NASA Technical Memorandum 78750

(NASA-TM-78750) WIND-TUNNEL TESTING OF VTOL AND STOL AIRCRAFT (NASA) 81 p HC A05/MF A01 CSCL 01A

N78-30040

Unclas
G3/02 28584

WIND-TUNNEL TESTING OF VTOL AND STOL AIRCRAFT

HARRY H. HEYSON

JULY 1978

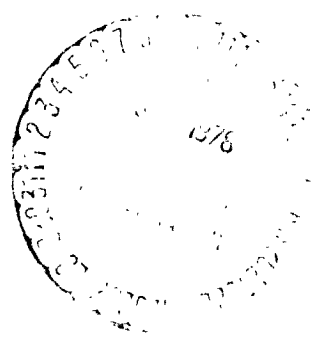

National Aeronautics and Space Administration

Langley Research Center
Hampton, Virginia 23665

WIND-TUNNEL TESTING OF VTOL AND STOL AIRCRAFT

Harry H. Heyson
Langley Research Center

SUMMARY

The basic concepts of wind-tunnel boundary interference are discussed and the development of the theory for VTOL-STOL aircraft is described. Features affecting the wall interference, such as wake roll-up, configuration differences, recirculation limits, and interference nonuniformity, are discussed. The effects of the level of correction on allowable model size are shown to be amenable to generalized presentation. Finally, experimental confirmation of wind-tunnel interference theory is presented for jet-flap, rotor, and fan-in-wing models.

INTRODUCTION

Theoretical aerodynamics is firmly based upon both implicit and explicit assumptions of small perturbations. These assumptions are grossly violated by VTOL aircraft in low speed transition flight, and theory is often an unreliable guide to efficient design. Under such circumstances, the wind tunnel generally stands as the sole source of reasonably good quantitative data in transition flight. Although the fact is not generally recognized, wind tunnels also have problems in low-speed testing. Indeed, it has been observed that nobody believes a theory except the man who developed it, and nobody disbelieves a wind-tunnel test except the man who ran it.

Many of the problems of wind-tunnel testing are purely mechanical. These problems are intensified with VTOL tests because the models invariably are powered and they require large amounts of power. The power may be electrical, hydraulic, or pheumatic; however, irrespective of the type of power, there are severe problems in transmitting this power across balances without either fouling or large taces. It is also often a problem to contain the power source within the model without grossly altering the desired configuration lines.

Another class of problem is aerodynamic imperfections in the flow. A wind tunnel does not produce a flow which is "straight down the tube." Locally, the flow may differ by several degrees from the main flow. It is really a necessity to have detailed flow surveys over most of the usable test volume to provide not only the basic velocity calibration but also the variations in upwash, sidewash, and static-pressure gradient at any model location. All too often, such measurements do not exist! The existerce of problems of this character often appears in upright-and-inverted testing and in tare runs. Unfortunately, these fundamental elements of a meaningful test program are also often omitted to obtain the suspect "economy" of reduced tunnel occupancy time.

The final problem in low-speed wind-tunnel testing is generally classed as "wall effects." This problem, in large degree, is accessible to theoretical treatment provided that the magnitude of the wall interference is kept within reasonable bounds. The wall interference tends to be proportional to lift coefficient and, therefore, becomes of great significance for VTOL configurations where the lift coefficient approaches infinity as the forward speed approaches zero.

The present paper is largely concerned with wall-interference at low speed. Numerous aspects of the theory are treated. Experimentally determined low-speed test results are discussed. Several examples of experimental measurements to determine the adequacy of the theory are also presented.

SYMBOLS

A	aspect ratio
A_L	V/STOL lifting element area
A_M	momentum area of lifting system
b	distance of center of lifting system from right-hand sidewall of tunnel
B	semiwidth of wind tunnel
C_L	lift coefficient
$C_{N,t}$	normal-force coefficient of tail
C_μ	momentum coefficient of jet, jet momentum/qS
$d\theta/dt$	pitching velocity
D	drag (sometimes used interchangeably with D_i)
D_i	induced drag
h	height of model above wind-tunnel floor
H	semi-height of wind tunnel
L	lift
m,n,N	integers
m^*	doublet intensity per unit area
M_u	longitudinal component of mass flow from model
M_w	vertical component of mass flow from model

M_T	mass flow through wind tunnel
n	ratio of final to initial induced velocities (also used to denote perpendicular direction
p	static pressure
p_o	static pressure for upstream
q	dynamic pressure, $\frac{1}{2}\rho V^2$
q_c	corrected dynamic pressure
s	semispan of wing
S	area
S_F	fan area
S_W	wing area
T_s	static thrust
u,v,w	velocities directed positive outward parallel to the X,Y,Z axes
u_o	momentum theory value of the longitudinal component of induced velocity
V	forward (or tunnel)velocity
V_j	exhaust velocity of lifting fan or jet
w_0	momentum theory value of the vertical component of induced velocity
w_h	the value of w_0 when hovering in free air
x,y,z	distances along X,Y,Z axes, positive outward from origin
X,Y,Z	Cartesian coordinates centered in model, X-axis runs directly aft (drag direction); Z axis directed upward (lift direction); and Y-axis directed to the side to form a right hand system
α	angle of attack
α_c	corrected angle of attack
$\alpha_{L=0}$	angle of attack for zero lift
γ	width-height ratio of tunnel

Γ	circulation
δ	wind tunnel interference factor
$\delta_{u,D}$	wind tunnel interference factor for longitudinal velocity due to induced drag
$\delta_{u,L}$	wind tunnel interference factor for longitudinal velocity due to induced lift
$\delta_{w,D}$	wind tunnel interference factor for vertical velocity due to induced drag
$\delta_{w,L}$	wind tunnel interference factor for vertical velocity due to induced lift
ΔL_i	fan induced lift
Δu	total longitudinal interference velocity, $\Delta u_L + \Delta u_D$
Δu_D	longitudinal interference velocity due to induced drag
Δu_L	longitudinal interference velocity due to lift
Δw	total vertical interference velocity, $\Delta w_L + \Delta w_D$
Δw_D	vertical interference velocity due to lift
Δw_L	vertical interference velocity due to induced drag
ϵ	downwash angle
θ	wake deflection downward from horizontal
θ_f	final rolled-up value of θ
θ_i	initial value of θ at the lifting system
Λ	wing sweep angle
μ	rotor tip-speed ratio
ρ	mass density of fluid
σ	ratio of span of model to width of tunnel
ϕ	potential
χ	wake deflection, aft and upward from vertical

DISCUSSION

BASIC CONCEPTS

Closed Tunnel

Physically, the nature of boundary effects can be illustrated as in figure 1. If the tunnel has closed walls, it is obvious that the general downward flow generated by producing lift will be stopped at the walls. This is equivalent to adding to the flow an additional interference flow whose strength at floor and ceiling is exactly opposite to the free air flow. Thus, in general, for a closed tunnel

$$\alpha_c = \alpha + \Delta\alpha \tag{1}$$

where $\Delta\alpha$ will be some positive quanitity; that is, the angle-of-attack set in the tunnel is increased effectively by the inteference.

Open Tunnel

The opposite effect is generated by a completely open wind-tunnel. Here the wind-tunnel stream is smaller than the infinitely large stream upon which the aircraft acts in free air. Since the aircraft is acting on less air, it must deflect the stream to a greater degree in the tunnel than in flight in order to maintain the same lift. This is equivalent to adding some downward flow to the free-air flow; thus, in an open tunnel, the $\Delta\alpha$ of the preceeding equation will generally be negative, reducing the effective angle-of-attack from that set in the tunnel.

BOUNDARY CONDITIONS

Closed Boundary

Evaluating wall effects is a theoretical boundary value problem. The appropriate conditions at a closed boundary are clear and unequivocable - the velocity normal to the wall must vanish; that is, in terms of the velocity potential ϕ

$$\frac{\partial\phi}{\phi n} = 0 \tag{2}$$

Open Boundary

The boundary condition at a free surface is not as obvious. The pressure throughout the exterior of the jet is constant and must be continuous across the boundary. Thus, we may consider Bernoulli's theorem on a streamline barely within the jet, at a point far upstream and at a point near the model, to yield

$$p + \frac{\rho}{2}\left[u^2 + (V + u)^2 + w^2\right] = p_o + \frac{\rho}{2} V^2 \tag{3}$$

where u, v, and w are the perturbations introduced by the model. Since the static pressure is constant along the edge of the jet $p = p_o$, equation (3) becomes

$$u^2 + v^2 + w^2 + 2\,Vv = 0 \tag{4}$$

If we now assume that the disturbances of the model are small, the squares of the perturbation velocities are negligible compared to Vv, and the boundary conditions becomes

$$v = 0 \tag{5}$$

Thus, for the open jet the longitudinal (rather than the normal) component of velocity vanishes at the boundary.

Two cautions must be observed: first, the open boundaries will alter their locations under the influence of the model; secondly, for conditions encountered by rotors and VTOL's at low speeds, the perturbation velocities may be much larger than the free stream velocities (fig. 2). Both effects violate the foregoing analysis and are not treated anywhere in the literature. Thus, great caution must be used in interpreting the results of tests at low speed in open tunnels.

CLASSICAL CORRECTIONS

Prandtl (ref. 2), Glauert (ref. 3), Theodorsen (ref. 4), and many subsequent authors developed theoretical treatments of wall effects computing general inteference factors for practical application in wind-tunnel testing. These results tyrically give the δ in the equation

$$\Delta\alpha = \delta \frac{S}{A_T} C_L \tag{6}$$

This formulation presented problems as soon as rotors and VTOL models began to be tested. At constant lift, C_L increased as V decreased so that $\Delta\alpha$ became infinite in hovering. Actually, this difficulty was merely a manifestation of small angle assumptions, for the full equation was

$$\tan \Delta\alpha = \frac{\Delta w}{V} = \delta \frac{S}{A_T} C_L \tag{7}$$

In this full form, infinite C_L in hover merely said that $\Delta\alpha$ was 90^o; that is, the interference was a pure upwash in a closed tunnel. Unfortunately, the magnitude of the upwash was unavailable. An even greater problem was that the wake assumed for the calculation was totally incorrect, for the wake of a hovering aircraft passes directly downward and not directly rearward.

VTOL-STOL CORRECTIONS

Figure 3 shows the wake of classical theory, which under small perturbation assumptions, was assumed to progress directly downstream without deflection. The main feature lacking was the large wake deflection characteristic of low-speed powered-lift aircraft. This feature was added by the analysis of reference 5. In that paper, the wake is assumed to be deflected from the vertical at some arbitrary angle χ until it meets the floor, at which point it turns and runs off along the floor. The results are given in terms of interference factors which yield the horizontal as well as the vertical interference velocities, and these, in turn, are separated into thos caused by the model lift forces and those caused by the drag forces. Characteristically, the wall effects yield a change in effective velocity as well as in angle-of-attack.

THE WAKE SKEW ANGLE

Momentum Considerations

It is already obvious that the wall effects will depend upon the skew angle χ. It will evolve that they also depend upon u_0 and w_0, the mean induced velocities at the lifting system. Simple V/STOL momentum theory (ref. 6) shows that

$$\left(\frac{w_o}{w_h}\right)^4 = \frac{1}{1 + \left(\frac{V}{w_0} + \frac{D_i}{L}\right)^2} \tag{8}$$

where

$$w_h = -\sqrt{\frac{L}{n\rho A_M}} = \sqrt{\frac{2\ C_L}{n\pi A}}\ V \tag{9}$$

The solution of equation (8) is shown graphically in figure 5. Values of w_o/w_h may be read directly from figure 5 for desired values of V/w_h and

The solution of equation (8) is shown graphically in figure 5. Values of w_o/w_h may be read directly from figure 5 for desired values of V/w_h and D_i/L. The corresponding value of u_o/w_h is simply $(D_i/L)(w_o/w_h)$ and the wake skew angle is found as

$$\cos \chi = \sqrt{\frac{w_o}{w_h}} \tag{10}$$

The momentum analysis of reference 6 is relatively crude; however, it has been found to provide good agreement with experiments for a wide variety of diverse configurations. Figure 6, from reference 7, illustrates the agreement obtained for jet flaps and for a ducted fan combined with external flaps. Other investigations have obtained comparable agreement for lifting propellers, helicopter rotors, and fan-in-wing configurations.

Wake Rollup

The angle obtained from momentum theory is the angle at which the main flow leaves the lifting device. The wind tunnel analysis is based on the deflection of the vorticity in the wake, which is not necessarily the same angle. Consider the wake of a uniformly loaded wing, a simple horseshoe vortex, as shown in figure 7. At the center of lift on the bound vortex, the bound vortex contributes nothing to the induced velocity; however, each trailing leg contributes $w_o/2$, so that the total induced velocity at the center of lift is w_o. In the center of the wake far behind the wing, the bound vortex is too far away to have any effect; however, each trailing leg is now effectively doubly infinite in length and contributes w_o to the induced velocity, for a total induced velocity of $2\ w_o$. This is a typical $n = 2$ system, where the induced velocities double at infinity. In contrast, consider the induced velocity in the far wake on one of the trailing legs. Because it is straight, this leg induces no velocity on itself. The other vortex, being twice as far from this vortex as it is from the center of the wake, contributes only $w_o/2$. Thus, the vortex wake itself is grogressing downward only half as rapidly as would be indicted by the induced velocity at the lifting system. A more elaborate analysis for an elliptically loaded wing based on reference 8 indicates a similar factor of $\pi^2/4$.

Even though a simple wing may seem vastly different from a rotor of a VTOL aircraft, the effect of rollup is similar. Figure 8 shows contours of vorticity measured behind a lifting rotor (ref. 9). If undistorted, the wake would be a skewed cylinder, and one would expect to find the vorticity within the elliptic intersection of the wake and the survey plane. In reality, most of the wake rolls up immediately into rather concentrated vortices centered only hald as far below the rotor as indicated by momentum theory. Even the complex flows from multiple jets roll up (fig. 9 from ref. 10) and obey a similar trend.

Figure 10 illustrates some plausible relationships between the final and initial wake deflections. A simple factor between initial and final values will yield an obviously incorrect vlaue in hover. This may be corrected by noting that tangents should be used for the large deflections near hovering as indicated on the figure. In any event, most wind-tunnel tests will involve deflection angles of 60^0 or less, and the use of any of these relationships will make little difference, provided that one of them is used.

General Wake Model

Next, a simple inclusive wake model is required. Consider two such diverse lifting systems as a rotor and a wing (fig. 11). The rotor wake may be considered as an assemblage of vortex rings of strength , while the wind wake is a simple horseshoe vortex. Prandtl has shown the identity between a area surrounded by vortices and the same area covered by a uniform doublet distribution. Thus, the rotor wake in this concept becomes a stack of circular doublet sheets, and the wing wake becomes a single continuous doublet sheet. If these wakes are examined from greater and greater distances, they appear progressively more narrow until the point is reached where either system appears to be a uniform distribution of point doublets along a line. This is an admirable economy, for this singlet wake concept may be used to represent almost any lifting system. This is the wake model used in reference 5.

Calculating Correction Factors

The conditions at the edge of the test section may be met by setting up a doubly infinite image system as in figure 12. The varying conditions for open boundaries and closed walls are obtained by a suitable choice of sign effect pair. This pair is obtained by the superpositions shown schematically in figure 13. Wall effects are the difference between the wind tunnel and free air. Rather than actually perform the subtraction, the central free-air wake is merely omitted from the superpositions. The entire procedure is executed within the computer. While tables of correction factors have been published, many facilities have the same, or similar, programs operational on their computers.

Applying Corrections

The application of corrections to data can become very involved; however, in the simplest case, the equation are shown in figure 14. The interference factors are obtained from the digital computer. The increments in the horizontal and vertical induced velocities are defined in terms of the interference factors, the momentum area of the lifting system 9generall $A_M = \pi\, b^2/4$), the cross sectional area of the tunnel A_T, and the induced velocities u_o and w_o at the lifting system. These interference velocities combine as shown to obtain a correction $\Delta\alpha$ to angle of attack and a ratio qc/q by which to correct the dynamic pressure.

The typical behavior of the interference factors in a closed tunnel is illustrated in figure 15. The vertical interference due to lift $_{w,L}$ corresponds to the of classical theory. When the wake trails directly rearward (= 90°), the value of $_{w,L}$ is identical to the classical (with a factor of -4 because of an altered definition) and the other three interference factors are zero. Thus, the V/STOL theory includes classical theory as a special case. As the wake is depressed downward toward 0°, the magnitude of the vertical interference increases and $_{u,L}$ takes on a positive value resulting in a decrease of effective forward velocity. The factors $_{w,D}$ and $_{u,D}$ are such as to magnify these effects for positive drag and to decrease them for negative drag.

It is tempting to think that wall effects depend upon the ratio of the momentums in the wake and through the tunnel. Such, however, is not the case, for the derivation shown in figure 16 indicates that the interference depends upon the mass-flow ratios rather than the momentum ratios. Thus, for equal interference factors, an efficient system obtaining lift by giving a small impetus to a large mass of air will have larger wall effects than an inefficient system which lifts by giving a large impetus to a small mass of air.

Large Models

Up to this point, the wake of the model has been represented by only a single string of doublets. Although this procedure is useful, such a wake is a satisfactory representation only of models which are "vanishingly small" with respect to the wind-tunnel dimensions. Glauert pointed out decades ago (ref. 3). that such an assumption was inadequate for classical corrections if the span of the model exceeded 10 percent of the tunnel width. The same conclusion is true for V/STOL corrections.

Simple superposition of the "vanishingly small: wakes may be used to provide reasonably adequate representations of the wakes of large models. A few rudimentary examples of this technique were presented in reference 5; however, the systematic elaboration of the method was first published in reference 12 for V/STOL aircraft. That paper presents a set of procedures for the digital computer which result directly in the average interference and its distribution for rotors, swept wings, jet-lift VTOL's and a number of combined systems.

Figure 17 illustrates the procedure of reference 12 for a swept wing. The wing is represented by ten doublet strings. The result is the summation of figure 18 which is evaluated within the computer. A similar summation and computer procedure is provided for a rotor by using a wake consisting of an assemblage of 20 doublet strings as in figure 19. The set of computer programs for these calculations is available in the literature, and the programs are operational at many wind-tunnel facilities.

A certain amount of thought prior to choosing the model may be necessary for rational application of corrections. Certain types of configuration such as

those illustrated in the upper portion of figure 20 result in a more or less blended wake. In most cases, these can be treated as if they were simple wings. In other cases, two very distinct wakes may be generated (lower portion of figure 20). In such cases, the wall effects must consider, in addition, the contribution on each piece engendered by the presence of the other piece within the tunnel walls. Successful application of corrections to such models probably requires the provision of internal balances to separate the forces arising from each portion of the aircraft.

Increasingly more complicated configurations may be built up from their separate elements as indicated in figure 21. However, the successful application of corrections depends on the ability to measure the actual performance of each of the elements while they are operating in the presence of each other. This may not be a great penalty. Such information is highly desirable as basic information for such configurations and the instrumentation should be provided in any event.

LIMITS OF CORRECTION

Nonuniformity of Interference

There are limits to the magnitude of the corrections that can be tolerated without distorting the wind-tunnel flow so badly that the resulting data loses meaning. One obvious limitation is the crude nature of the theoretical treatment itself. Refinement is not truly necessary provided that the overall magnitude of the corrections is modest; after all, even a 10 percent error in a 10 to 20 percent effect is only 1 to 2 percent of the total. Generally, the combined effect of the measurement-system accuracies is that great.

The nonuniform nature of the interference can be illustrated by computing the flow field in the central plane of a helicopter rotor (fig. 22), and adding to that field the interference velocities caused by the tunnel walls. The resulting flow is shown in figure 23. For the condition chose, the correction angle $\Delta\alpha$ is 8.3 degrees. Thus, the flow angles in free air are those measured with respect to a new axis system cocked by this angle with respect to tunnel axis. This may improve things at the rotor, but it obviously makes the comparison worse far in front of, and far behind the rotor. In short, the amount of wall effect varies with tunnel location; the flow is highly distorted.

Figure 24 illustrates the effect of some of the types of distortion which may be encountered. If the interference increases laterally from the center of the model, the wing tips ses a greater local angle-of-attack. The same effect could be generated in a uniform flow by twisting the tiops upward (wash-in). Effectively, with respect to the air, the model is distorted in the tunnel and may be subject to premature tip stall.

Interference generall increases for some distance downstream from the model. This generates a curved flow. With respect to a uniform flow, the model would see the same local angles only if it had an increased camber.

Similarly, this curvature effectively results in an altered tail height and tail setting. All of these effects may be considered as distortions of the model.

Figure 25 presents an alternate viewpoint. Here the model is subjected to a linearly varying wall-interference. As shown on the right-hand side of the figure, this nonuniformity is equivalent to operating in free air at a different angle-of-attack and also with an imposed rate of pitch.

Removing the effects of nonuniform flow from the model data is exceedingly difficult, and it imposes a limit on the allowable magnitude of the wall effects. The old rule-of-thumb was that $\Delta\alpha$ should be less than 2^0. Such small limits insure that nonuniformity will be small; however, 2^0 also partially accounts for the even more approximate nature of classical wall corrections. A larger limit may be allowable when using the more elaborate corrections of references 5 and 12.

Recirculation

The complete flow in the tunnel has been explored in depth in reference 13. Figures 26-29 show isometrics of the flow in the central plane of a rotor and in the plane of the floor for wake skew angles of 70^0 to 10^0. In each case, the flow in free air is shown on the left, and the flow in a closed wind-tunnel is shown on the right. For $\chi = 70^0$ (fig. 26), the two flows are very similar within a diameter or so of the rotor. For $\chi = 50^0$ (fig. 27), the flows are fairly similar except for a stagnant region immediately in front of the intersection of the wake and floow. In this region, the wind tunnel flow becomes stagnant, and the velocity around the sides of the intersection is greater in the tunnel. When the skew angle is 30^0 (fig. 28), the flow ahead of the intersection is strongly reversed and there is a notable outward flow from the intersection. At $\chi = 10^0$ (fig. 29), these effects are greatly magnified, a large vortex-like motion involves the forward portion of the rotor, and the flow is reversed, and will separate from, the ceiling aft of the rotor.

It is clear that the rotor wake will be grossly altered by flows such as shown in the preceeding figures. Figure 30 illustrates the deformations. The flow squirts forward ahead of the rotor, in a manner sure woll up into a vortex, and is drawn aft and upward behind the rotor. Examination of the deformed wake (fig. 30) indicates that the deformation will magnify the theoretical effects. The overall flow to be expected is sketched in figure 31. A large cylindrical sheet of vorticity forms ahead of the rotor and passes off to the sides. As it approaches the walls, it sees the effect of its own image in the wall and climbs upward. The initial portion of the vortex sheet is clearly shown in the tuft-grid photograph of figure 32.

Obviously the flow in the tunnel can be so unlike free-air flow that tests may produce invalid results. The theory, which does not include wake deformation is inadequate to predict the limits of testing. Instead, controlled testing is necessary to determine limits; indeed, this "recirculation" limit was initially found in such tests by Rae at the University of Washington (ref. 14). His results are function of wind-tunnel width-height ratio, and can be recast in the form shown in figure 33. The criterion is a function of the distance

behind the model at which the theoretical wake strikes the floor. Additional values placed on figure 33 indicate that grossly different models follow the same rule.

Wind-Tunnel Boundary Layer

The limits of figure 33 may be far more generous when testing to obtain data for ground effect since a somewhat similar recirculation occurs in ground effect as well. Here a different problem arises because of the wind-tunnel boundary layer. Figure 34 illustrates the effect schematically. When there is no boundary layer as in the upper part of the figure, the initial flow reversal is relatively small; however, this disturbance can propagate forward in the low energy tunnel boundary-layer, locally causing increased angles in the flow near the nose until the model stalls at the nose. These effects can be eliminated by eliminating the boundary layer on the floor; the most direct way is to provide a belt moving with free stream velocity as the floor. Figure 35 (from ref. 15) shows one experimental determination of the conditions which require such treatment.

CHOOSING MODEL SIZE

The complexity of the corrections at low speed makes it rather difficult to predict the allowable size of a model for a given test. Reference 16 attempts to provide a set of generalized correction charts to provide some guidance in selecting sizes. As the starting point, reference 16 uses momentum theory to form the results upon C_L rather than the momentum skew angle χ. The definition of C_L is first divided by $(w_h/w_h)^2$, to obtain

$$C_L = \frac{L}{\frac{1}{2}\rho V^2 S\,(w_h/w_h)^2} \tag{11}$$

Now substitute equation (9) into equation (11) to yield

$$C_L = \frac{L}{\frac{1}{2}\rho \left(\frac{V}{w_h}\right)^2 S\left(\frac{L}{n\rho A m}\right)} \tag{12}$$

Simplifying equation (12) and noting that $A = 4S^2/S$ yields

$$C_L = \frac{\pi n A}{2\left(\frac{2}{w_h}\right)^2} \tag{13}$$

From momentum theory (ref. 6)

$$\frac{V}{w_0} = -\left(\tan \chi + \frac{D_i}{L}\right) \tag{14}$$

Substitute equations (10) and (14) (noting that $V/w_h = (V/w_o)(w_o/w_h)$) into equation (14) to obtain (for n = 2)

$$\frac{C_L}{A} \quad \frac{\pi}{\left(\tan \chi + \frac{D_i}{L}\right)^2 \cos \chi} \tag{15}$$

Figure 36 has been prepared by calculating C_L/A for a range of χ and D_i/L. In the simple case of an unpowered wing, examination of the "shaft" power by momentum theory shows that $D_i/L = \cot \chi$. In that case, equation (15) reduces to

$$\frac{C_L}{A} = \sin^2 \chi \cos \chi \tag{15}$$

Equation (15) is also shown in figure 36. Observe that one of the most fundamental and far-reaching consequences of powered lift is that the conventional relationship between induced drag and lift is destroyed. A V/STOL aircraft can operate anywhere in the plane of figure 36. Any lift coefficient can be obtained by the V/STOL aircraft. This is in distinct contrast to the conventional wing where the relationship between induced drag and lift restricts the maximum lift coefficient to

$$C_L + 1.209 A \tag{16}$$

The parameters displayed on figure 36 are sufficient to calculate the wall interference for a given span-width ratio σ in any given wind tunnel. This interference can be plotted in terms of $\Delta\alpha$ and qc/q on the same plane as in figure 37. Similar charts are also presented for the difference in corrections at the wing and at the tail, as well as for the distortions across the span of the wing.

Maximum plausible values for these various quantities can be assigned according to how much detail is to be incorporated into the data reduction for a given wind-tunnel test. Then a simple chart such as figure 38, shows the maximum C_L/A for which acceptable data can be obtained. It is interesting that $\Delta\alpha$ seldom limits testing, and that Rae's recirculation limit largely is applicable to small models only. In most cases, various nonuniformities of interference set the limits.

The degree of effort expended in correcting data can have a large effect on the usable testing range. Reference 16 sets three levels ranging from no corrections at all to a maximum effort where the details of span loading are involved. As shown in figure 39, the level of corrections applied to the data can affect the allowable range of lift coefficient by an entire order of magnitude.

EXPERIMENTAL VERIFICATION

Over a period of years, a substantial effort has been made to verify the wall effects predicted by the theory of reference 5. Figure 40 provides a listing of a number of these test programs, and many of the test models are shown in figures 41 to 43. In general, the experimental results were quite encouraging, with the preciseness of correlation being largely a function of the rigor with which the corrections were applied. The general results are illustrated by the following samples:

Jet Flap

The first test presented herein was conducted on the jet flap model shown in figure 44. This model had a full-span trailing-edge jet flap with a fixed 90^{o} deflection angle. The model was mounted on a strain-gage sting balance. A separate balance was provided for the simple rectangular tail. Tests were conducted in Langley's 300-mph 7x10-foot tunnel and in a smaller 2.70x1.88-foot test section. These results were originally presented in reference 17.

The test results for lift are presented in figures 45 and 46. At $C_{\mu} = 1.5$, where the model has a distinct stall, correcting the data has brought the stall angle into complete agreement with a correction angle $\Delta\alpha$ of about 5^{o}. At $C_{\mu} = 10$, corrections fail at angles of attack in excess of about 10^{o}. This angle of attack corresponds to Rae's recirculation limit as presented earlier in figure 33. A comparison based on the tail normal-forces is presented in figure 47. The corrected data is again coincident within the accuracy of the data.

Lifting Rotor

The second example concerns a tail behind a lifting rotor (ref. 18). This system, shown earlier in figure 41, was tested in the University of Washington 8x12-foot tunnel, as well as within a 4x6-foot insert in that tunnel. The data is presented directly as a wall effect, in that the difference in tail zero-lift angle is shown as a function of tip-speed ratio. The line marked recirculation limit was determined from earlier tests (ref. 14) and not from this test. Above this limit line, the theoretical corrections eliminate the effect of the walls to a point within the order of accuracy of the tests.

Fan-in-Wing

The final example is an extensive study (ref. 19) on the fan-in-wing model shown in figure 49. The model was equipped with two tip-turbine-driven fans and tail was equipped with a separate strain-gage balance. Overall forces were obtained from the wind-tunnel balances. This model was tested in a number of

different test sections. Figure 50 illustrates the comparative model and test-section sizes. In addition to those shown, the model was also tested in the 30x60-foot and 40x80-foot tunnels.

One early criteria for testing without corrections was developed empirically in reference 20. The appropriate ratios given by that reference for this test are shown in figure 51. These values indicate that in many cases there should be no wall effects. In contrast, the uncorrected data (fig. 52a) indicate rather large wall effects in all of the smaller tunnels. These differences collapse into a single data set when corrections are applied (fig. 52b).

Considerable effort has been expended in the past measuring and correlating the "fan-induced" lift of fan configurations. One such correlation (ref. 21) is shown in figure 53. The chosen conditions are $= 0^{o}$ and $V/V_j = 0.4$. There are, of course, significant differences between forward and aft locations; however, those configurations which are reasonable balanced in moments appear to be along the shaded region. The uncorrected values from the present test in the 44x88-inch section for the complete configuration, both with and without the tail load, bracket the same shaded area. Unfortunately, the "fan-induced" lift vanishes (fig. 52a) when the data is corrected. Indeed, the corrected data closely follows a theoretical analysis (ref. 22) in which the interference between the fans and the wing is totally neglected.

Figure 54 and 56 demonstrate the effectiveness of corrections at higher angles of attack and at the tail. In almost all cases, the correlation degenerates at very low values of V/V_j. This effect is caused by recirculation, which is more suitably predicted in the present case by the results of Tyler and Williamson (refs. 23 and 24).

REFERENCES

1. POPE, ALAN: AND HARPER, JOHN J.: LOW-SPEED WIND TUNNEL TESTING., JOHN WILEY AND SONS, NEW YORK, 1952.

2. PRANDTL, L.: AND TEITJENS, O. G. (J. P. DEN HARTOG, TRANS.): APPLIED HYDRO- AND AEROMECHANICS. DOVER PUB., INC., 1957. PP 222-225.

3. GLAUERT, H.: THE ELEMENTS OF AEROFOIL AND AIRSCREW THEORY., 2ND ED., CAMBRIDGE UNIV. PRESS, 1948. PP 189-198.

4. THEODORSEN, THEODORE: THE THEORY OF WIND-TUNNEL WALL INTERFERENCE. NACA REP. 410, 1931.

5. HEYSON,HARRY H.: LINEARIZED THEORY OF WIND-TUNNEL JET-BOUNDARY CORRECTIONS AND GROUND EFFECT FOR VTOL/STOL AIRCRAFT. NASA TR R-124, 1962.

6. HEYSON,HARRY H.: NOMOGRAPHIC SOLUTION OF THE MOMENTUM EQUATION FOR VTOL-STOL AIRCRAFT. NASA TN D-814,1961 (ALSO AVAILABLE AS: V/STOL MOMENTUM EQUATION, SPACE/AERON. VOL.38,NO.2, JULY,1962, PP B-18 TO B-20.)

7. NEWSOM, WILLIAM A., JR.: WIND-TUNNEL INVESTIGATION OF A DEFLECTED-SLIPSTREAM CRUISE-FAN V/STOL AIRCRAFT WING. NASA TN D-4262, 1967.

8. CONE, CLARENCE D.: A THEORETICAL INVESTIGATION OF VORTEX-SHEET DEFORMATION BEHIND A HIGHLY LOADED WING AND ITS EFFECT ON LIFT. NASA TN D-657, 1961.

9. HEYSON, HARRY H.: AND KATZOFF, S.: INDUCED VELOCITIES NEAR A LIFTING ROTOR WITH NONUNIFORM DISK LOADING. NASA REP. 1319, 1957. (SUPERSEDES NACA TN 3690 BY HEYSON AND KATZOFF AND NACA TN 3691 BY HEYSON.)

10. MARGASON, RICHARD J.: JET-INDUCED EFFECTS IN TRANSITION CONF. ON V/STOL AND STOL AIRCRAFT. NASA SP-116, 1966. PP 170-190.

11. PRANDTL, L.: AND TEITJENS, O. G. (L. ROSENHEAD, TRANS.): FUNDAMENTALS OF HYDRO- AND AEROMECHANICS. DOVER PUB., INC., 1957. PP 200-207.

12. HEYSON, HARRY H.: USE OF SUPERPOSITION IN DIGITAL COMPUTERS TO OBTAIN WIND-TUNNEL INTERFERENCE FACTORS FOR ARBITRARY CONFIGURATIONS, WITH PARTICULAR REFERENCE TO V/STOL MODELS. NASA TR R-302, 1969.

13. HEYSON, HARRY H.: THEORETICAL STUDY OF CONDITIONS LIMITING V/STOL TESTING IN WIND TUNNELS WITH SOLID FLOOR. NASA TN D-5819, 1970.

14. RAE, WILLIAM H.,JR.: LIMITS ON MINIMUM-SPEED V/STOL WIND-TUNNEL TESTS. JOUR.OF AIRCRAFT, VOL.4, NO.3, MAY-JUNE, 1967, PP 249-254.

15. TURNER, THOMAS R.: A MOVING-BELT GROUND PLANE FOR WIND-TUNNEL GROUND SIMULATION AND RESULTS FOR TWO JET-FLAP CONFIGURATIONS. NASA TN D-4228, 1967.

16. HEYSON, HARRY H.: RAPID ESTIMATION OF WIND TUNNEL CORRECTIONS WITH APPLICATIONS TO WIND TUNNEL AND MODEL DESIGN. NASA TN D-6416, 1971.

17. HEYSON, HARRY H.; AND GRUNWALD, KALMAN J.: WIND TUNNEL BOUNDARY INTERFERENCE FOR V/STOL TESTING. CONFERENCE ON V/STOL AND STOL AIRCRAFT, NASA SP-116, 1966. PP 409-434.

18. RAE, WILLIAM H., JR.; AND SHINDO, SHOJIRO: COMMENTS ON V/STOL WIND TUNNEL DATA AT LOW FORWARD SPEEDS. PROCEED. THIRD CAL/AVLABS SYMPOSIUM ON AERODYNAMICS OF ROTARY WING AND V/STOL AIRCRAFT. VOL. 2, BUFFALO, N.Y., JUNE 18- 20, 1969.

19. HEYSON, HARRY H.: THE EFFECT OF WIND-TUNNEL WALL-INTERFERENCE ON THE PERFORMANCE OF A FAN-IN-WING VTOL MODEL. NASA TN D-7518, 1974.

20. COOK, WOODROW L.; AND HICKEY, DAVID H.: COMPARISON OF WIND-TUNNEL AND FLIGHT-TEST AERODYNAMIC DATA IN THE TRANSITION-FLIGHT SPEED RANGE FOR FIVE V/STOL AIRCRAFT. CONF. ON V/STOL AND STOL AIRCRAFT. NASA SP-116, 1966. PP 447-467. (ALSO AVAILABLE AS AGARD REPT 520, 1965.)

21. HICKEY, DAVID H.; AND COOK, WOODROW L.: AERODYNAMICS OF V/STOL AIRCRAFT POWERED BY LIFT FANS. AGARD CP 22, PAPER NO 15, SEPT 1967.

22. HEYSON, HARRY H.: THEORETICAL AND EXPERIMENTAL INVESTIGATION OF THE PERFORMANCE OF A FAN-IN-WING VTOL CONFIGURATION. NASA TN D-7498, 1973.

23. TYLER, R. A.; AND WILLIAMSON, R. G.: EXPERIENCE WITH THE NRC 10 FT.X20 FT. V/STOL PROPULSION TUNNEL - SOME PRACTICAL ASPECTS OF V/STOL ENGINE MODEL TESTING. CAN. AERO. AND SPACE JOUR.,VOL 10, NO 9, SEPT 1972. PP 191-199.

24. TYLER, R. A.; AND WILLIAMSON, R. G.: WIND TUNNEL TESTING OF V/STOL ENGINE MODELS - SOME OBSERVED FLOW INTERACTION AND TUNNEL EFFECTS. AGARD-CP-91-71, PAPER NO 8. DEC. 1971.

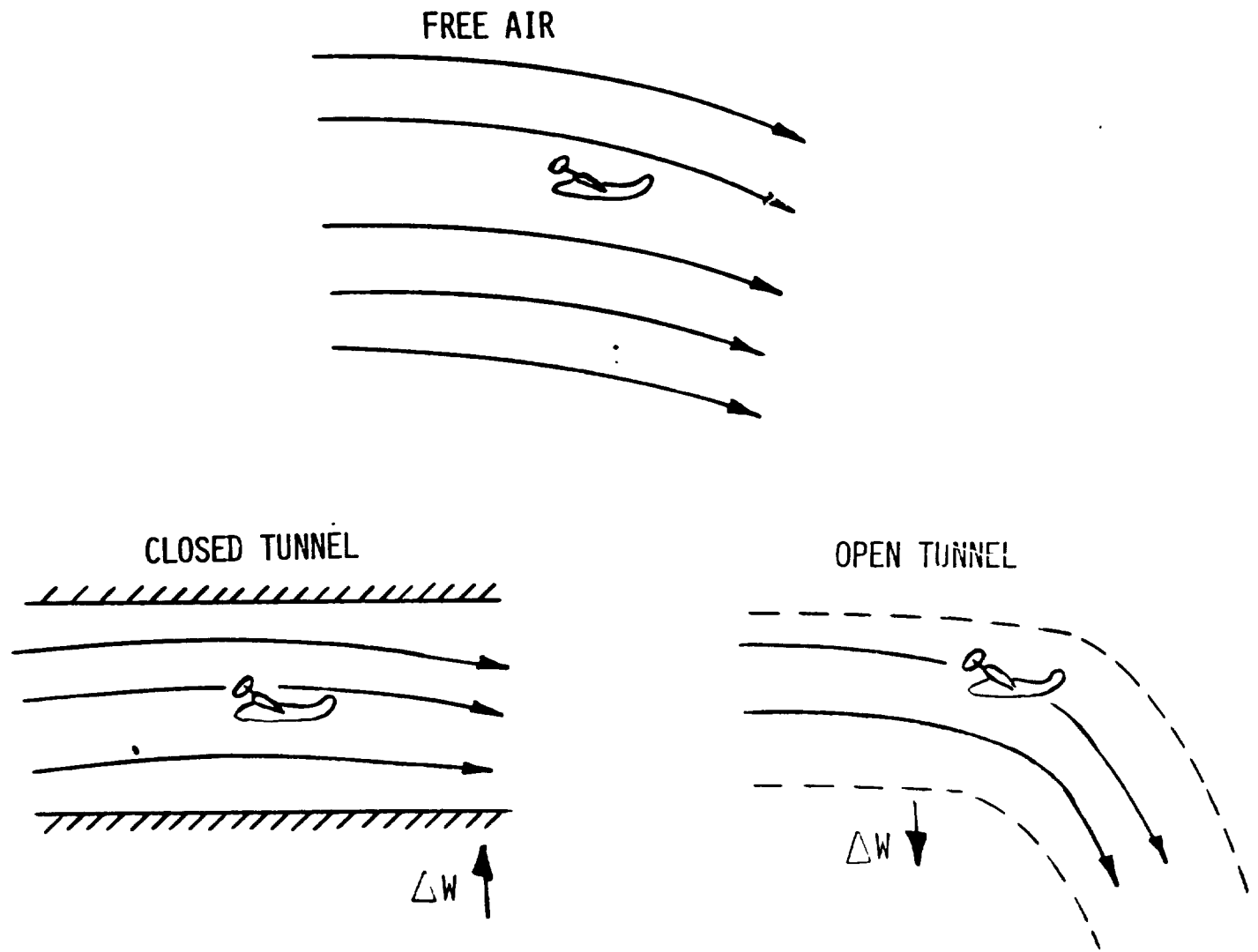

Figure 1.- Basic concepts of wind-tunnel boundary interference.

Figure 2. - Dust-flow photograph of a model rotor in an open tunnel.

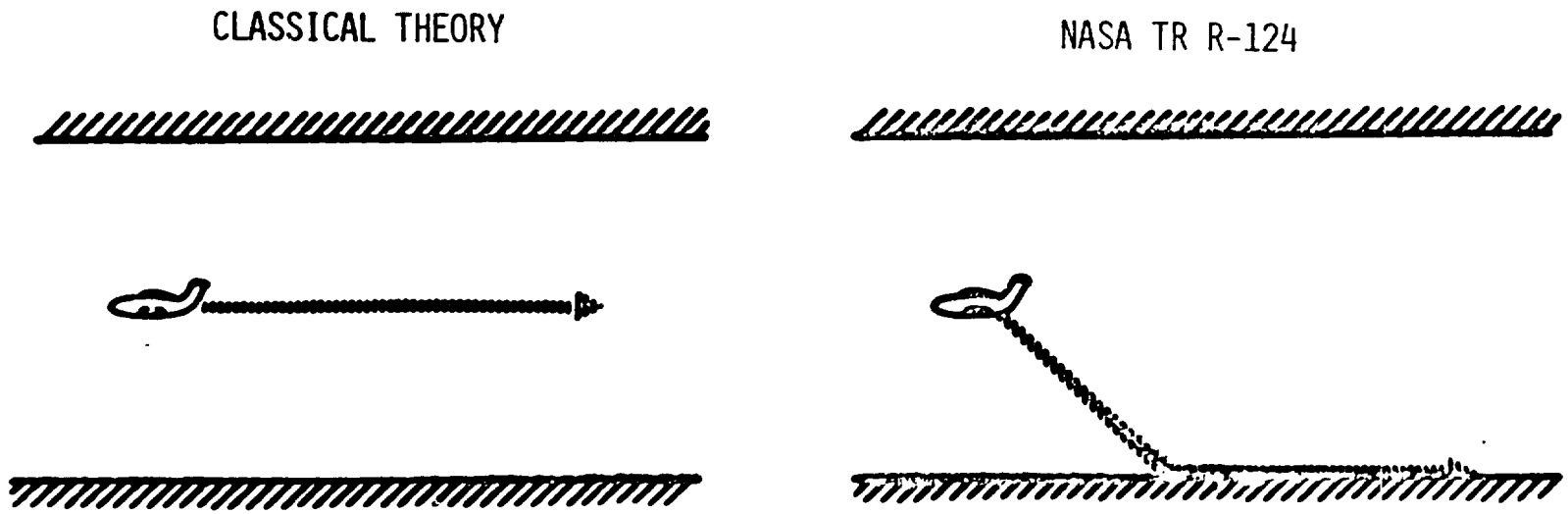

Figure 3. - Assumed wake of model.

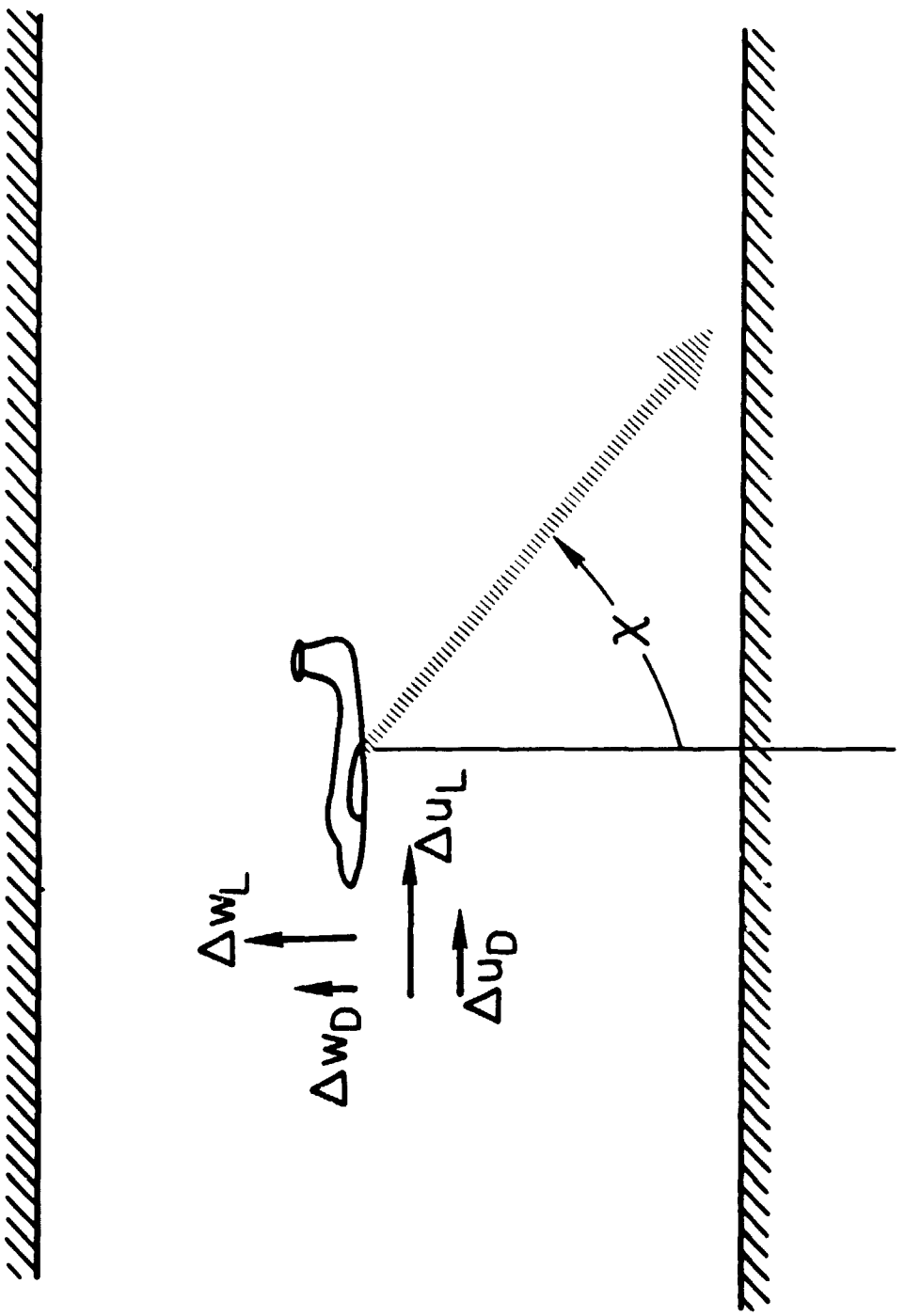

Figure 4. - Interference velocities for VTOL-STOL wind-tunnel corrections.

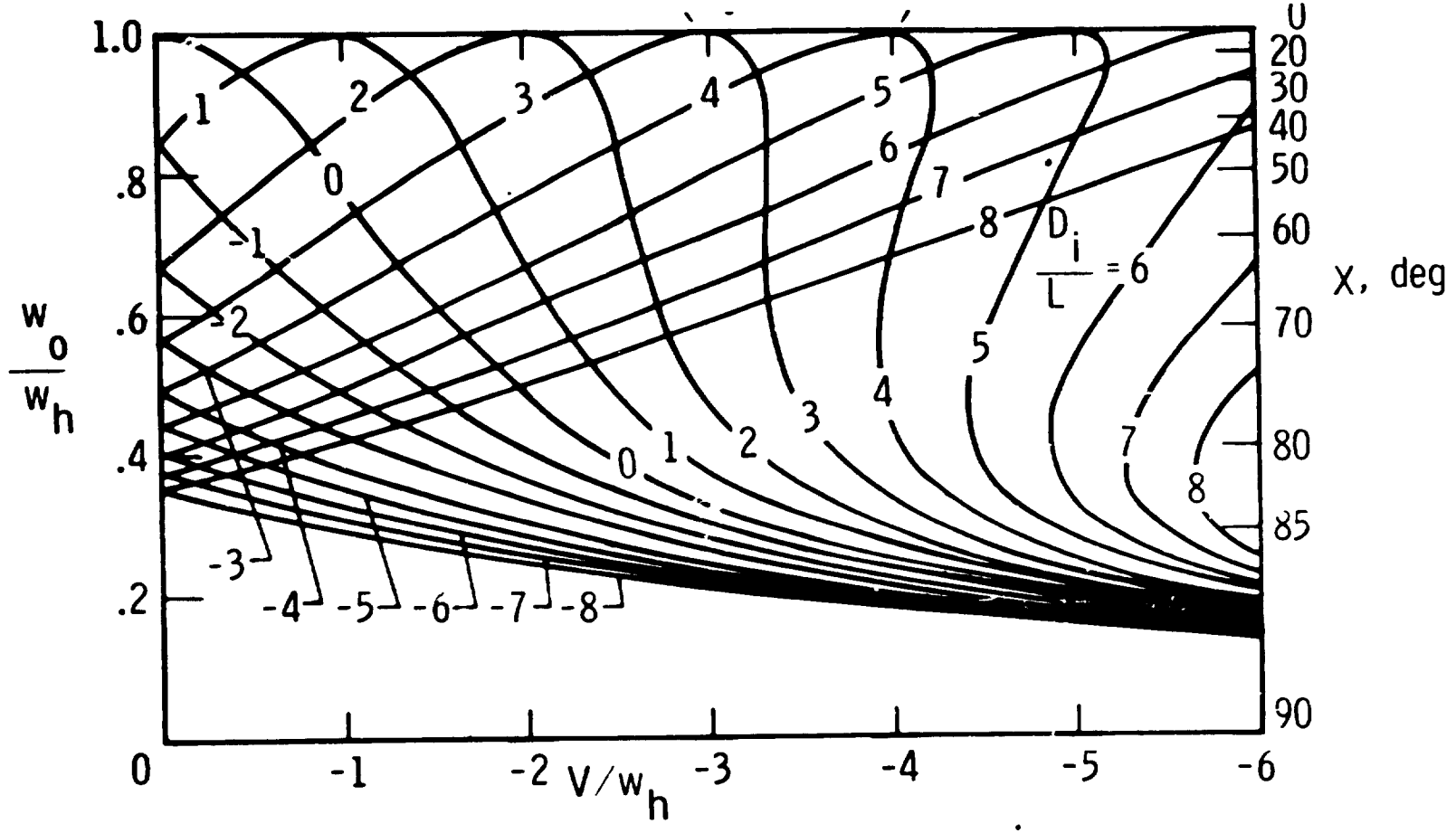

Figure 5. - Solution of VTOL-STOL momentum quartic.

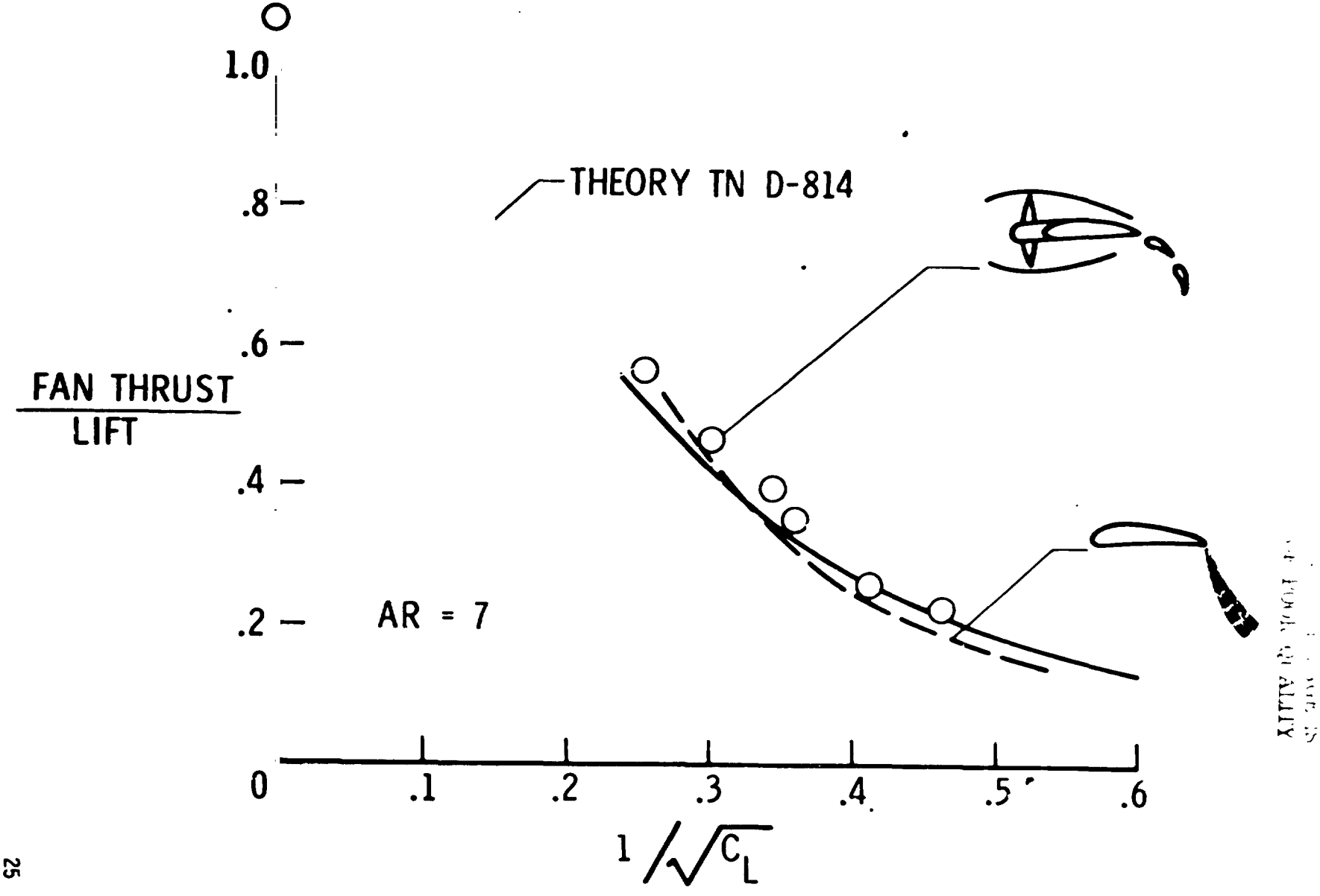

Figure 6. - Comparison of momentum theory with experiments.

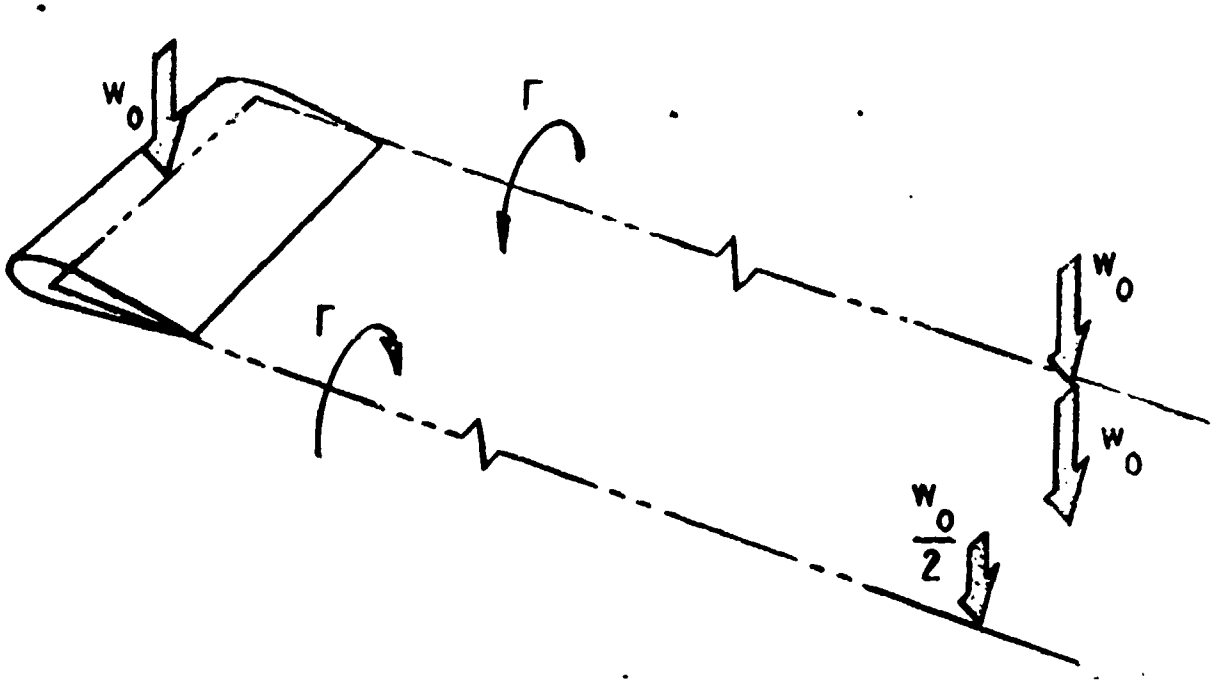

Figure 7. - Path of vorticity in the wake of a uniformly loaded wing.

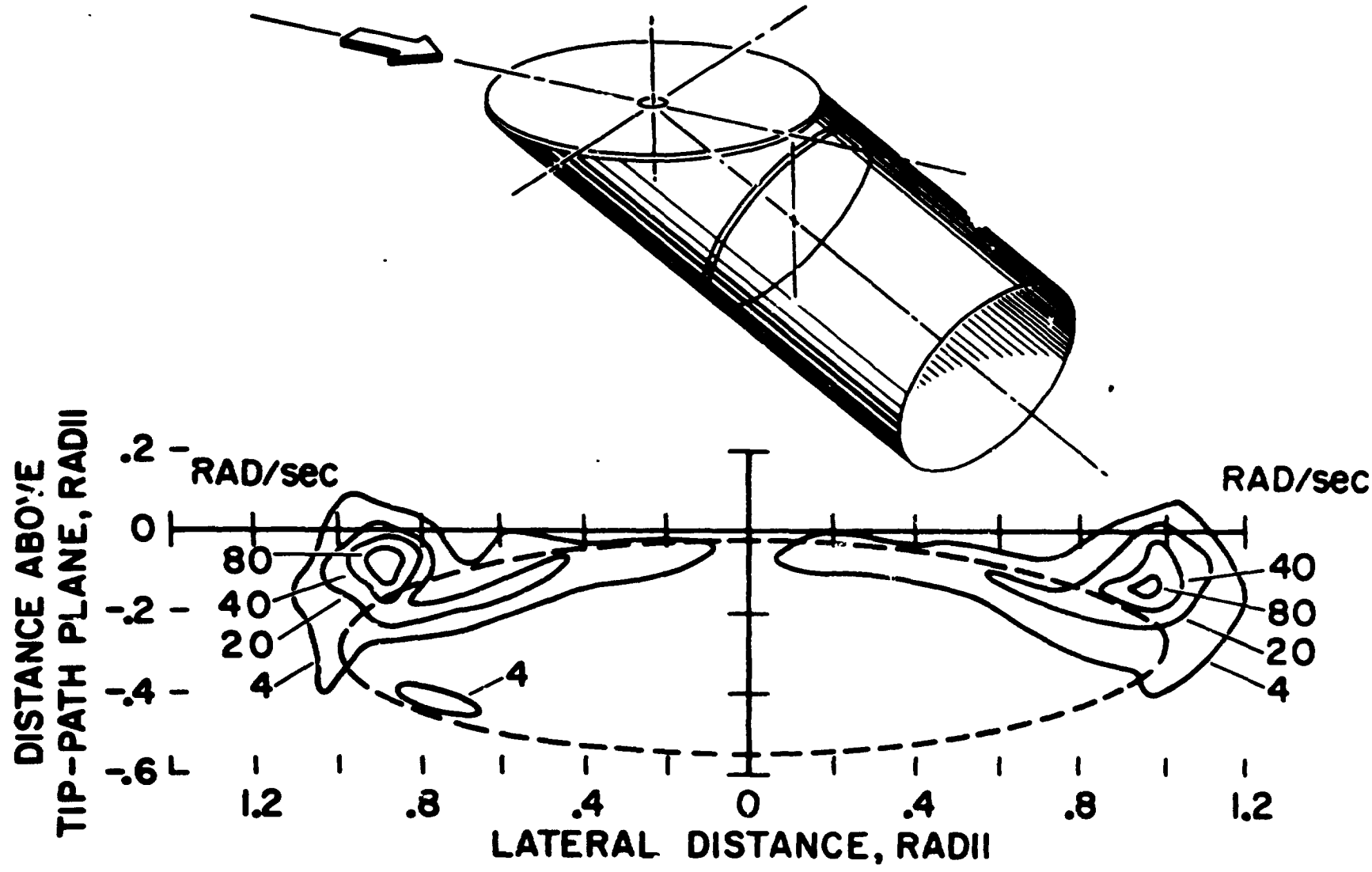

Figure 8. - Contours of equal value of vorticity measured seven percent of a radius behind the trailing edge of a rotor. $\chi = 75^{o}$.

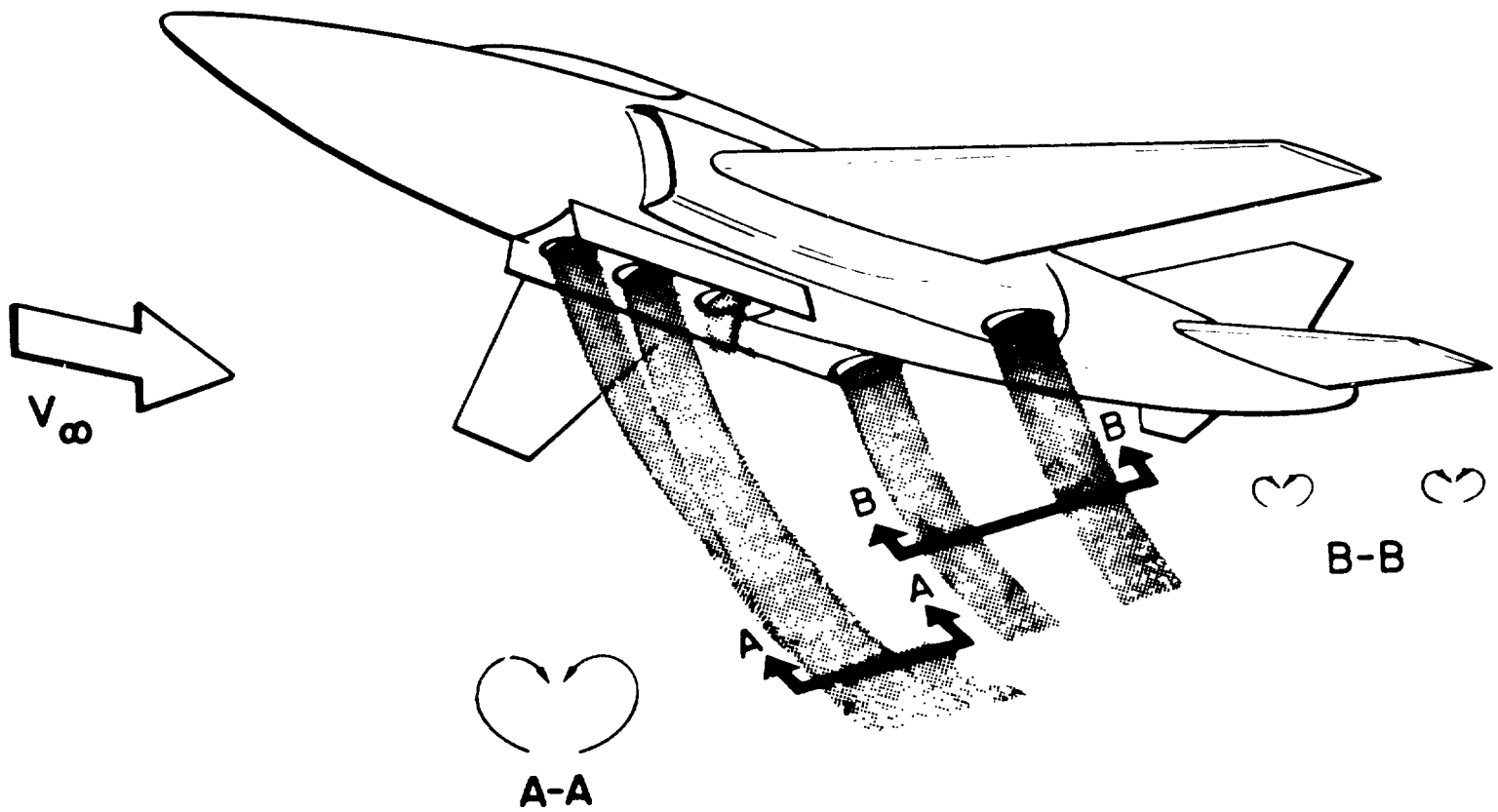

Figure 9. - Sketch of jet wakes observed behind a jet-lift fighter model.

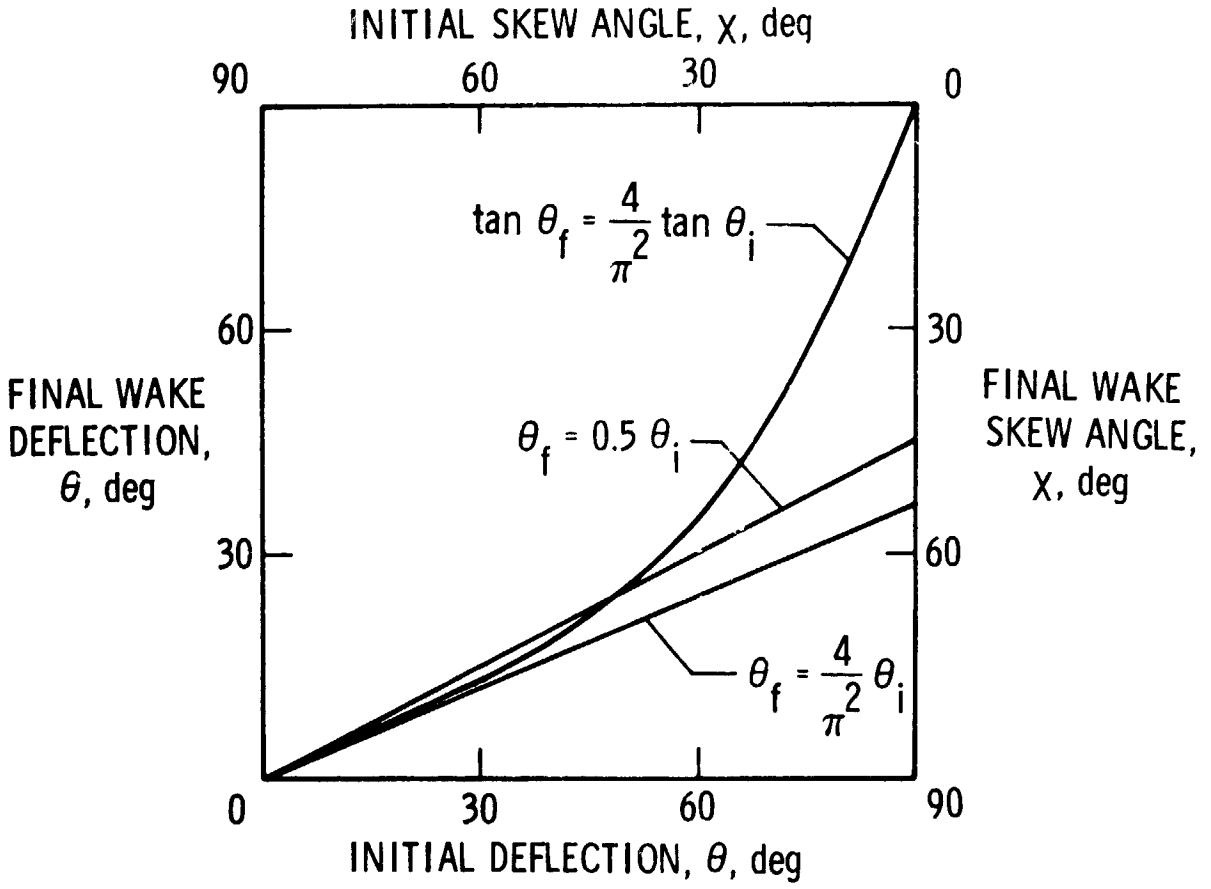

Figure 10. - Effect of wake roll-up on the final (or effective) wake inclination.

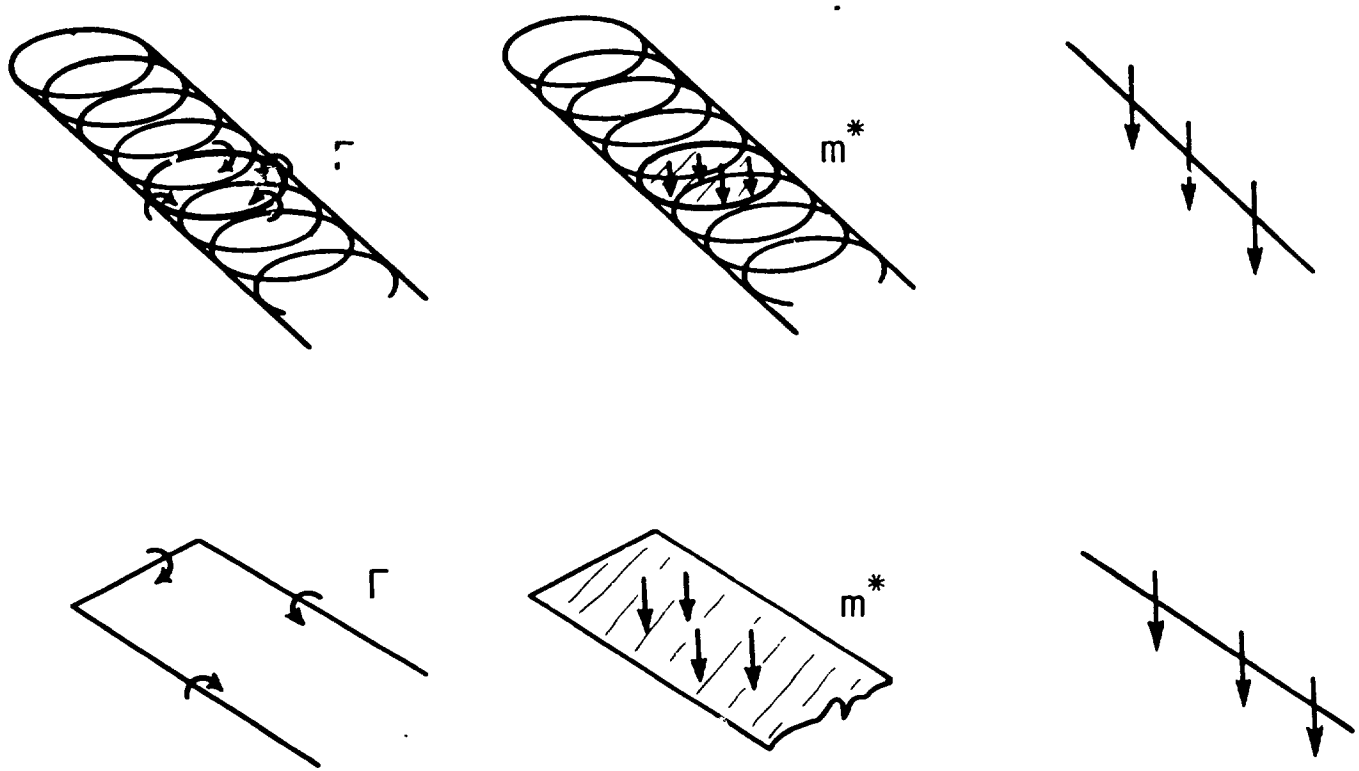

Figure 11. - Sketches illustrating the reduction of idealized rotor and wing wakes into a semi-infinite string of point doublets.

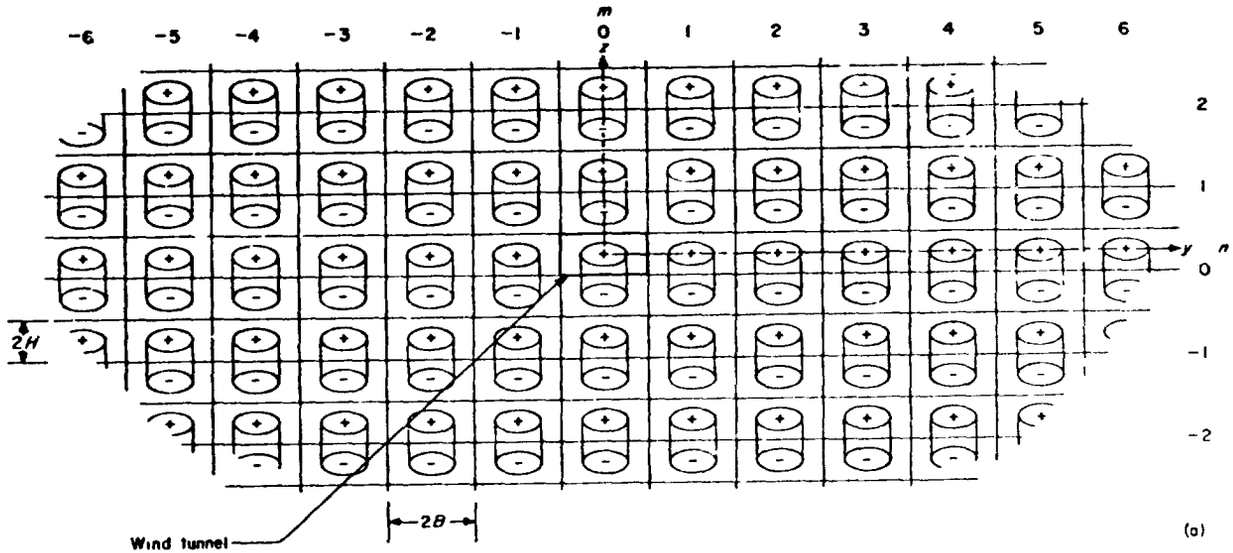

Figure 12. - Image system representing the effect of the walls of a closed wind tunnel. Plus signs indicate the same direction of vorticity as the real wake.

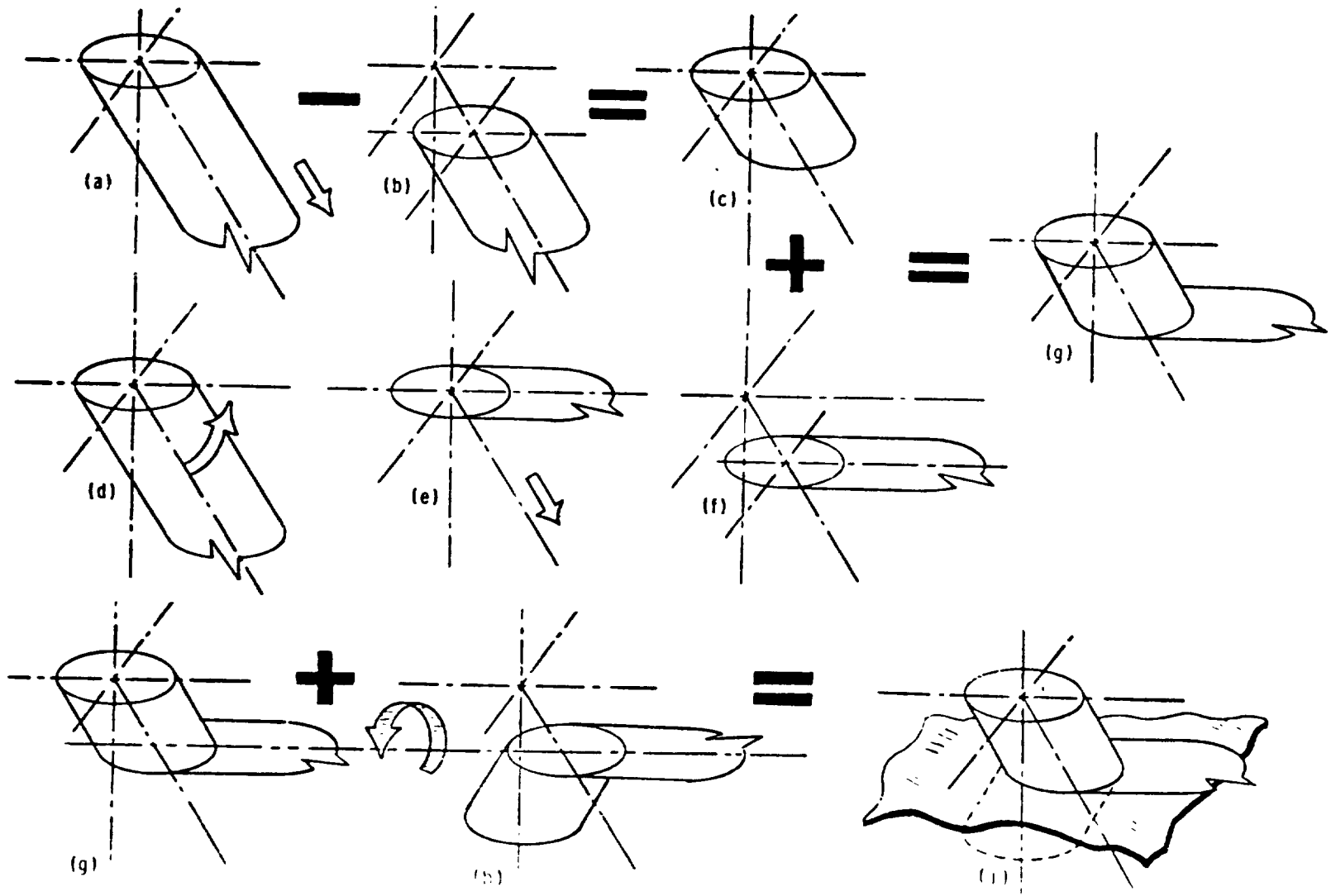

Figure 13. - Superpositions of the wake and its associated flow field used to obtain the wake and flow field in ground effect.

$$\Delta w_L = \delta_{w,L} \frac{A_M}{A_T} w_O \qquad \Delta w_D = \delta_{w,D} \frac{A_M}{A_T} u_O$$

$$\Delta u_L = \delta_{u,L} \frac{A_M}{A_T} w_O \qquad \Delta u_D = \delta_{u,D} \frac{A_M}{A_T} u_O$$

$$\Delta w = \Delta w_L + \Delta w_D$$

$$\Delta u = \Delta u_L + \Delta u_D$$

$$\text{TAN } \Delta\alpha = \frac{\frac{\Delta w}{V}}{1 + \frac{\Delta u}{V}}$$

$$\frac{q_c}{q} = \left(1 + \frac{\Delta u}{V}\right)^2 + \left(\frac{\Delta w}{V}\right)^2$$

Figure 14. - Basic equations for applying corrections to wind-tunnel data.

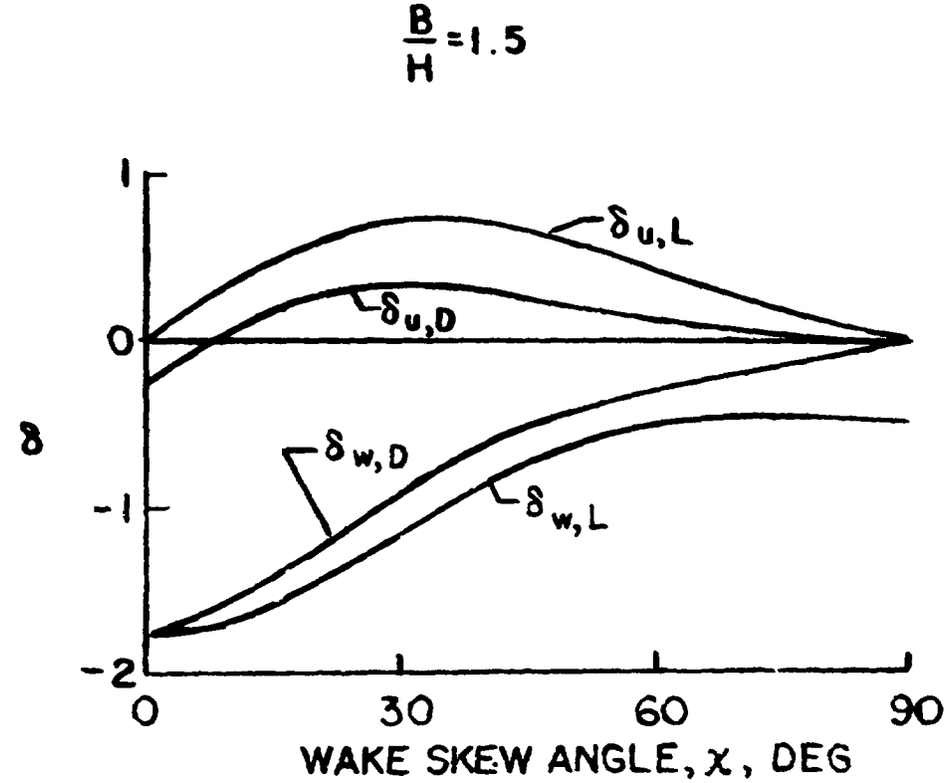

Figure 15. - Interference factors for a vanishingly small model in a closed wind tunnel.

$$\Delta w_L = \delta_{w,L} \frac{A_M}{A_T} w_O \qquad \Delta w_D = \delta_{w,D} \frac{A_M}{A_T} u_O$$

$$\Delta u_L = \delta_{u,L} \frac{A_M}{A_T} w_O \qquad \Delta u_D = \delta_{u,D} \frac{A_M}{A_T} u_O$$

DIVIDE BOTH SIDES BY V, MULTIPLY RIGHT HAND SIDE BY $\frac{\rho}{\rho}$

$$\frac{\Delta w_L}{V} = \delta_{w,L} \frac{\rho A_M w_O}{\rho A_T V} = \delta_{w,L} \frac{M_w}{M_T} \qquad \frac{\Delta w_D}{V} = \delta_{w,D} \frac{\rho A_M u_O}{\rho A_T V} = \delta_{w,D} \frac{M_u}{M_T}$$

$$\frac{\Delta u_L}{V} = \delta_{u,L} \frac{\rho A_M w_O}{\rho A_T V} = \delta_{u,L} \frac{M_w}{M_T} \qquad \frac{\Delta u_D}{V} = \delta_{u,D} \frac{\rho A_M u_O}{\rho A_T V} = \delta_{u,D} \frac{M_u}{M_T}$$

WHERE:

M_w = VERTICAL MASS FLOW PRODUCED BY MODEL

M_u = LONGITUDINAL MASS FLOW PRODUCED BY MODEL

M_T = MASS FLOW THROUGH WIND TUNNEL

Figure 16. - Proof that wall effects depend upon relative mass flow rather than relative momentum flux.

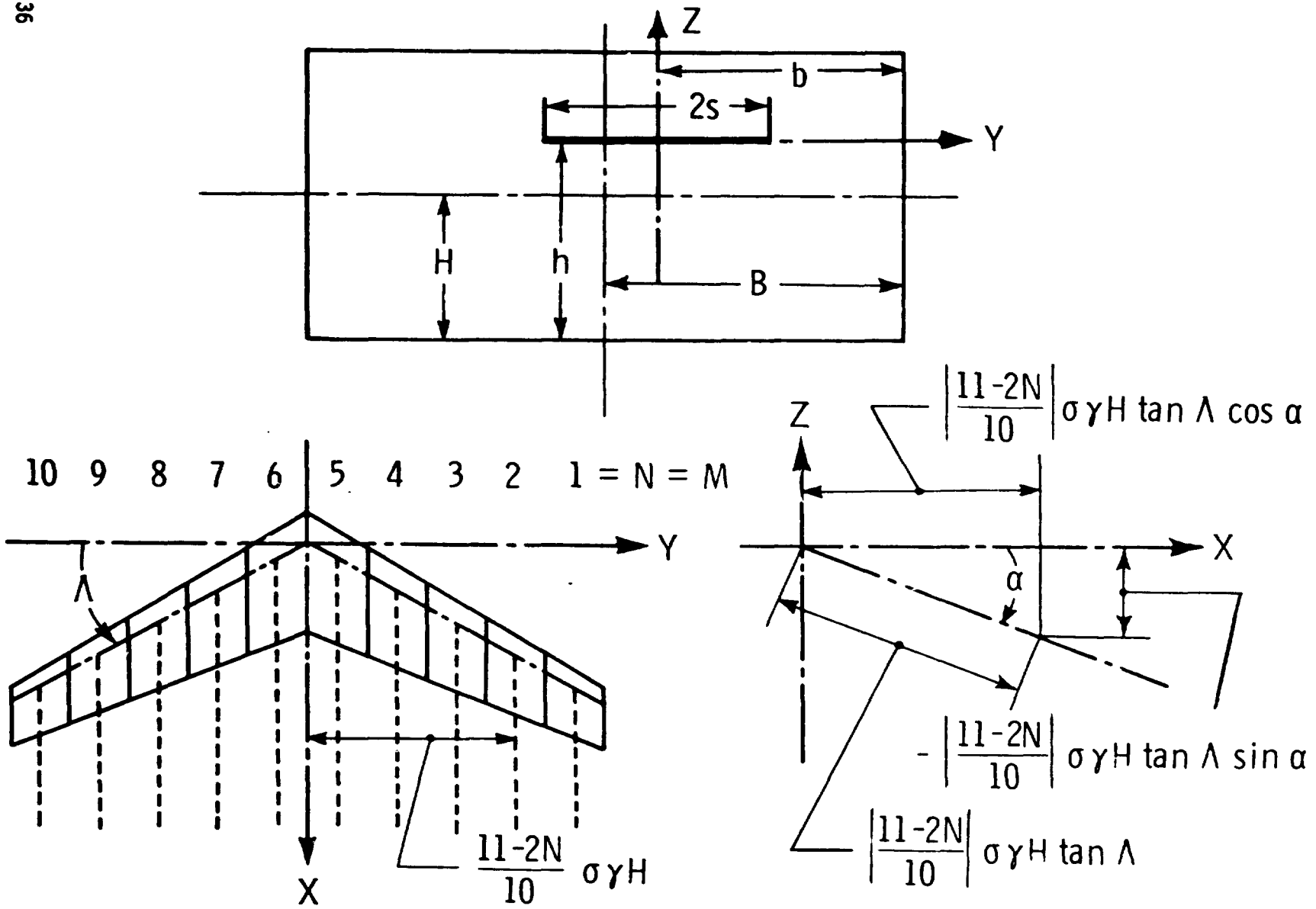

Figure 17. - Superposition scheme to obtain interference factors for a swept wing of finite span

$$\delta = \frac{1}{\sum_{N=1}^{10} L_N} \sum_{M=1}^{10} \sum_{N=1}^{10} L_N \cdot \delta \text{ AT } \left\{ \begin{array}{l} \zeta_N = \dfrac{\zeta}{1 - \left|\dfrac{2N-11}{10}\right| \sigma \gamma \zeta \text{ TAN } \Lambda \text{ SIN } \alpha} \\ \eta_N = \eta + \dfrac{2N-11}{10} \sigma \\ \left(\dfrac{x}{H}\right)_{N,M} = \sigma \gamma \text{TAN } \Lambda \text{ COS } \alpha \left[\left|\dfrac{11-2M}{10}\right| - \left|\dfrac{11-2N}{10}\right|\right] \\ \left(\dfrac{y}{H}\right)_{N,M} = \dfrac{\sigma \gamma (N-M)}{5} \\ \left(\dfrac{z}{H}\right)_{N,M} = \sigma \gamma \text{TAN } \Lambda \text{ SIN } \alpha \left[\left|\dfrac{11-2N}{10}\right| - \left|\dfrac{11-2M}{10}\right|\right] \end{array} \right\}$$

Figure 18. - Summation to obtain interference factors for a swept wing of finite span.

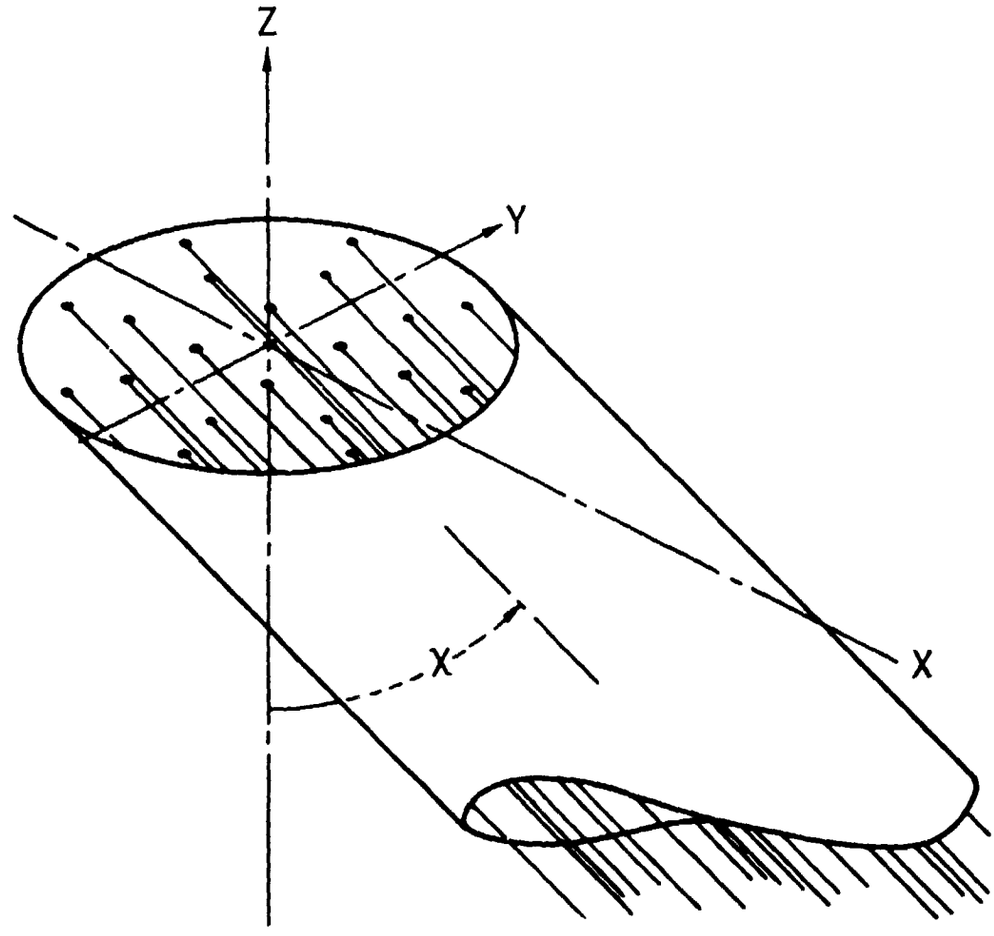

Figure 19. - Superposition of 20 doublet wakes to obtain the wake of a rotor with finite diameter.

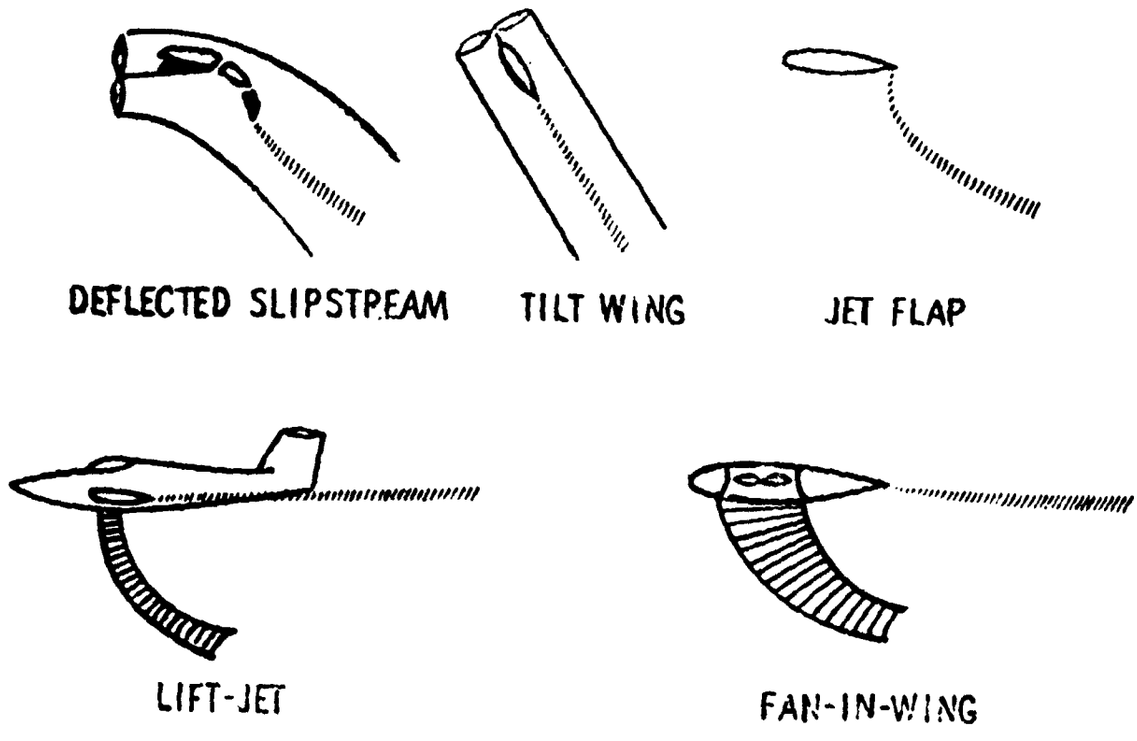

Figure 20. - Sketches illustrating wakes of several V/STOL model types.

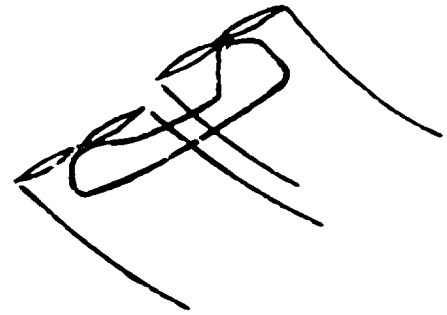

TANDEM ROTOR

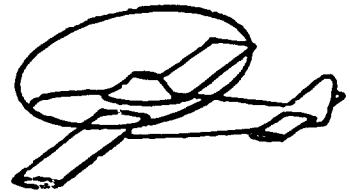

UNLOADED ROTOR

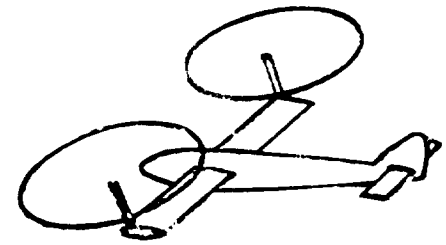

TILT ROTOR

Figure 21. - Several types of multi-element VTOL-STOL aircraft.

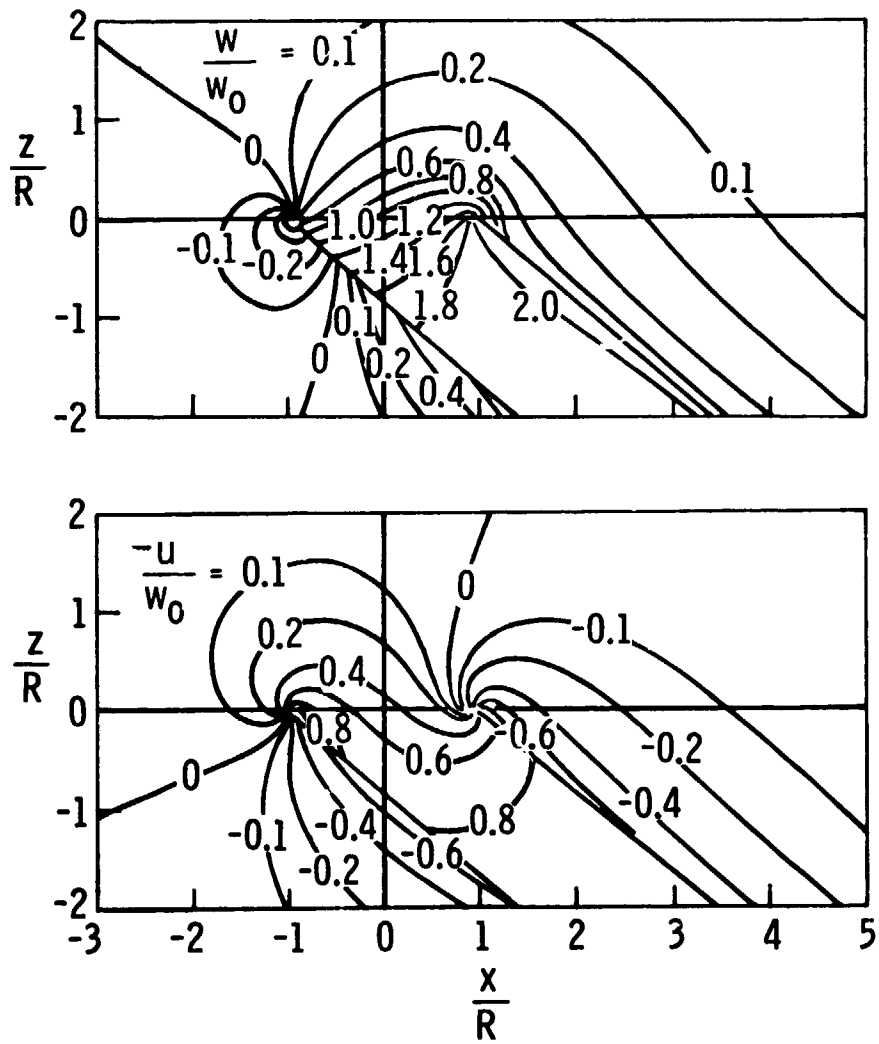

Figure 22. - Induced field of a uniformly loaded rotor. $\chi = 50^{o}$.

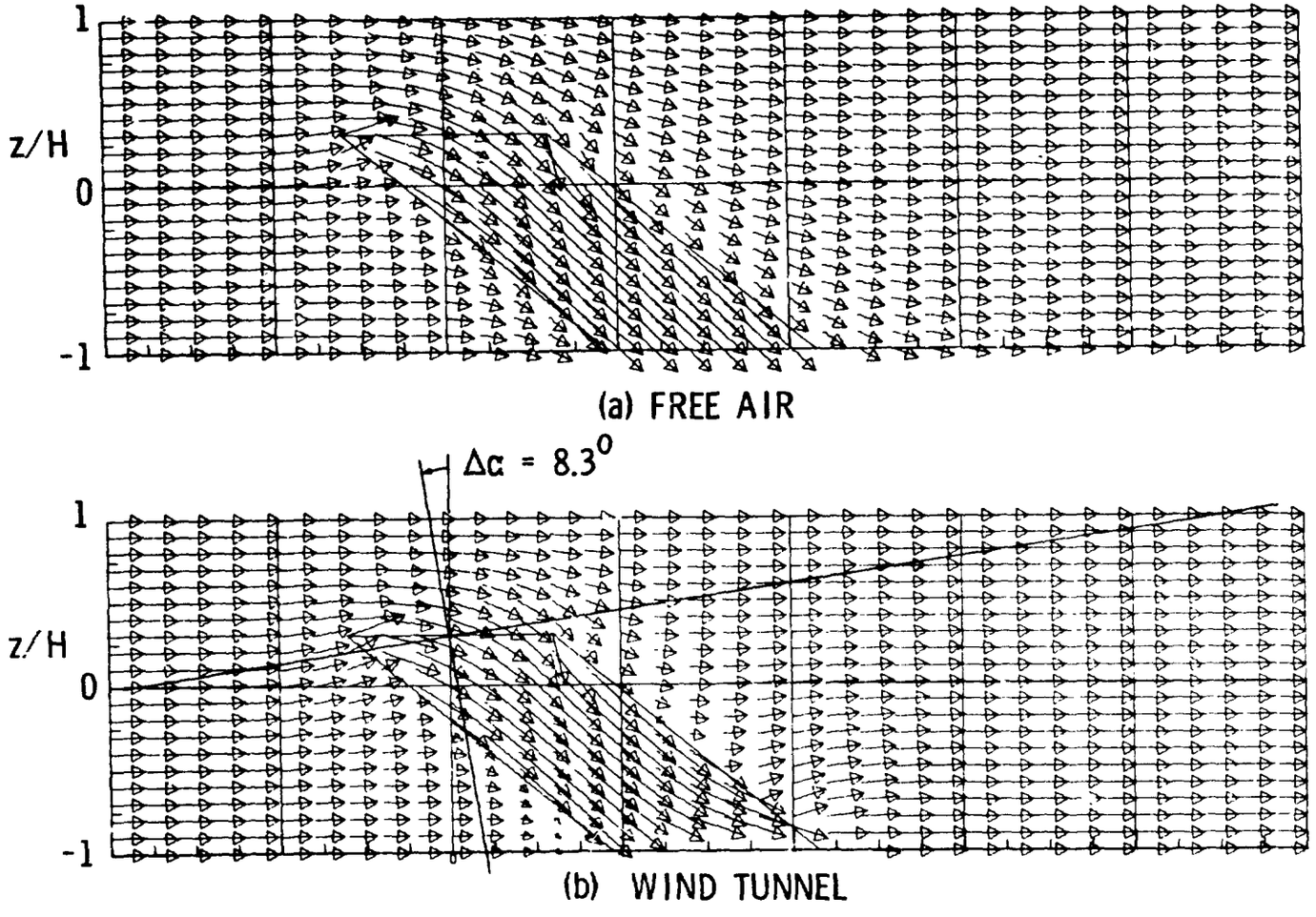

Figure 23. - Application of corrections to a rotor flow field. $\chi = 50^{o}$.

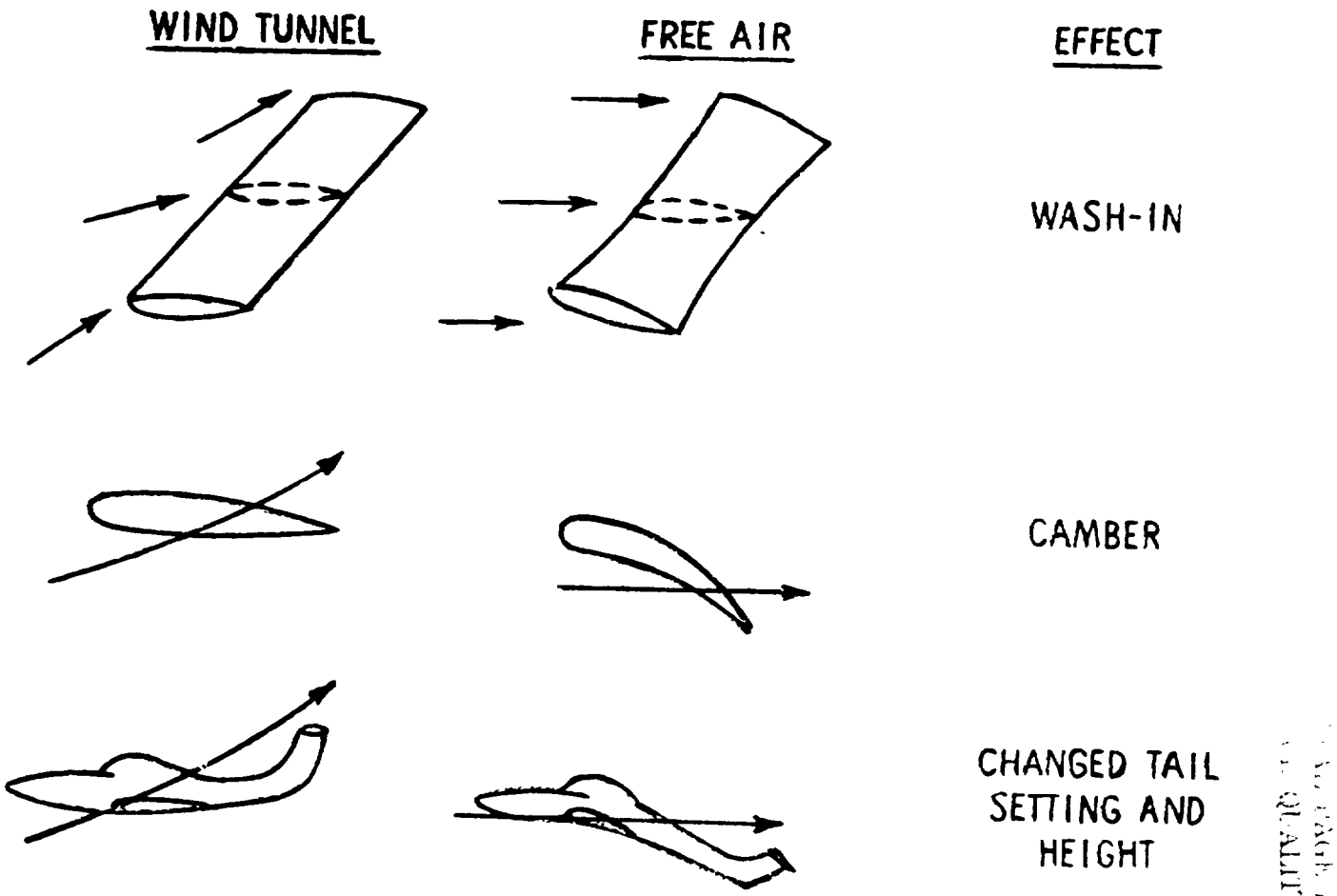

Figure 24. - Nonuniform interference as an effective distortion of the model.

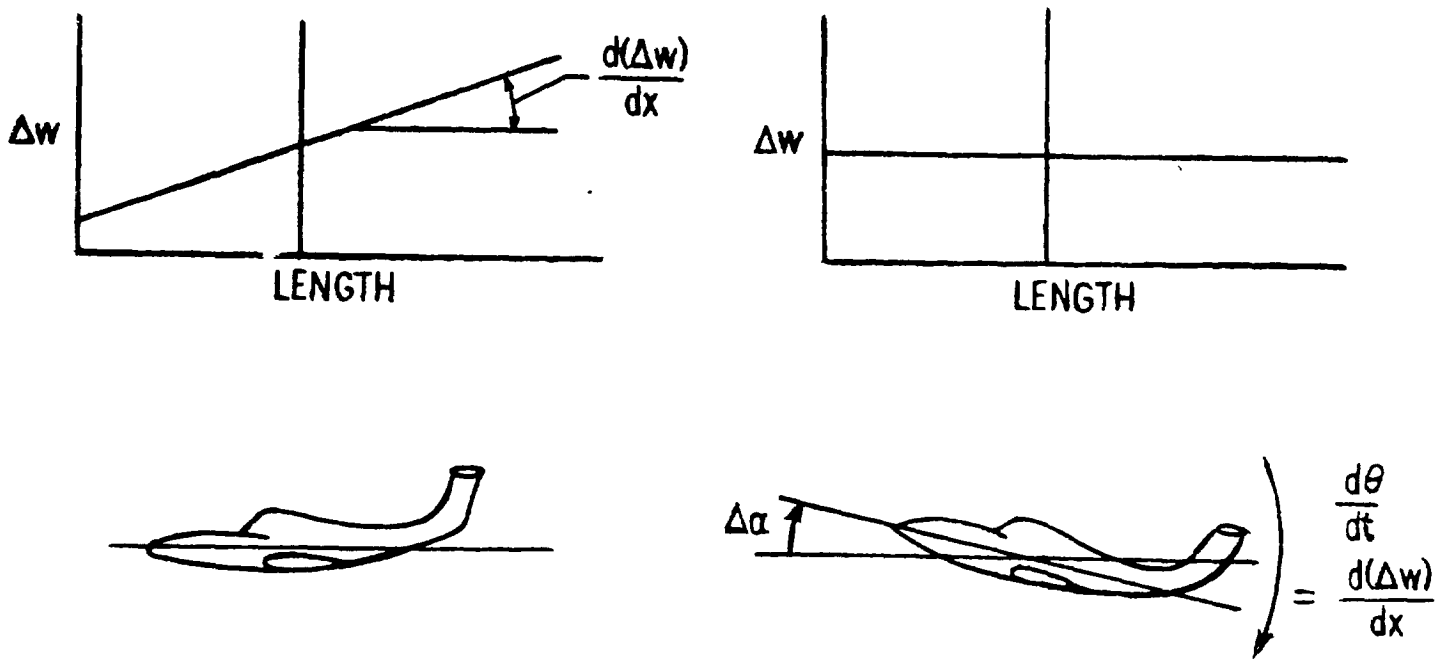

Figure 25. - Nonuniform interference as an effective rate of pitch.

Figure 26. - Flow in a tunnel with a rotor. $\gamma = 70^{\circ}$.

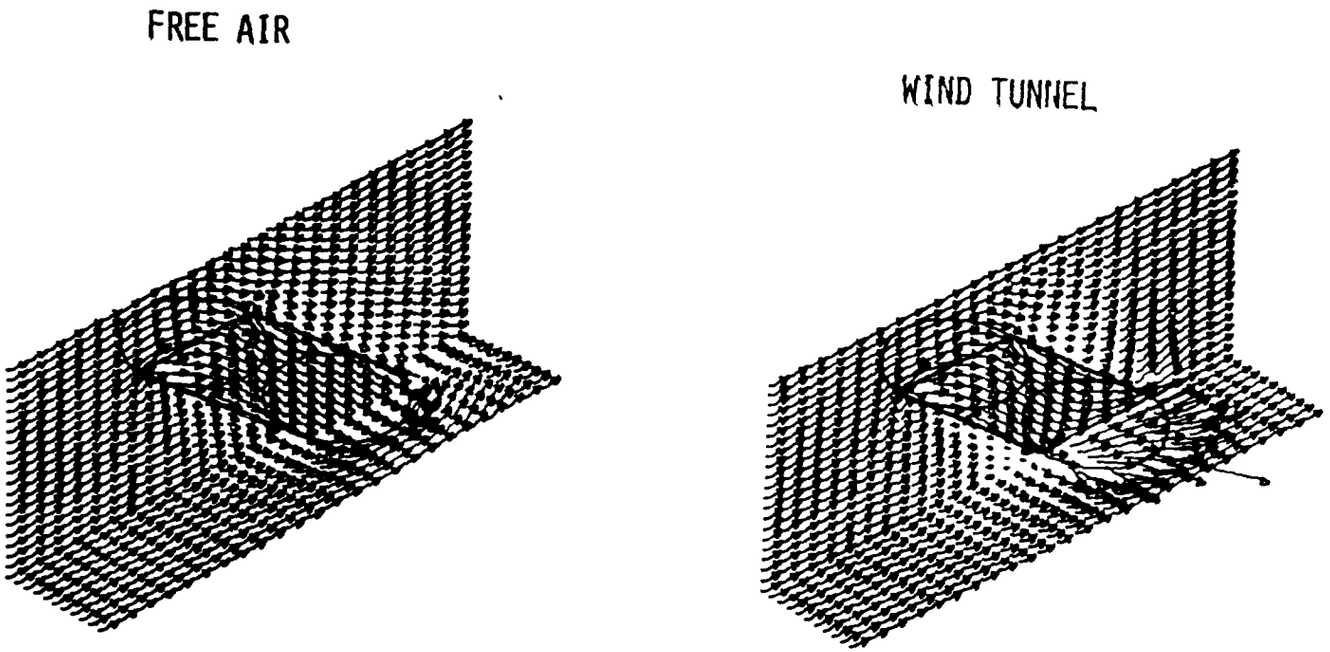

Figure 27. - Flow in a tunnel with a rotor. $\chi = 50^{o}$.

Figure 28. - Flow in a tunnel with a rotor. $\chi = 30^{o}$.

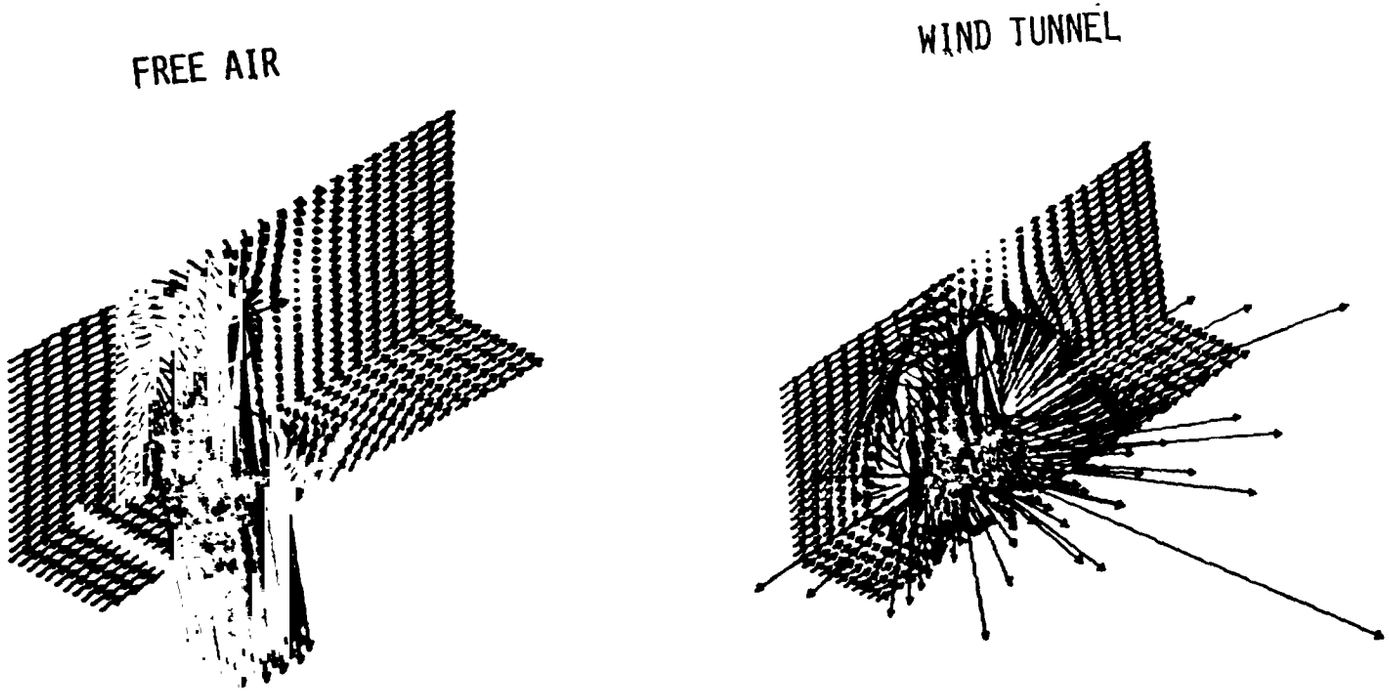

Figure 29. - Flow in a tunnel with a rotor. $\chi = 10^{o}$.

Figure 30. - The rotor wake near the floor with and without wake deformation.

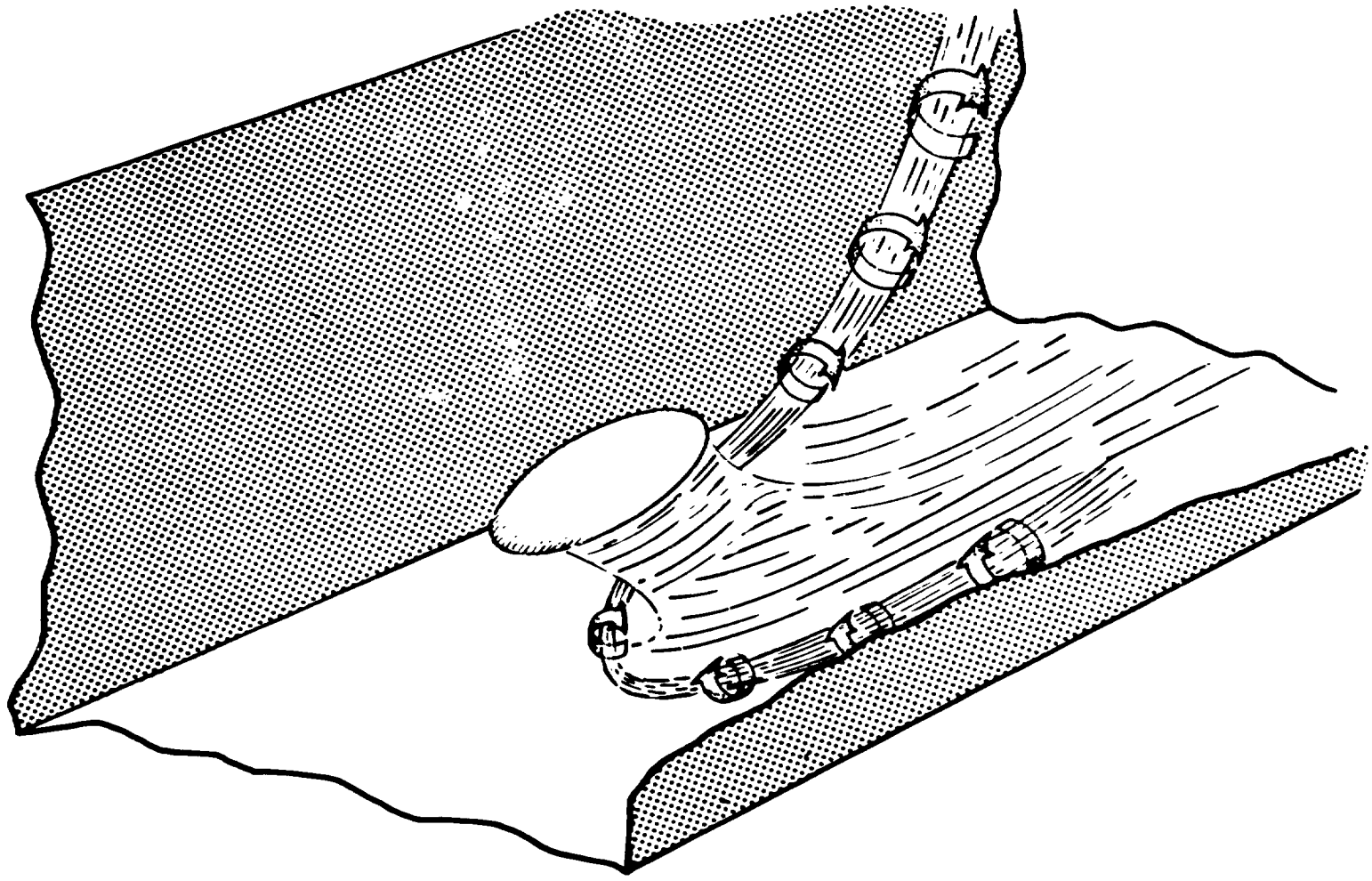

Figure 31. - Sketch of the flow generated by a severely deflected wake in a closed wind tunnel.

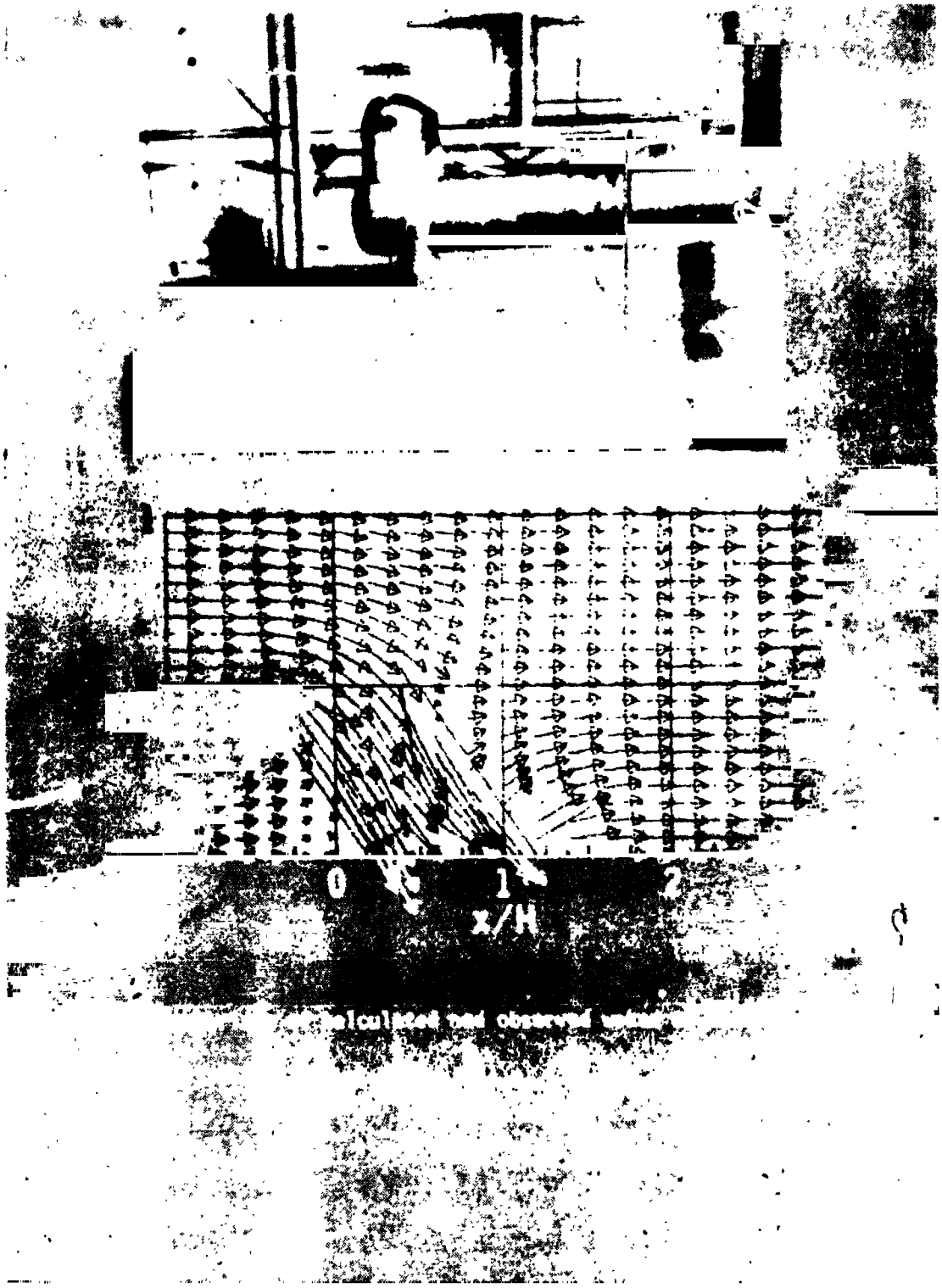

Calculated and Observed

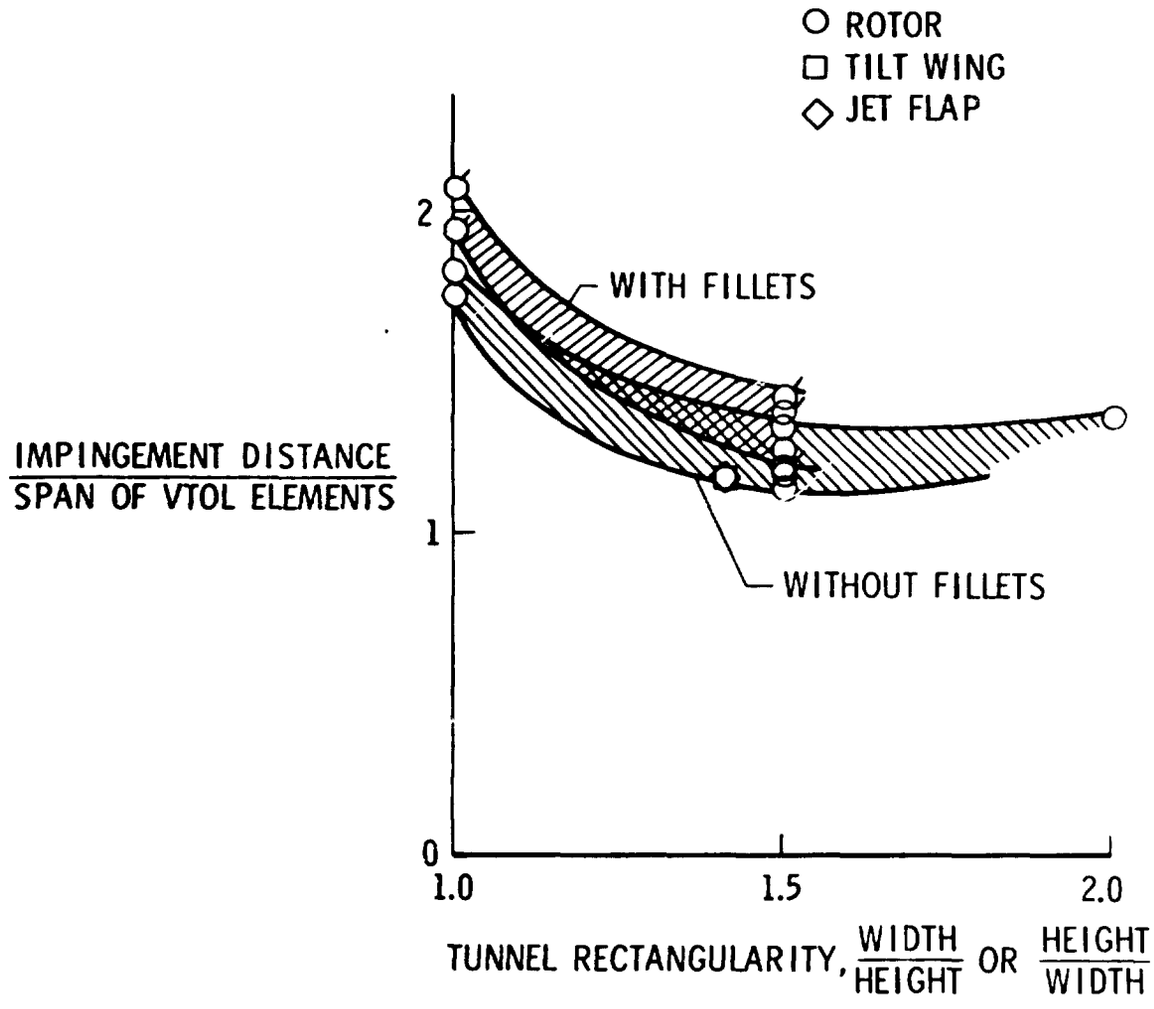

Figure 33. - Correlation of recirculation limits.

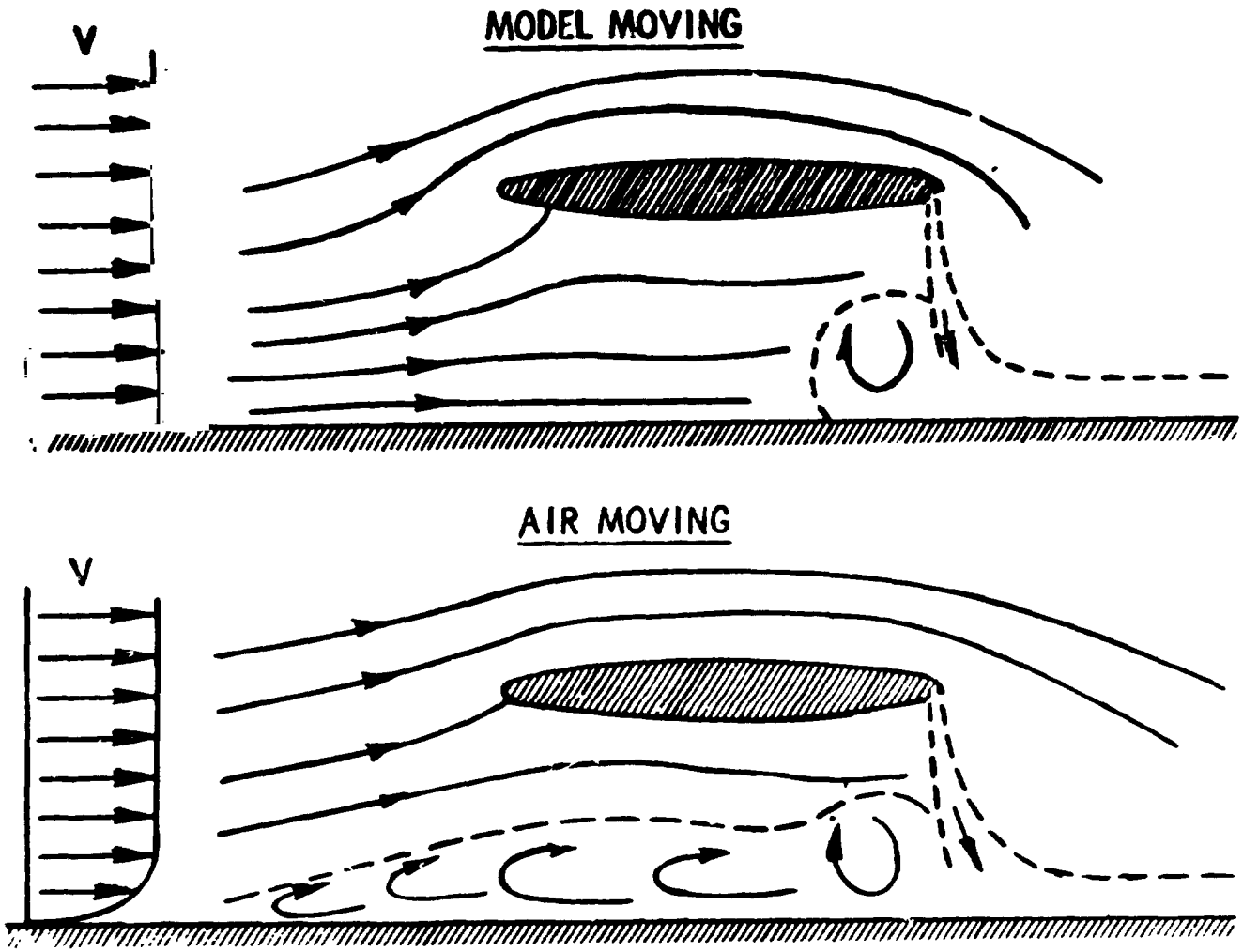

Figure 34. - Sketches of flow over a ground plane.

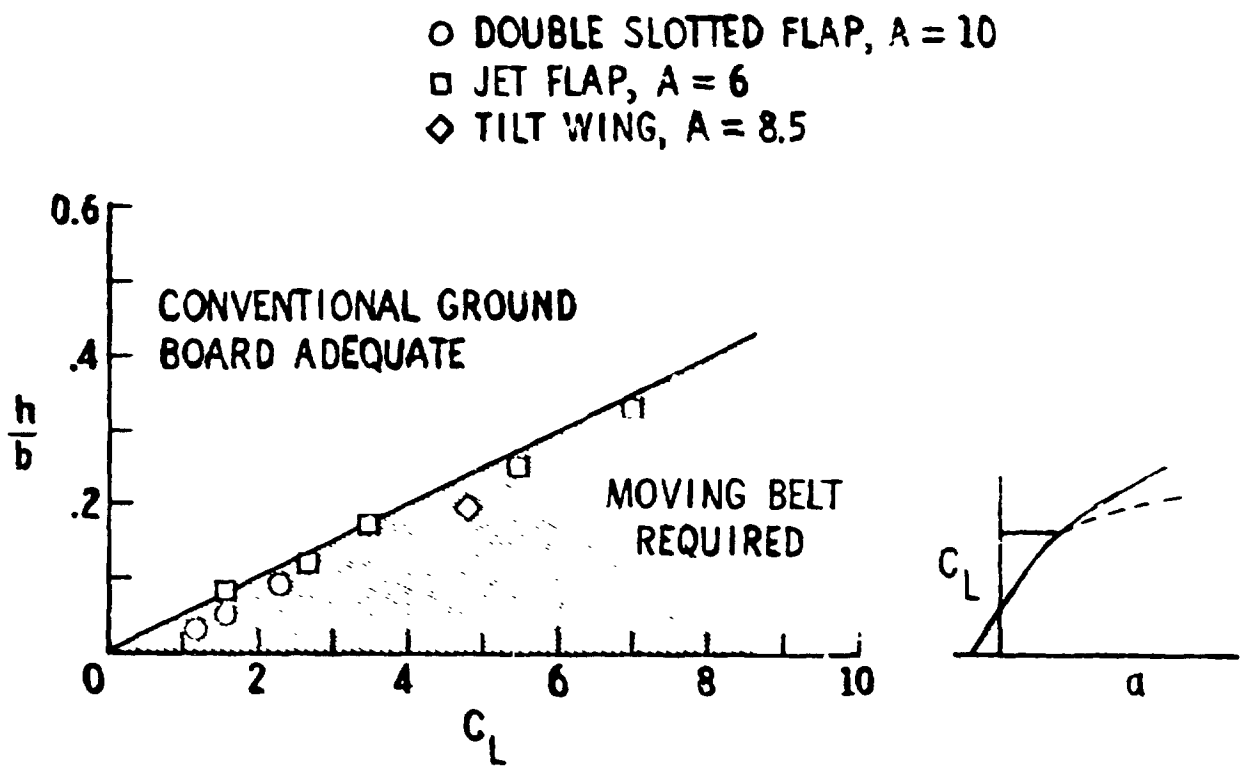

Figure 35. - Conditions requiring treatment of the boundary layer on a ground plane.

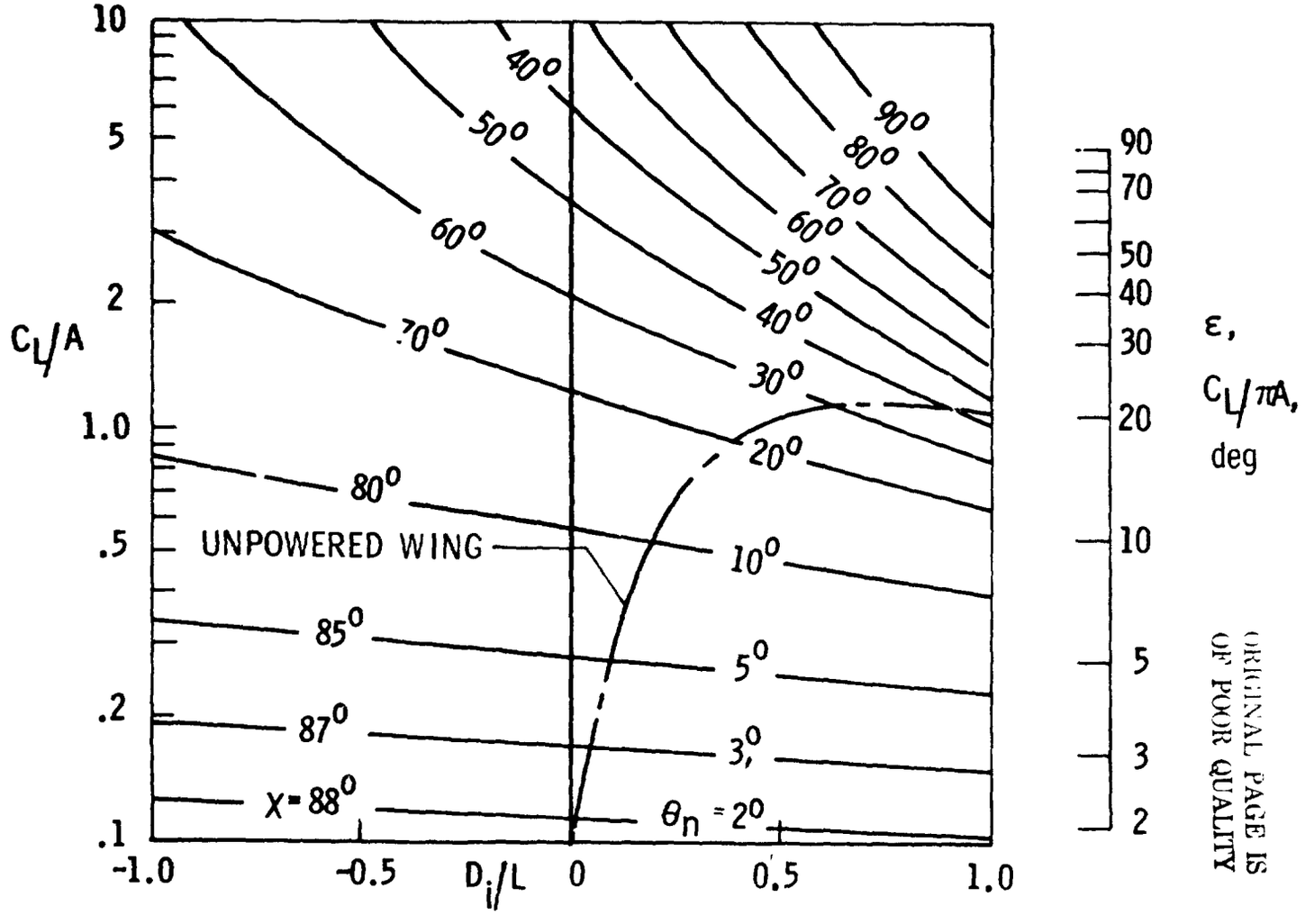

Figure 36. - Idealized performance of VTOL-STOL aircraft.

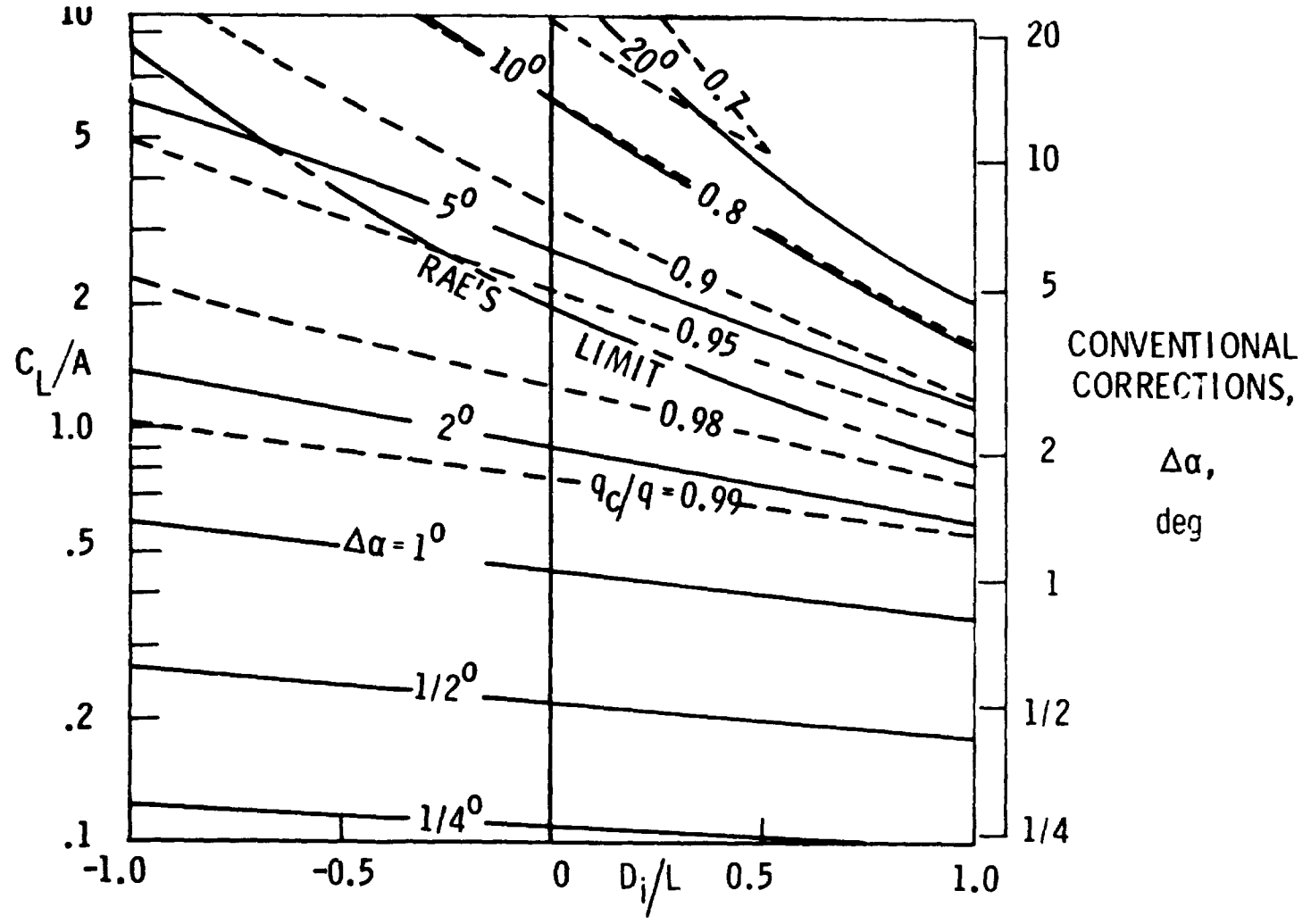

Figure 37. - Average corrections over a wing in a closed wind tunnel. B/H = 1.5, σ = 0.5.

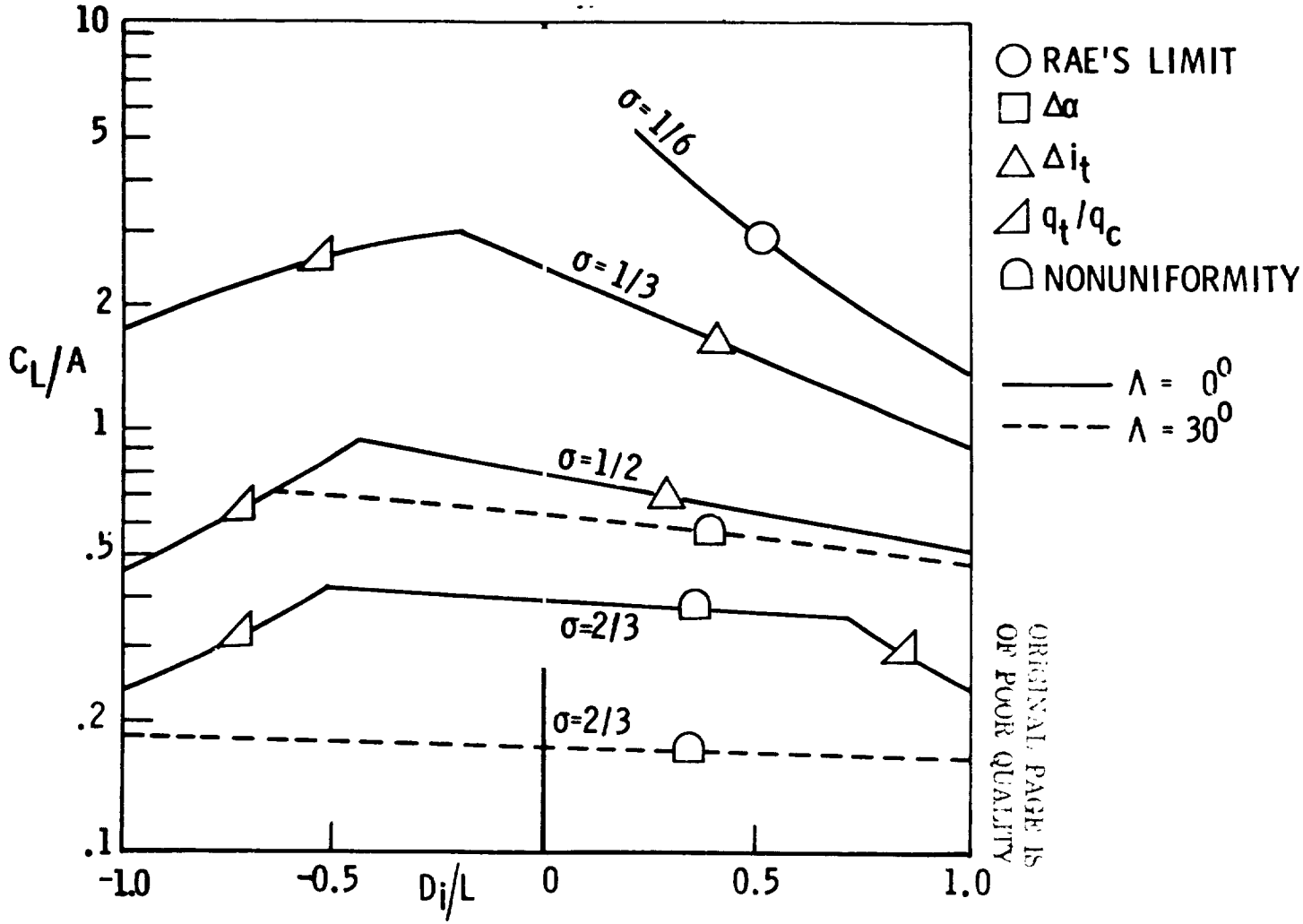

Figure 38. - Testing limits when applying a moderate level of correction to a wing in a closed wind tunnel. B/H = 1.5.

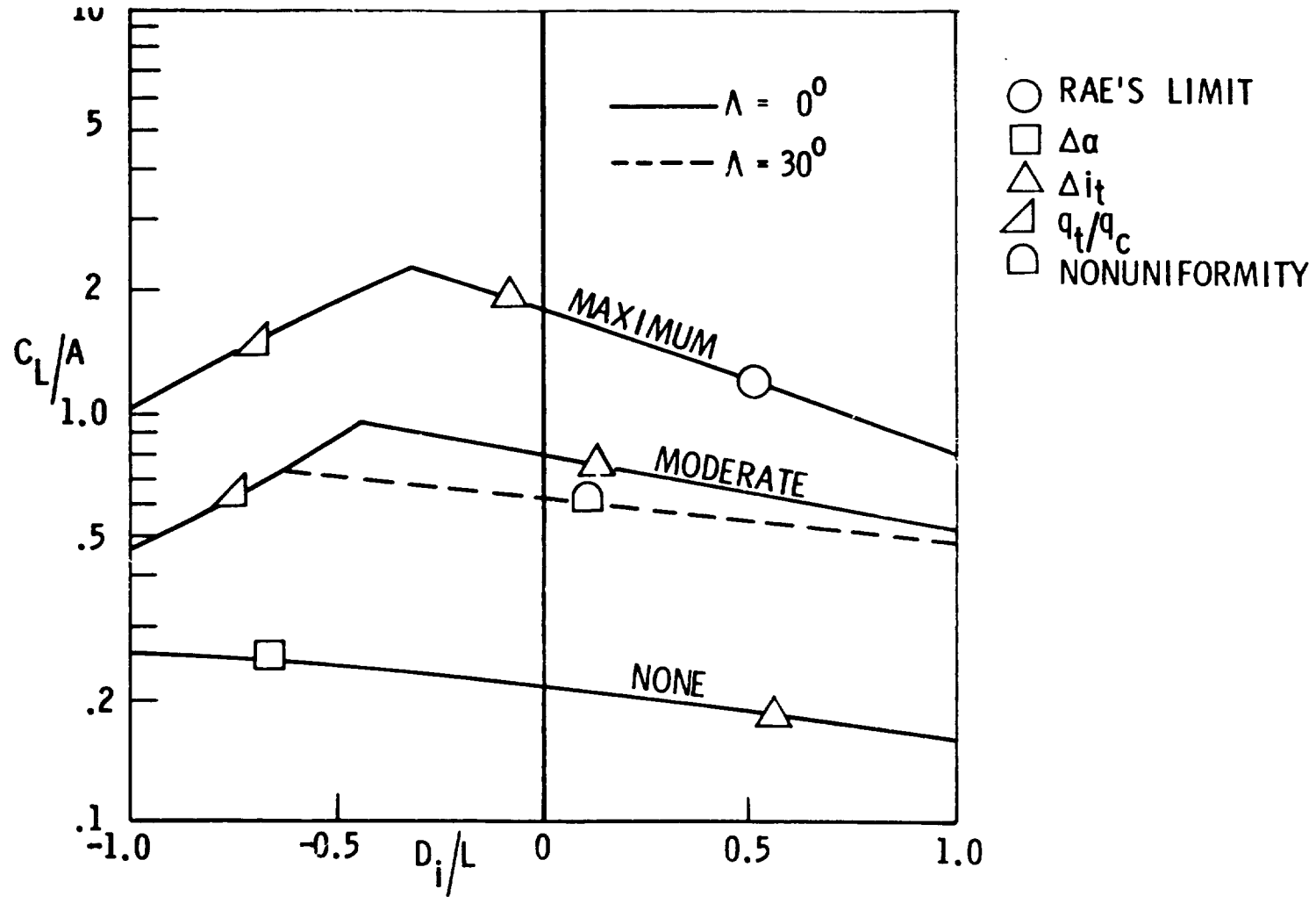

Figure 39. - Effect of the level of corrections on testing limits for a wing in a closed wind tunnel. B/H = 1.5, σ = 0.5.

UNIVERSITY OF WASHINGTON	ROTORS LIFTING PROPELLERS
BOEING COMPANY	JET FLAP JET LIFT
N.R.C. (CANADA)	TILT WING
LANGLEY RESEARCH CENTER	TILT WING FAN-IN-FUSELAGE FAN-IN-WING JET FLAP JET LIFT

Figure 40. - Table of some model tests conducted to verify VTOL-STOL corrections.

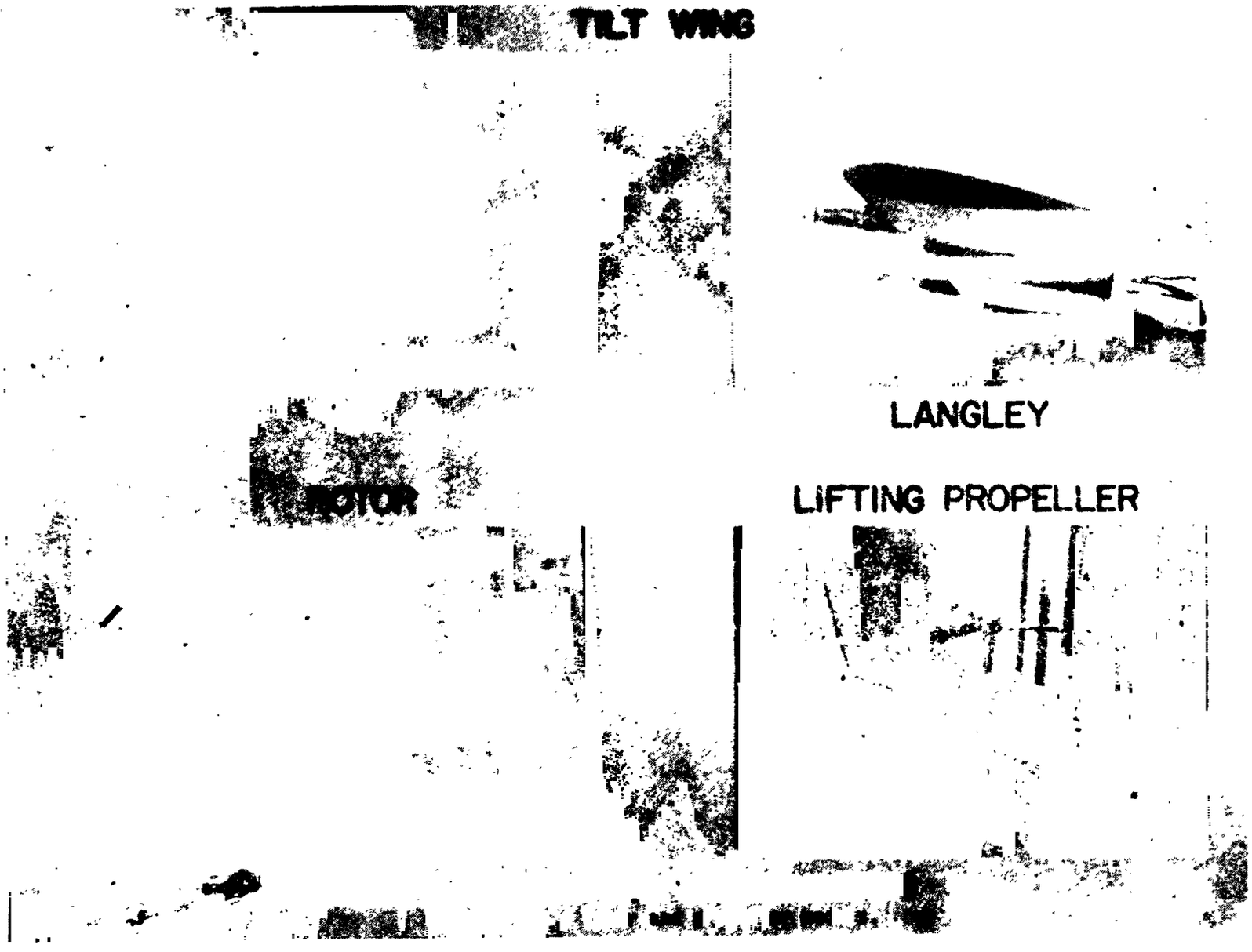
TILT WING
LANGLEY
ROTOR
LIFTING PROPELLER

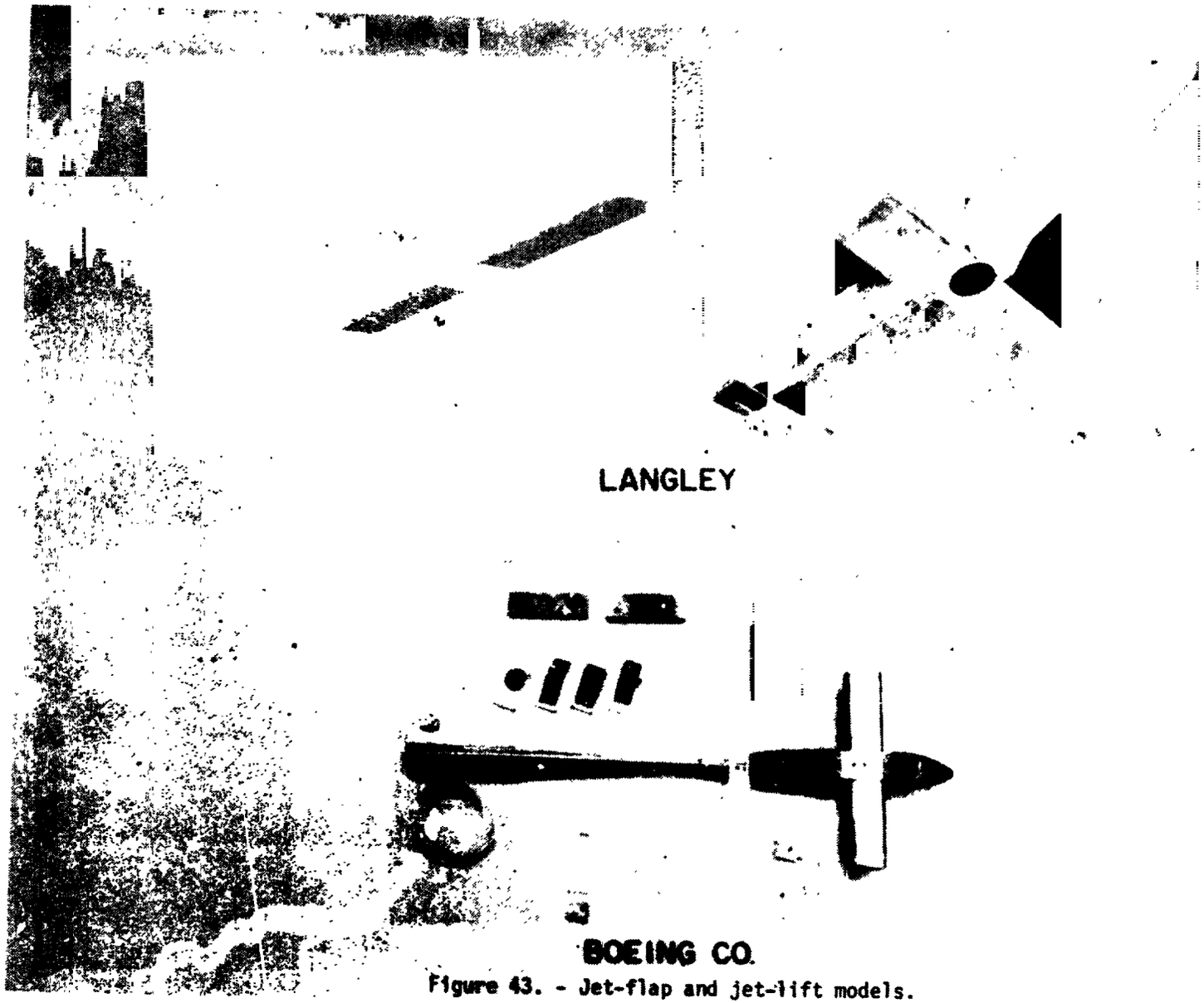

Figure 43. - Jet-flap and jet-lift models.

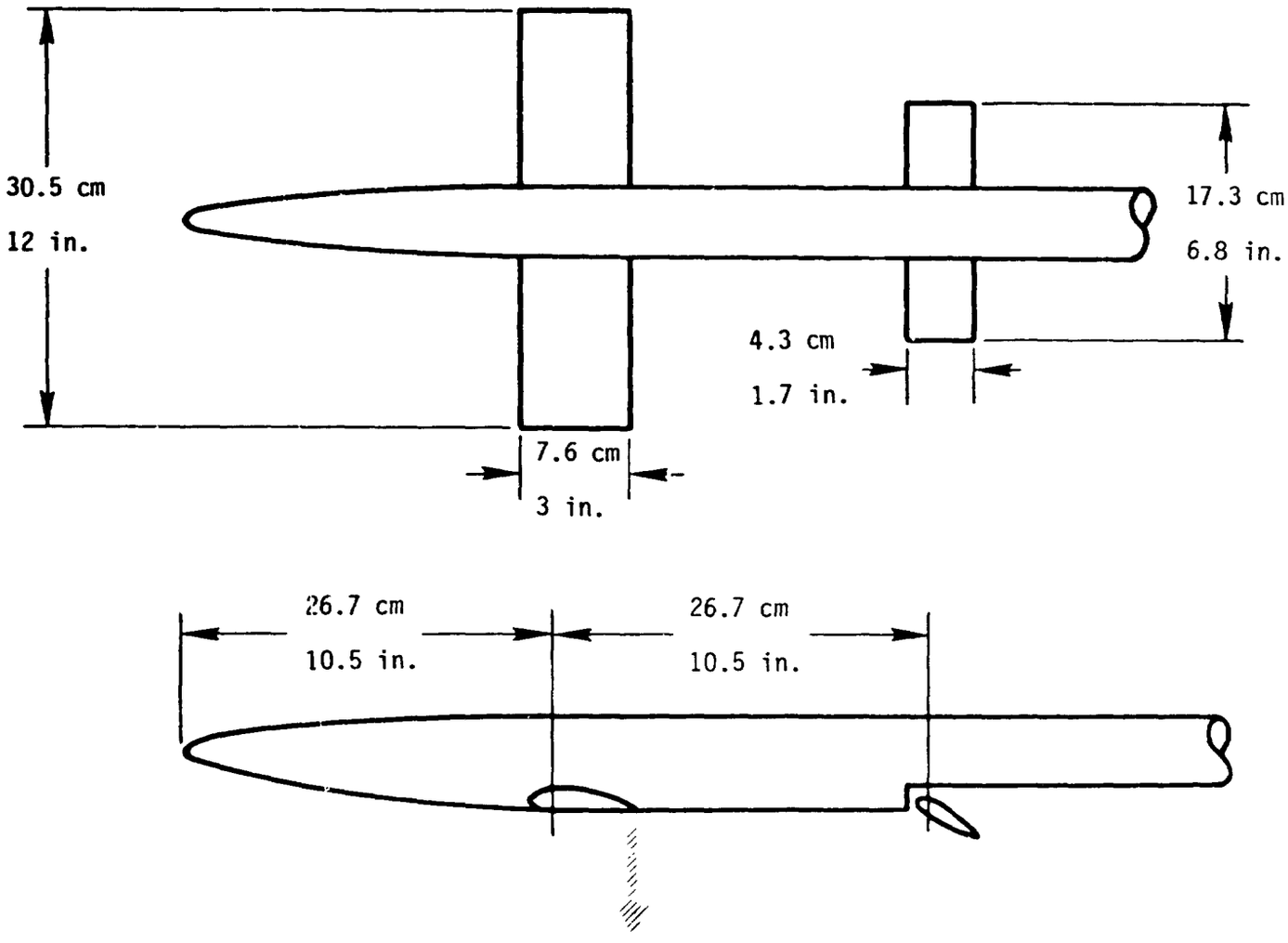

Figure 44. - Jet-flap model tested at Langley Research Center.

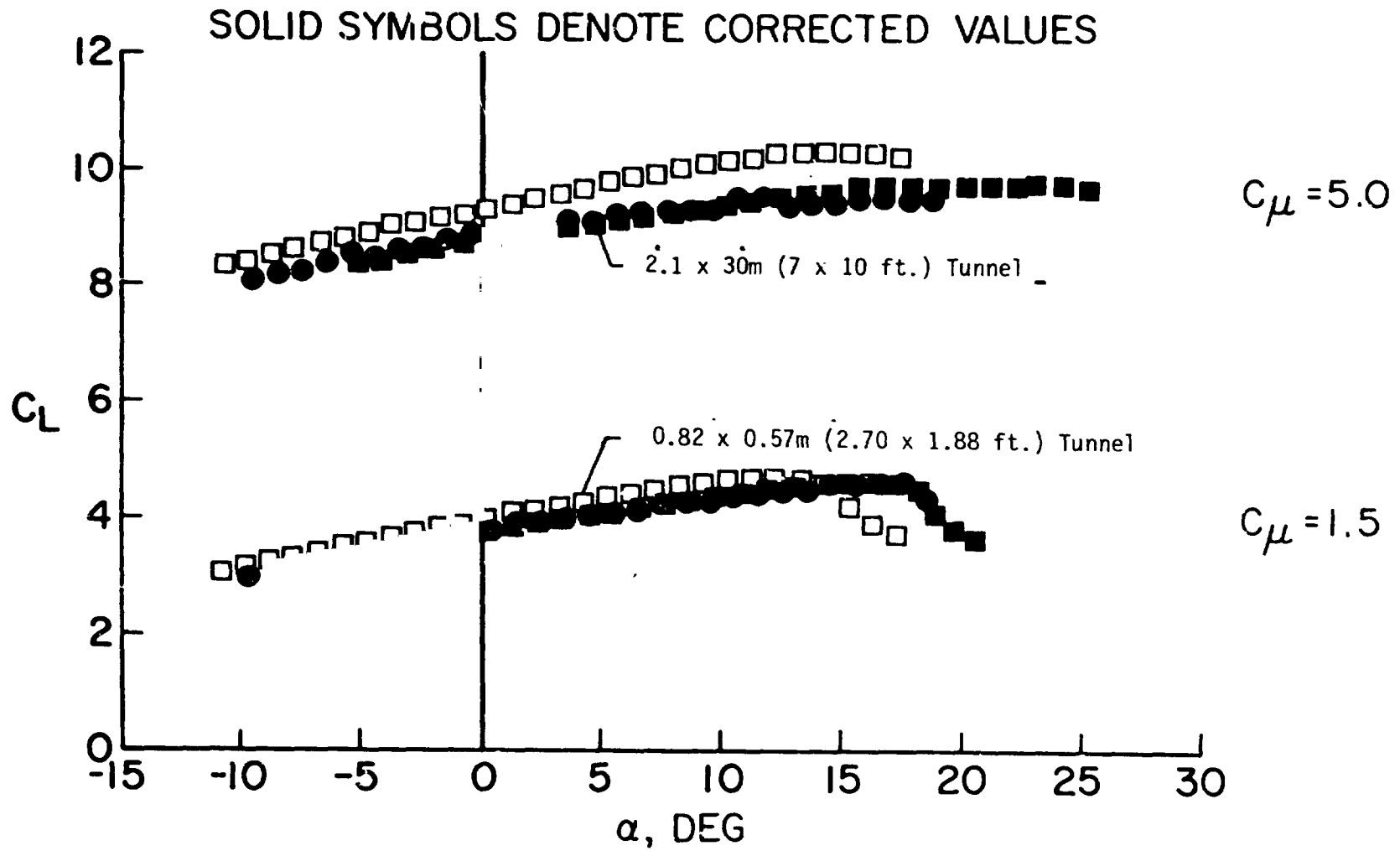

Figure 45. - Measured wall effects on the jet-flap model at modest values of C_μ.

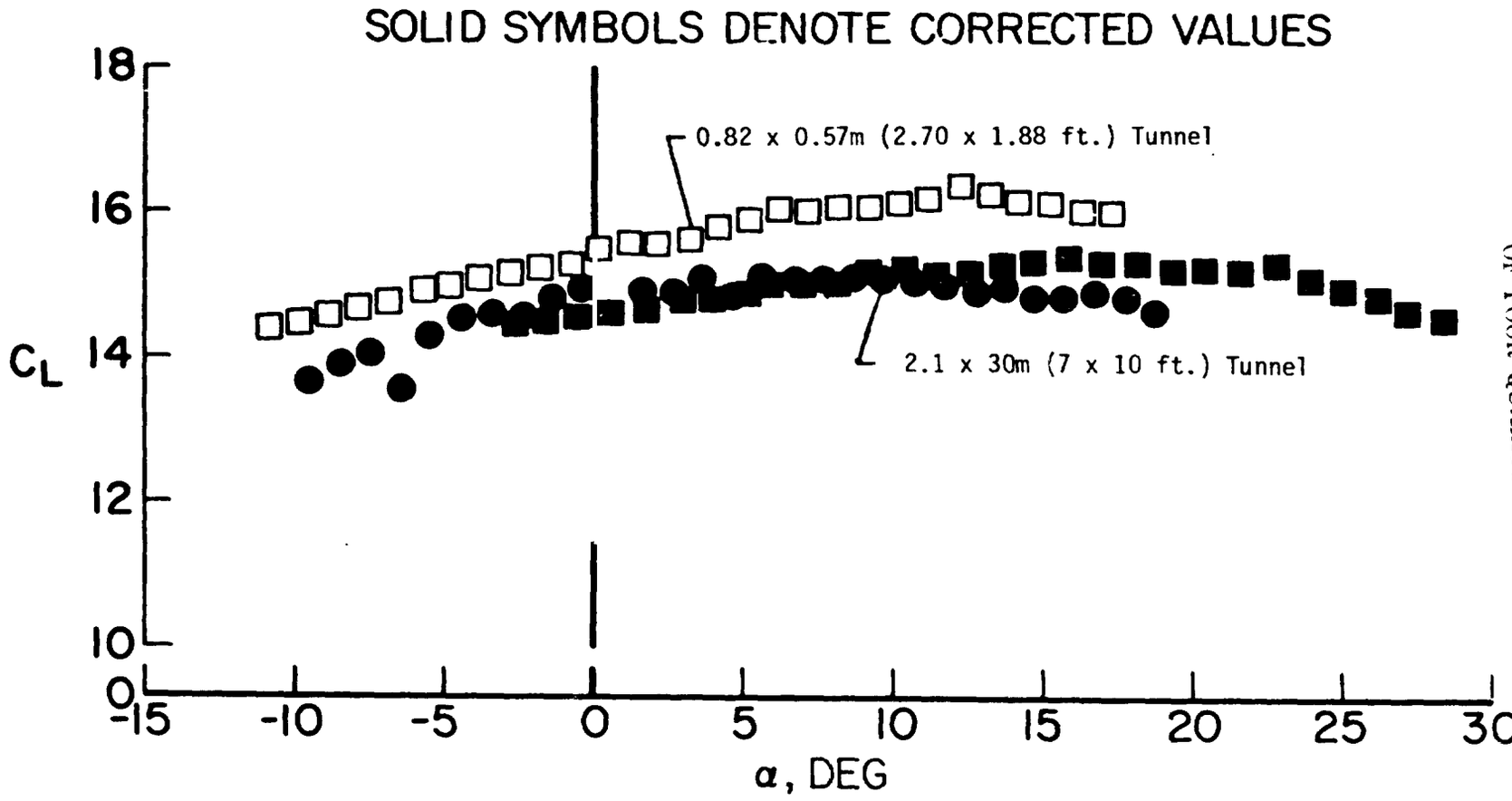

Figure 4c. - Measured wall effects on the jet-flap model at C_μ = 10.

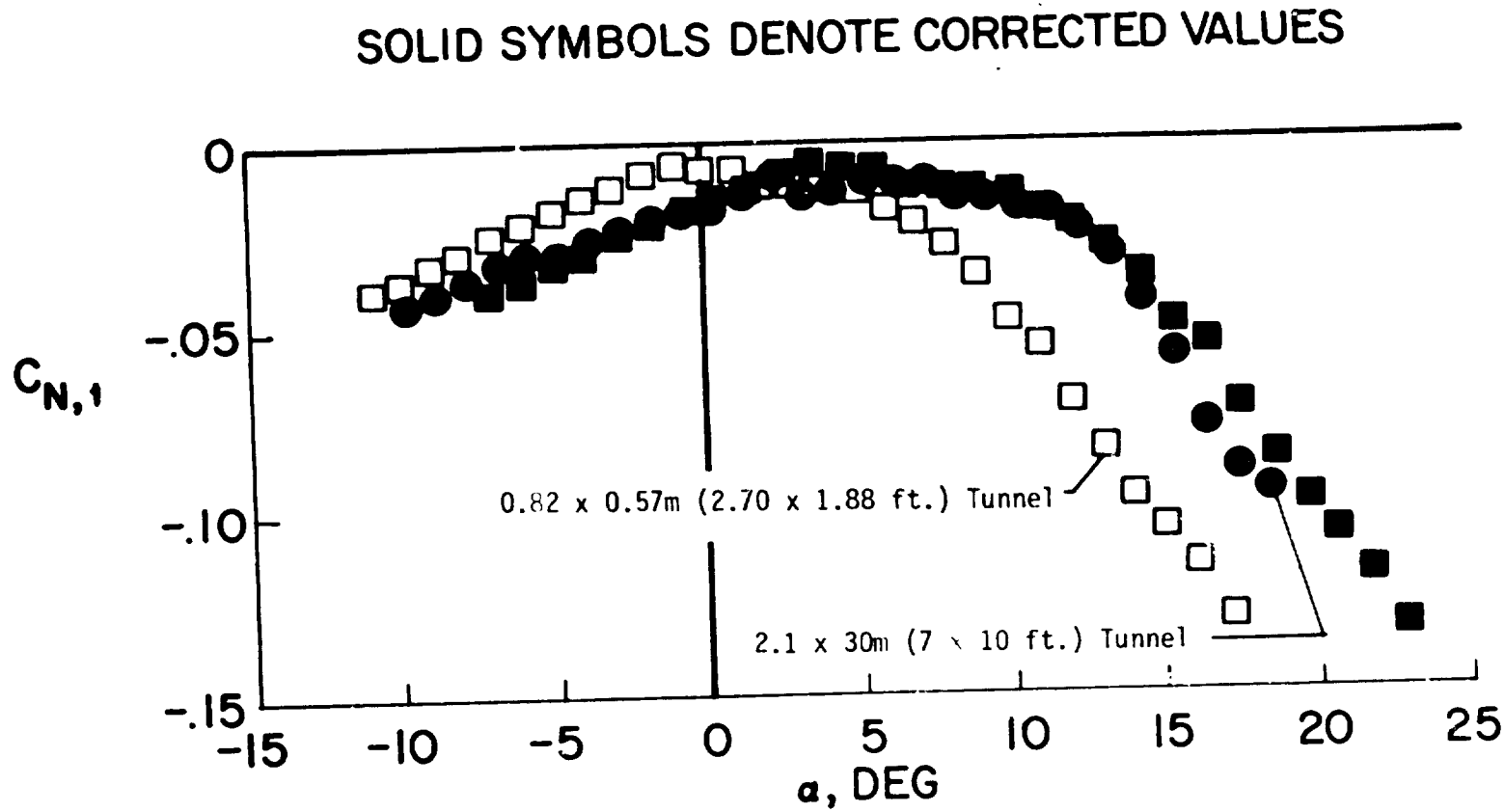

Figure 47. - Measured wall effects at the tail of the jet-flap model $C_\mu = 5$.

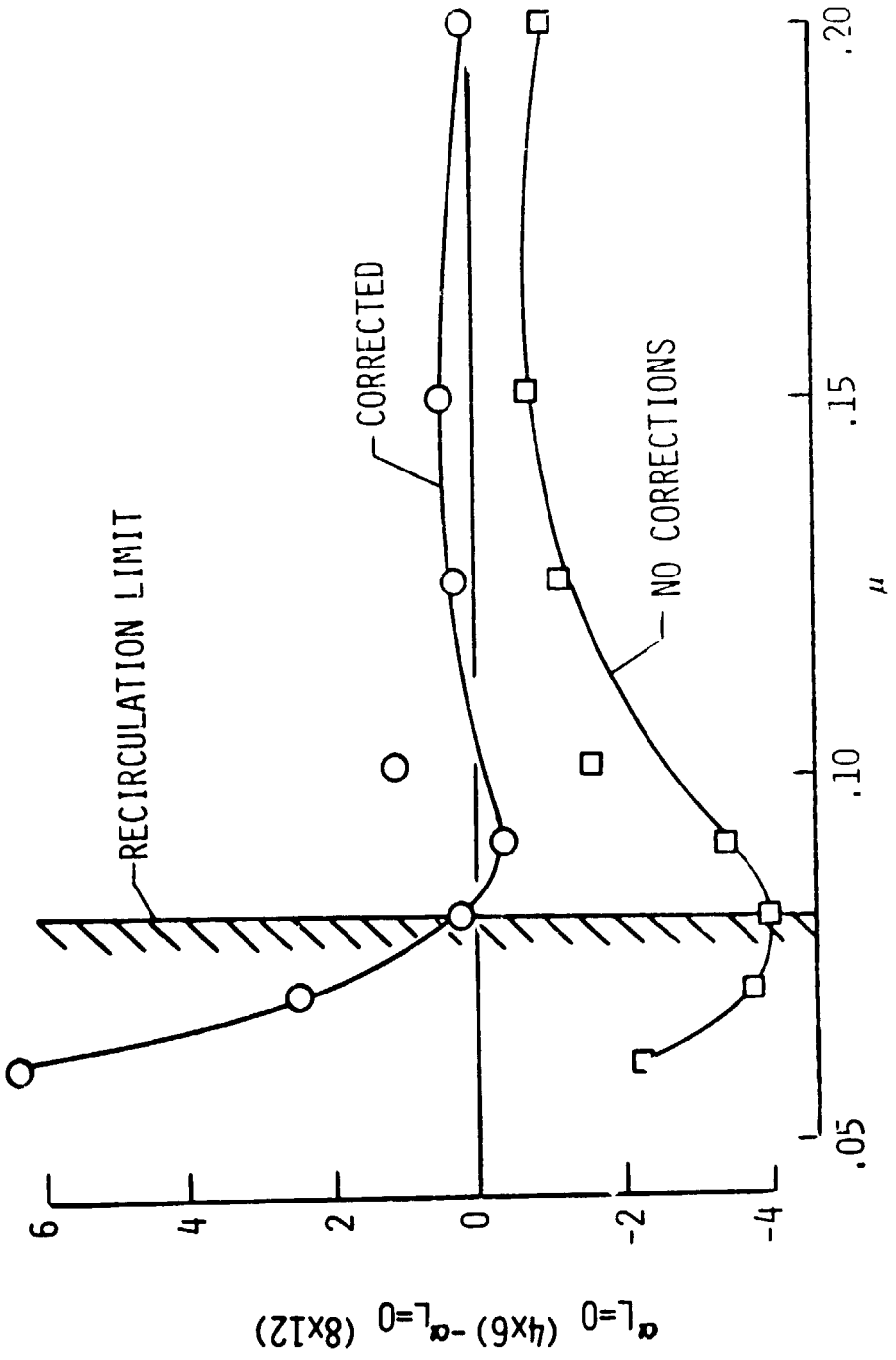

Figure 48.- Measured wall effects at a tail behind a rotor in the University of Washington wind tunnel.

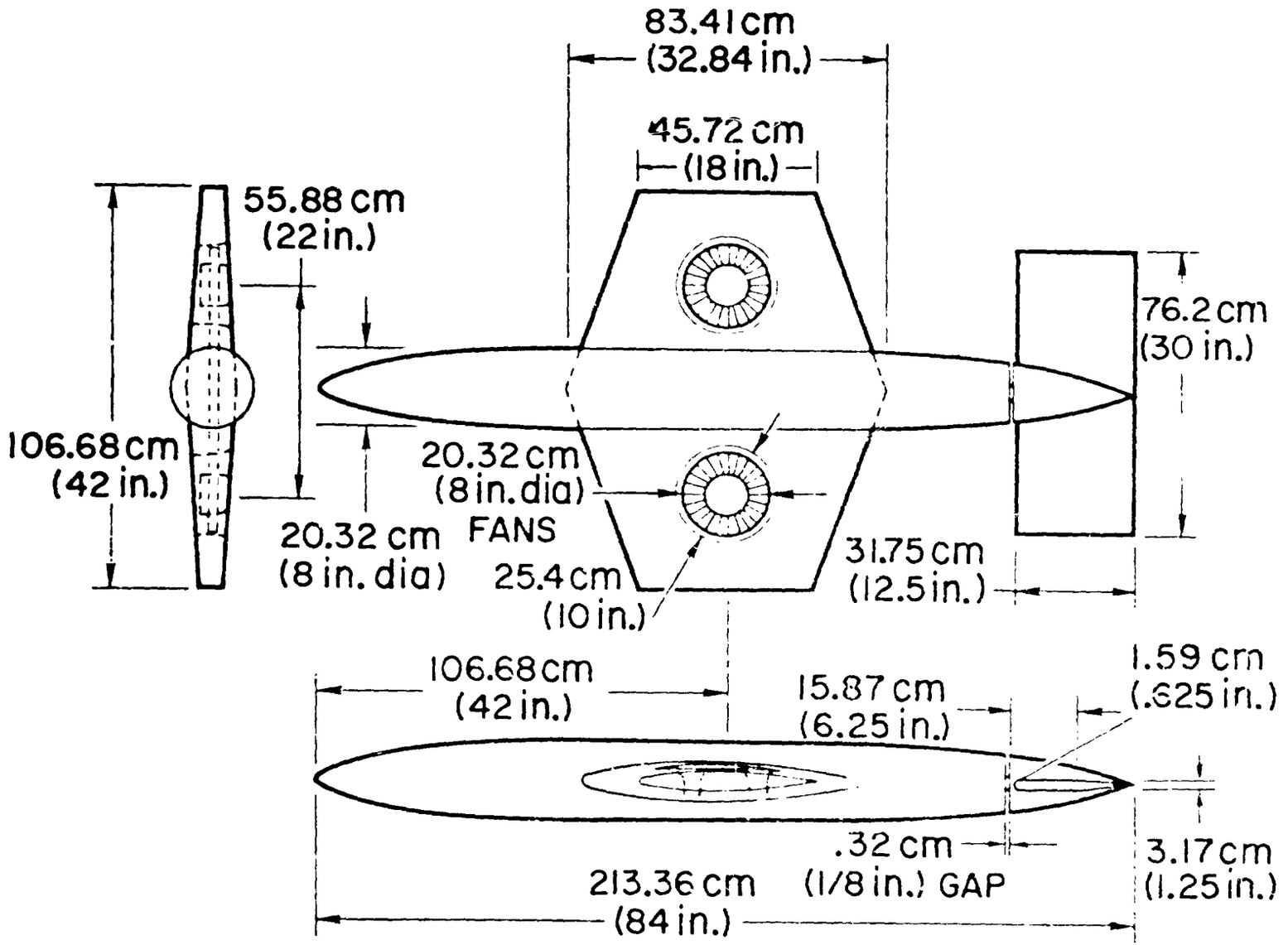

Figure 49. - Fan-in-wing model tested at Ames and Langley Research Center.

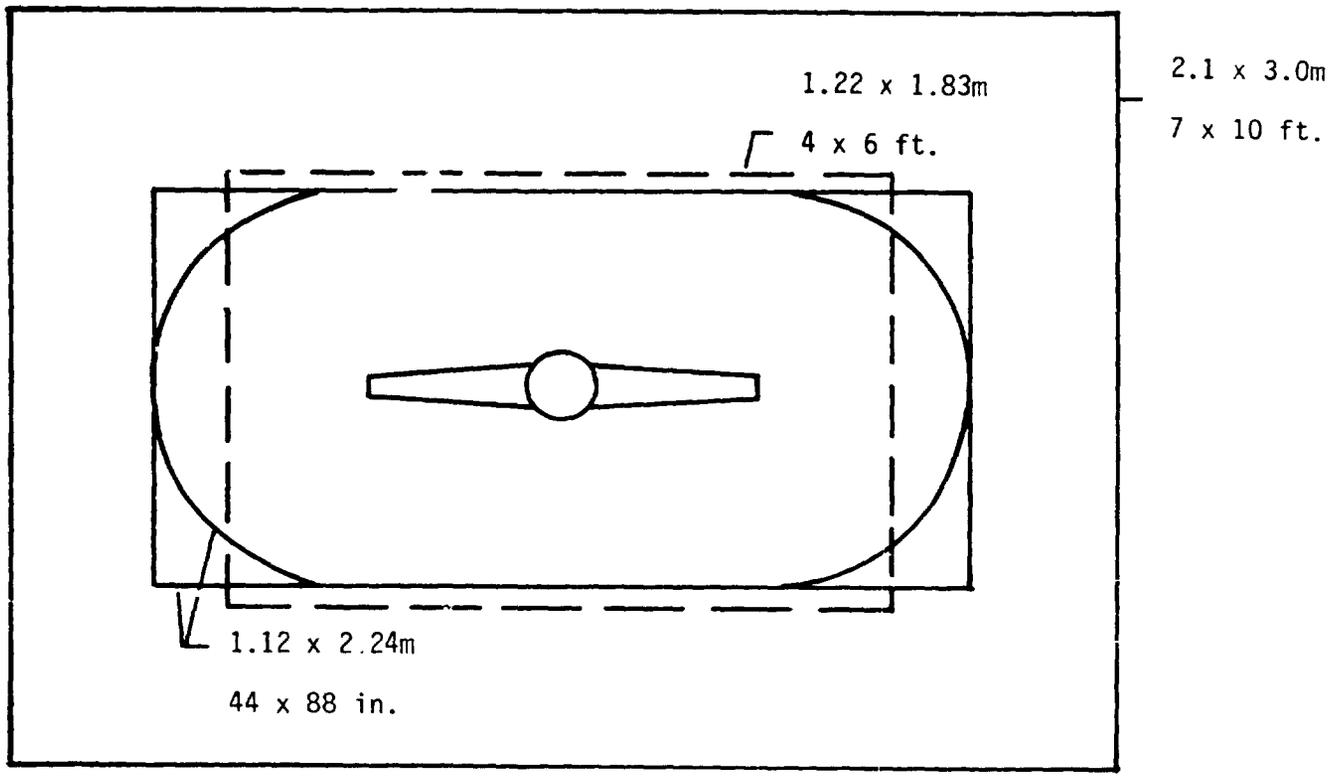

Figure 50. - Relative size of fan-in-wing model in the smaller test sections.

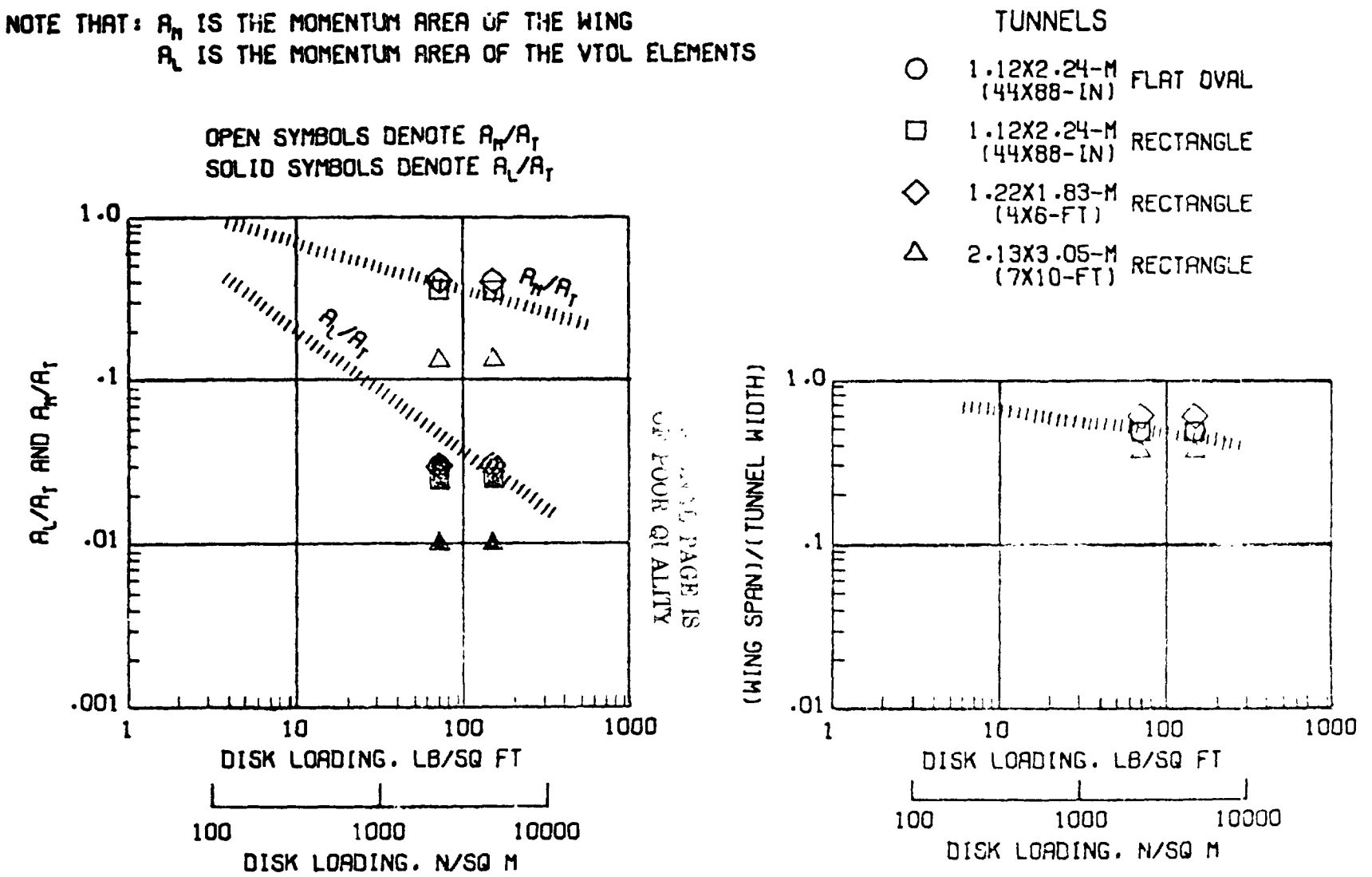

Figure 51. - An early criteria for testing VTOL-STOL models without corrections.

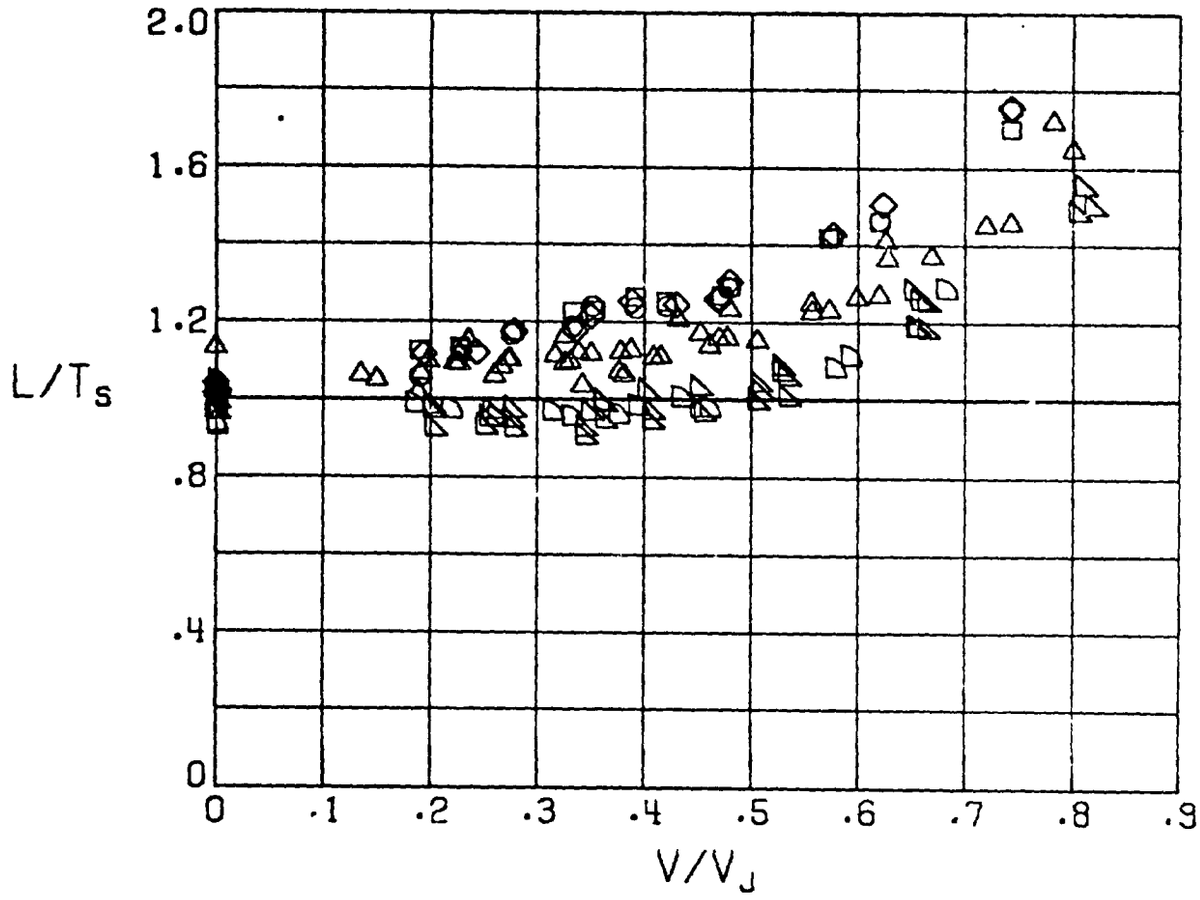

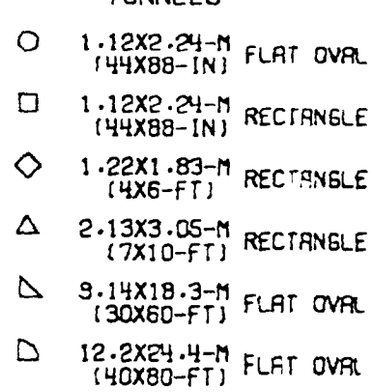

(a) Uncorrected data.

Figure 52. - Lift data from the fan-in-wing model. α = 00.

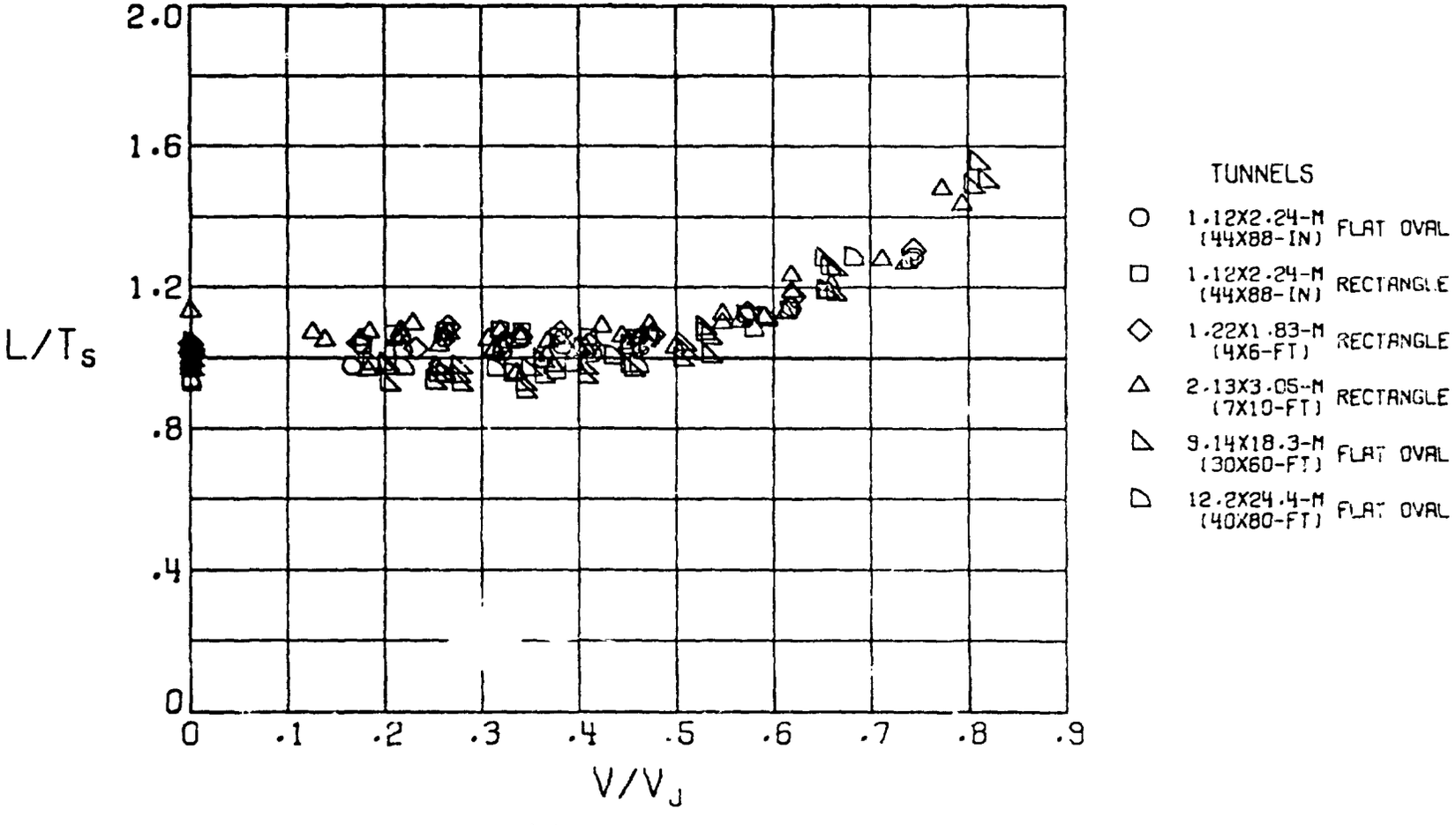

(b) Corrected data.
Figure 52. - Concluded.

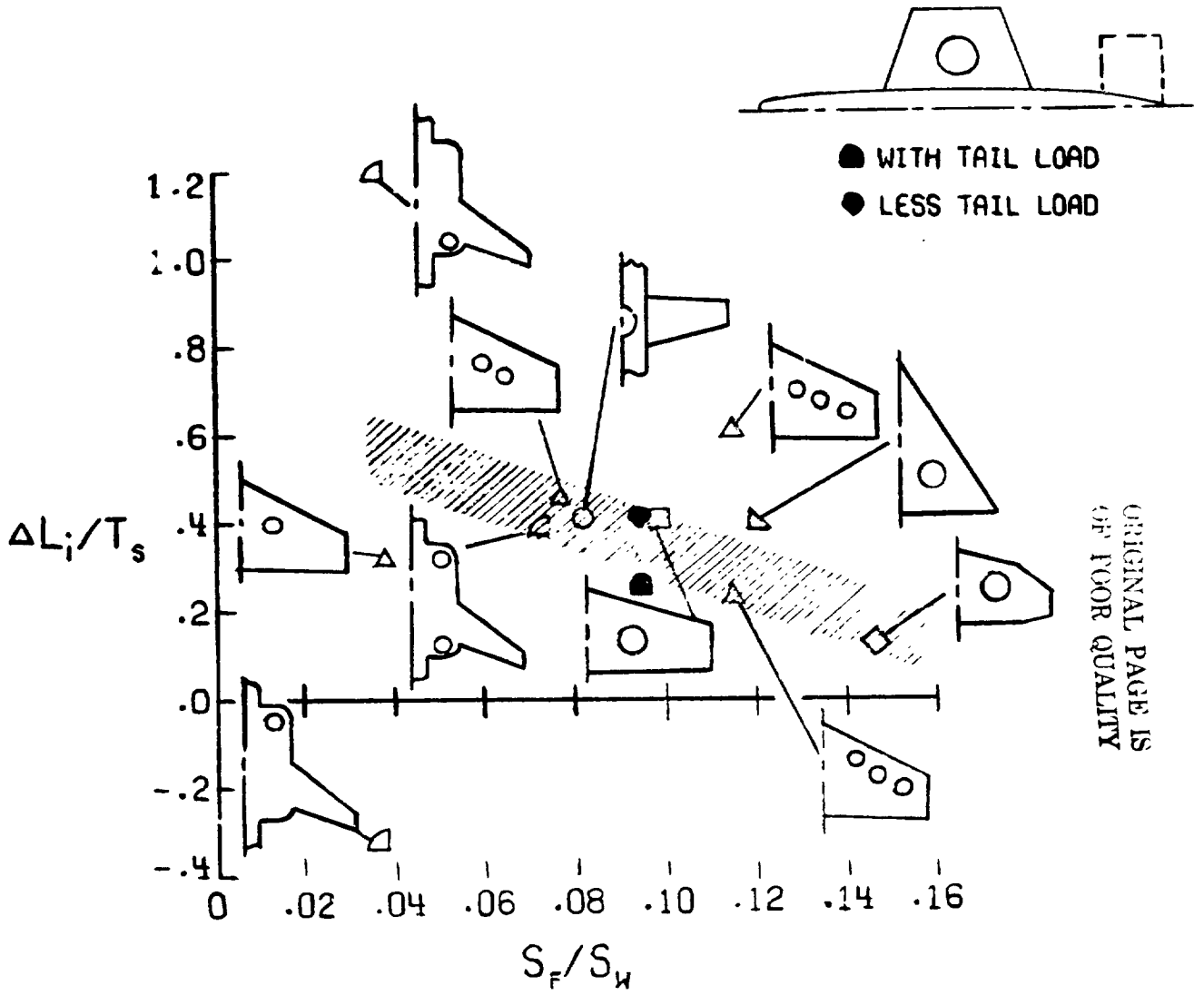

Figure 53. - Influence of the ratio of fan area to wing area on "fan-induced" lift as given by reference 21. The solid symbols show the equivalent values from figure 52(a) for the 1.12 x 2.24m (44 x 88 in.) flat-oval test section. $\alpha = 0^{o}$, v/vj = 0.4.

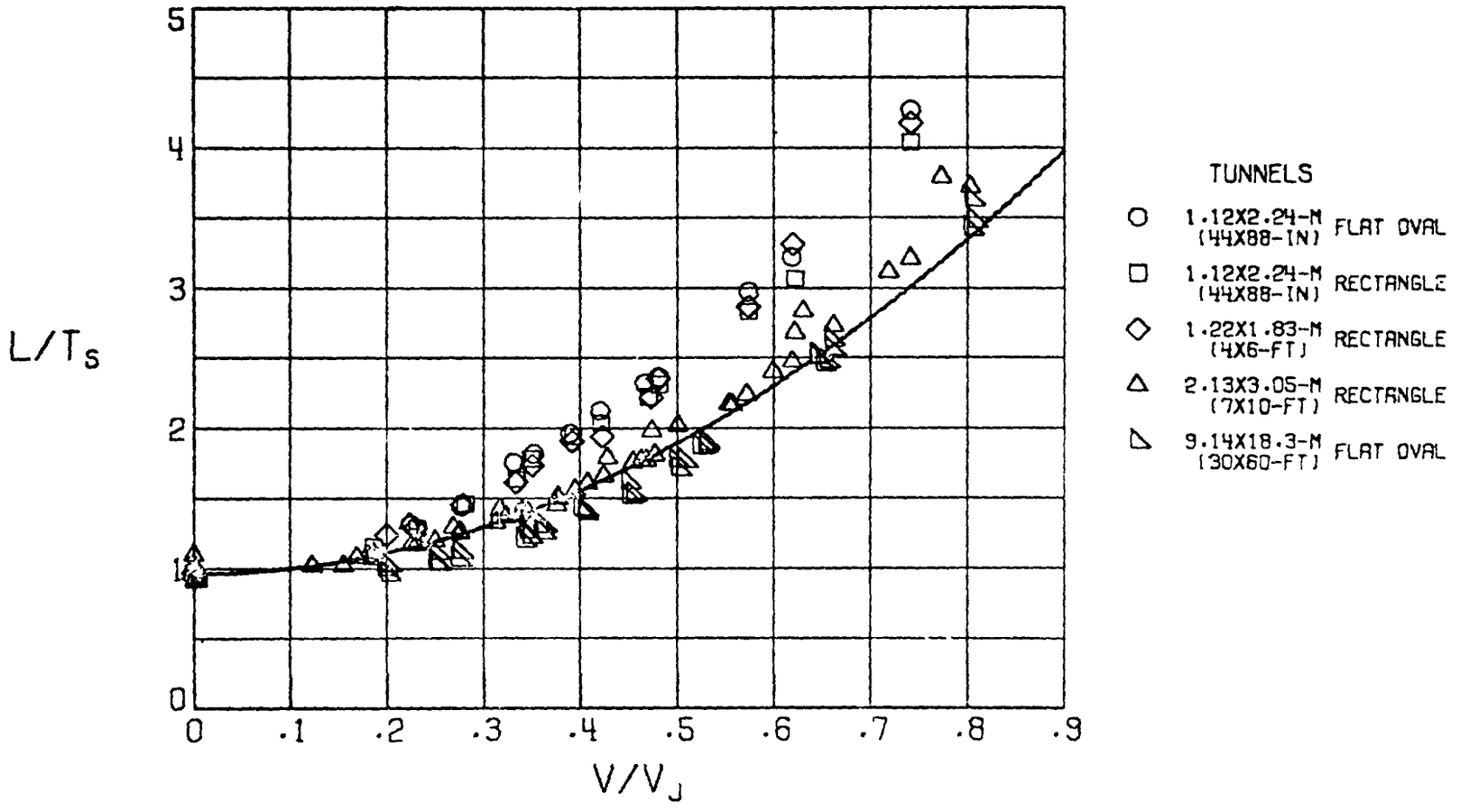

(a) Uncorrected data.

Figure 54. - Lift data from the fan-in-wing model. The solid line is the theoretical performance from reference 22. $\alpha = 16^{o}$.

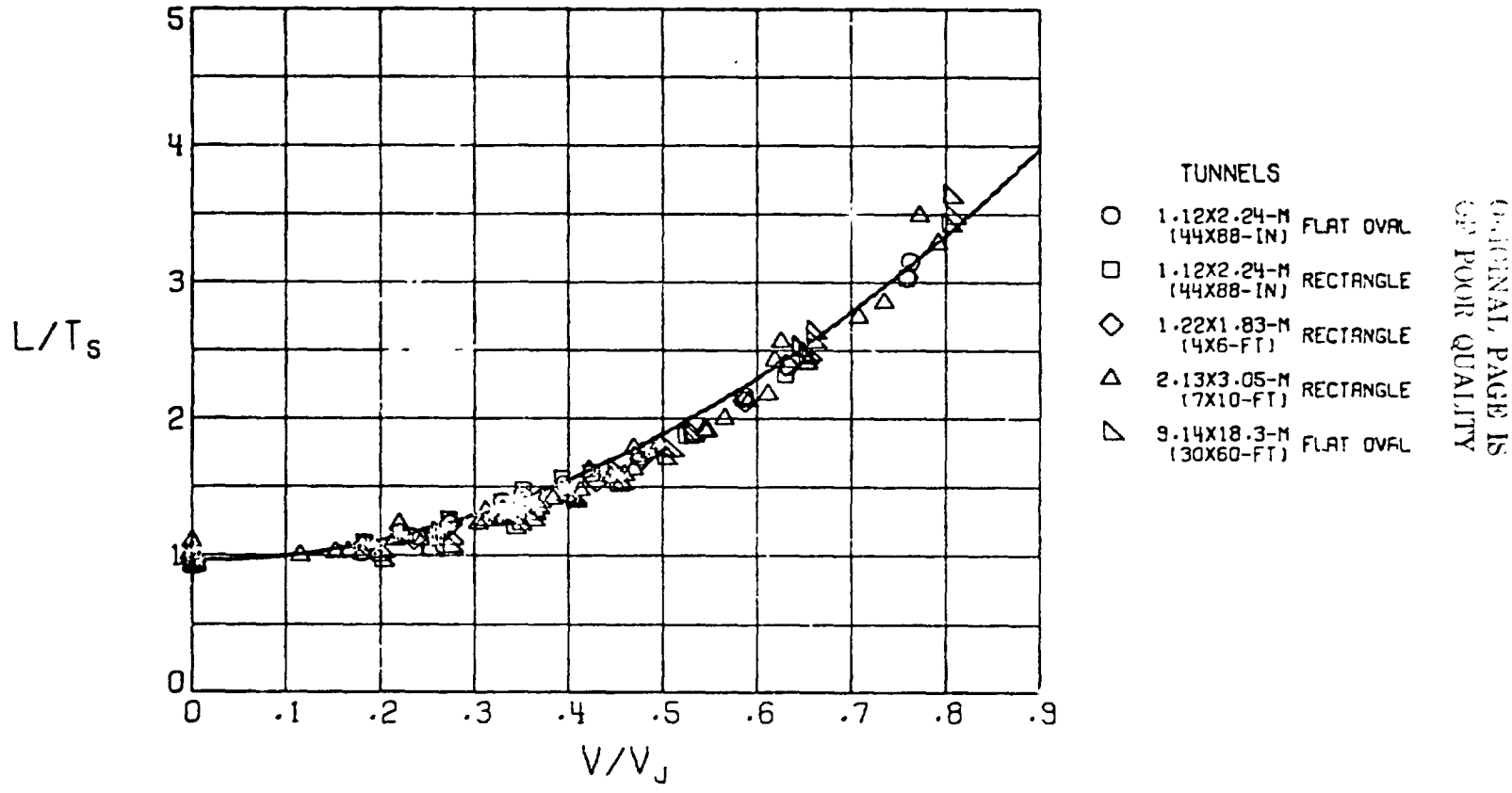

(b) Corrected data.

Figure 54. - Concluded.

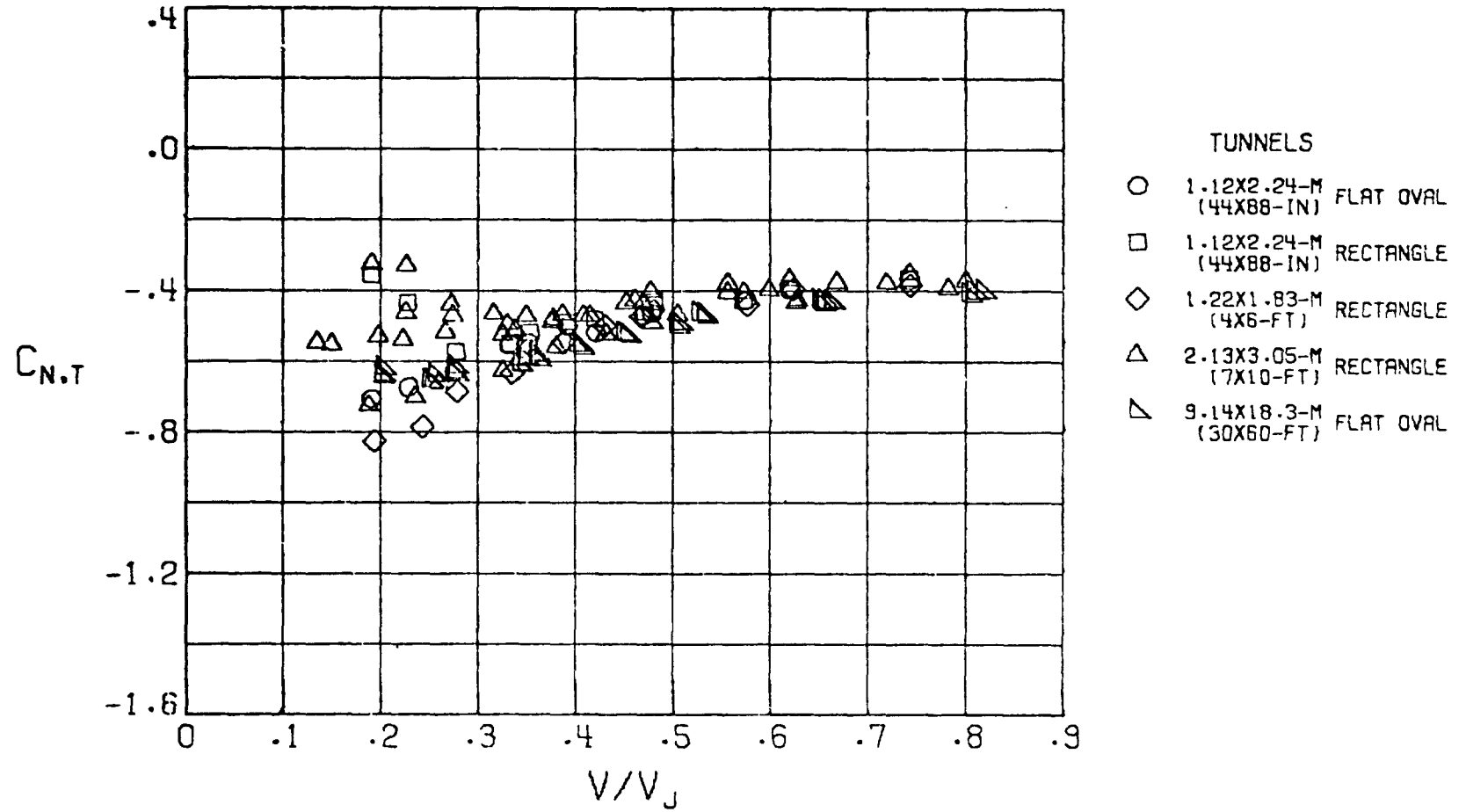

(a) Uncorrected data.

Figure 55. - Tail normal-force data from the fan-in-wing model. $\alpha = 0^{o}$.

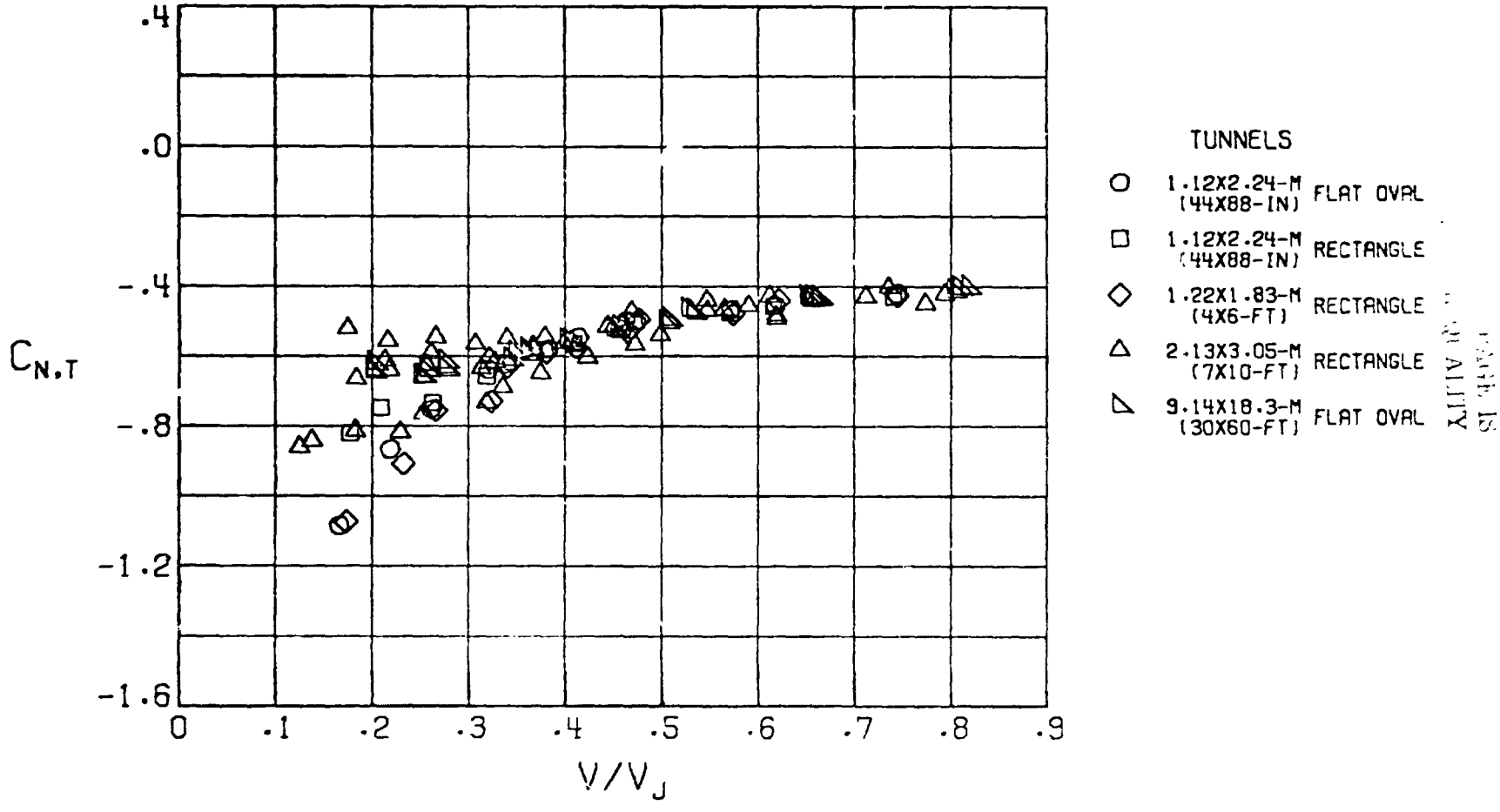

(b) Corrected data.
Figure 55. - Concluded.

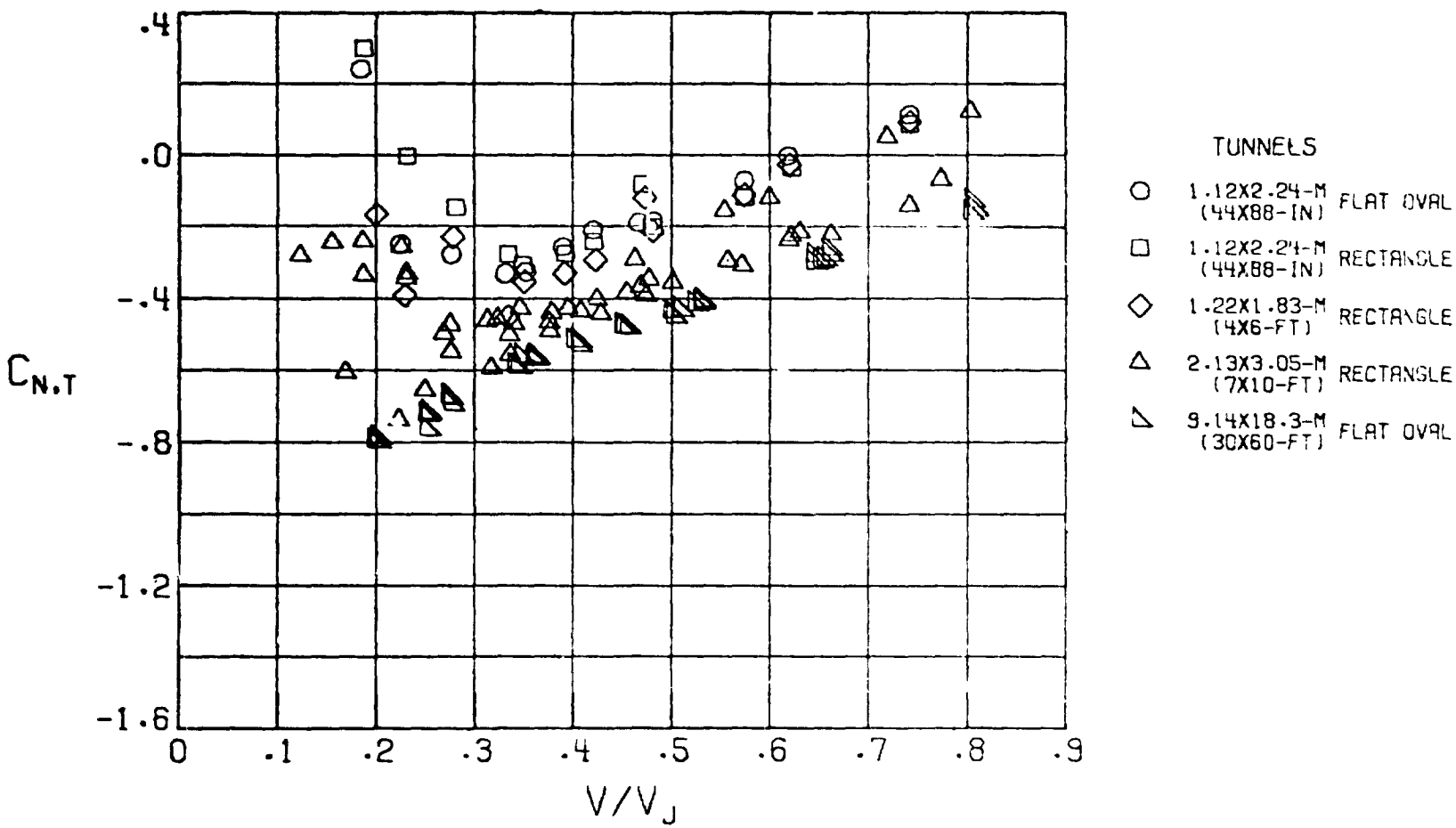

(a) Uncorrected data.

Figure 56. - Tail normal-force data from the fan-in-wing model. $\alpha = 16^{o}$.

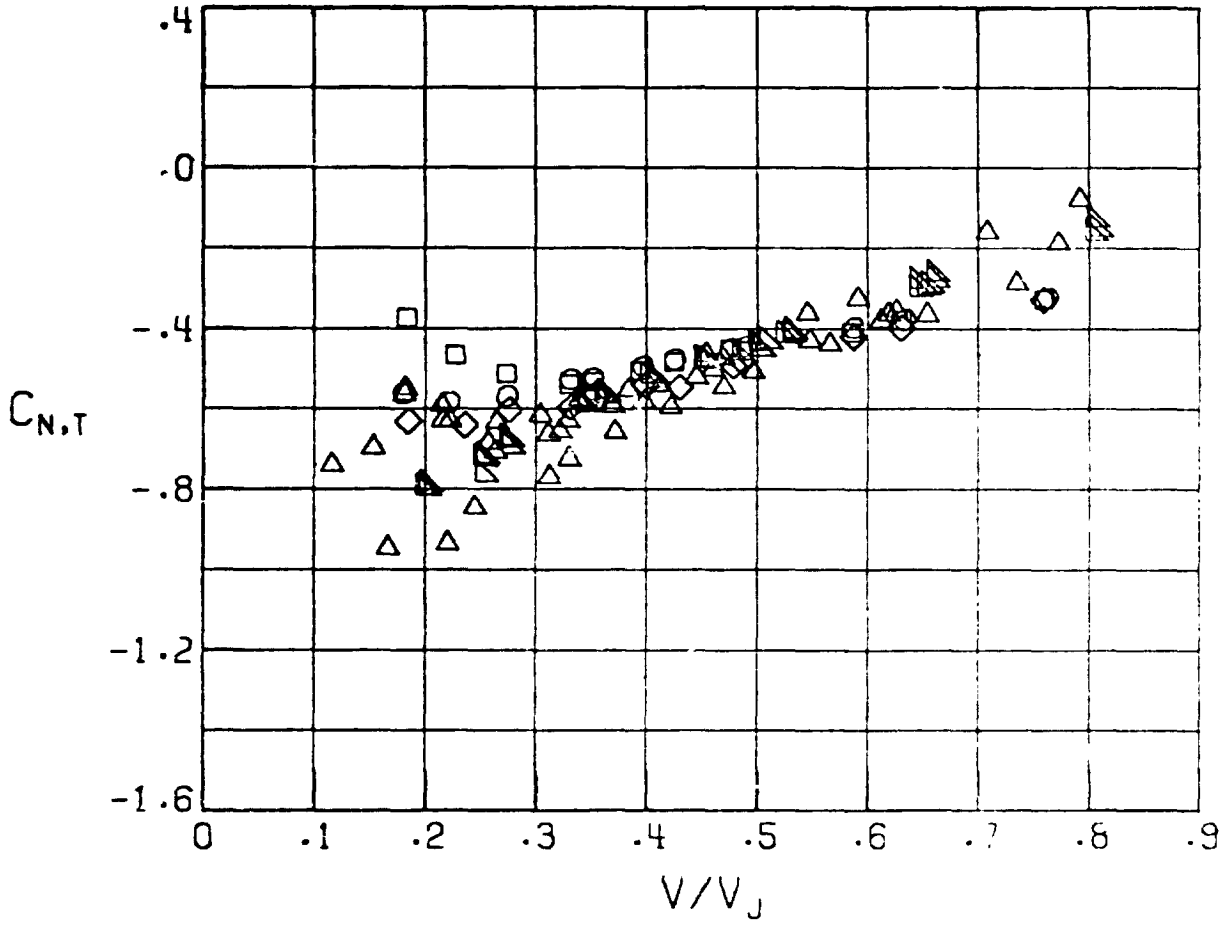

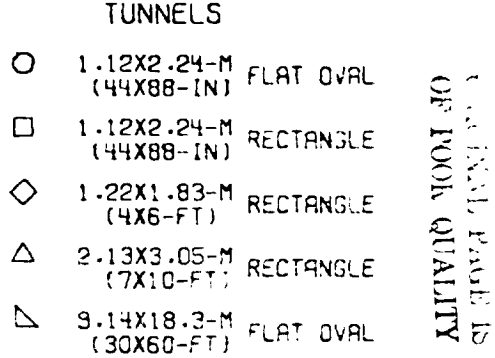

(b) Corrected data.
Figure 56. - Concluded.

1 Report No	2 Government Accession No	3 Recipient's Catalog No
NASA TM 78750		

4 Title and Subtitle	5 Report Date
WIND-TUNNEL TESTING OF VTOL AND STOL AIRCRAFT	July 1978
	6 Performing Organization Code 31.600
7 Author(s)	8 Performing Organization Report No
Harry H. Heyson	
9 Performing Organization Name and Address	10. Work Unit No
NASA Langley Research Center Hampton, Virginia 23665	516-50-23-01
	11 Contract or Grant No
	13 Type of Report and Period Covered
12 Sponsoring Agency Name and Address	Technical Memorandum
National Aeronautics and Space Administration Washington, DC 20546	14. Sponsoring Agency Code

15 Supplementary Notes Collateral release of notes for lecture presented in Seminar on Aerodynamics of V/STOL Aircraft and Helicopters at the Pennsylvania State University, University Park, PA, July 31-August 4, 1978.

16 Abstract

The basic concepts of wind-tunnel boundary interference are discussed and the development of the theory for VTOL-STOL aircraft is described. Features affecting the wall interference, such as wake roll-up, configuration differences, recirculation limits, and interference nonuniformity, are discussed. The effects of the level of correction on allowable model size are shown to be amenable to generalized presentation. Finally, experimental confirmation of wind-tunnel interference theory is presented for jet-flap, rotor, and fan-in-wing models.

17. Key Words (Suggested by Author(s))	18 Distribution Statement
Wind Tunnels Corrections V/STOL Helicopters	UNCLASSIFIED - UNLIMITED STAR Category: 02

19 Security Classif. (of this report)	20. Security Classif. (of this page)	21. No. of Pages	22 Price
UNCLASSIFIED	UNCLASSIFIED	79	$6.00

For sale by the National Technical Information Service, Springfield, Virginia 22161